Surface Myoelectric Signal Analysis and Enhancement for Improved Prosthesis Control

A thesis submitted for the degree of Doctor of Philosophy.

Centre for excellence in Signal and Image Processing,
Department of Electronic and Electrical Engineering,
University of Strathclyde

Paul McCool

2014

This thesis is the result of the author's original research. It has been composed by the author and has not been previously submitted for examination that has led to the award of a degree.

Signed:

Date:

Acknowledgements

I would like to thank my supervisors Dr Lykourgos ‘Akis’ Petropoulakis and Professor John J. Soraghan, who have been a source of tireless expertise and encouragement.

Thanks to Dr Navin Chatlani for advice and moral support.

I am grateful to Professor Adrian D. C. Chan of the Department of Systems and Computer Engineering at Carleton University, Ottawa, Ontario, Canada for his enthusiastic help, particularly during my placement at Carleton University.

I would also like to thank Radhika Menon for recording and providing Data Set 1 and Dr Christian Cipriani and Gunter R. Kanitz for providing Data Set 4.

Finally, thanks to my mum and dad, who gave me support and encouragement throughout this PhD.

Abstract

In this thesis, novel signal processing and machine learning techniques are presented in the field of myoelectric control. Specifically, algorithms for activity detection, noise identification and noise reduction are introduced, evaluated and discussed. The ultimate aim has been to develop algorithms to improve the performance of prosthetic control systems that use myoelectric signals.

Such systems must be an ability to distinguish between electromyographic signals and background noise. For this, the behaviour of One-Dimensional Local Binary Pattern histograms were used to identify the presence of myoelectric activity in recorded signals that originated from electrode sensors on the surface of the skin. This technique was compared against two other activity detection methods and it was found to give better performance in some circumstances. In particular, a lower False Positive Rate was achieved.

Noise is always present in myoelectric signals, and if it can be identified then steps can be taken to quantify and/or mitigate it. Pattern recognition was used to identify a single noise type in pre-recorded myoelectric signals. A set of Radial Basis Function Support Vector Machines were trained and tested on clean myoelectric signals that have been artificially contaminated with five typical noise types. The behaviour of the features and the nature of the confusion are discussed. Identification was shown to be possible, but confusion between noise types grew as the SNR increased.

Spectral Enhancement, which is normally used on speech signals, is applied to myoelectric signals in an attempt to mitigate noise. Spectral Enhancement based on Improved Minima Controlled Recursive Averaging (IMCRA) was found to improve the classification accuracy, and by corollary the signal quality, with signals that had white noise artificially added (which can be present in recorded myoelectric signals) and with intrinsically noisy signals. The improvement was higher when fewer channels were used.

List of Acronyms and Initialisms

1-D LBP	One-Dimensional Local Binary Pattern
AR	Autoregressive
AWGN	Additive White Gaussian Noise
BSS	Blind Source Separation
CCN	Correlation Coefficient Test for Normality
DC	Direct Control
DFT	Discrete Fourier Transform
DPR	Maximum-to-Minimum Drop in Power Density
ECG	Electrocardiogram
EMD	Empirical Mode Decomposition
EEG	Electroencephalogram
EMG	Electromyography/Electromyographic
FFT	Fast Fourier Transform
FPR	False Positive Rate
IMCRA	Improved Minima Controlled Recursive Averaging
IMCRA SE	Spectral Enhancement based on IMCRA
IMF	Intrinsic Mode Function
LBP	Local Binary Pattern
LBPAD	LBP-Based Activity Detection
LDA	Linear Discriminant Analysis
MAV	Mean of the Absolute Value
MMSE	Minimum Mean Square Error
MS	Minimum Statistics
MSE	Mean Square Error
MSNE	Minimum Statistics Noise Estimation
MUAP	Motor Unit Action Potential
MVC	Maximum Voluntary Contraction
OMLSA	Optimally Modified Log Spectral Amplitude
PCA	Principal Components Analysis
PDF	Probability Density Function
PR	Pattern Recognition
PSD	Power Spectral Density
RAD	Resistor Average Distance
RBF	Radial Basis Function
RI	Rotationally Invariant
sEMG	Surface Electromyographic/Surface Electromyogram
SENIAM	Surface ElectroMyoGraphy for the Non-Invasive Assessment of Muscles
SER	Signal to ECG Ratio
SMR	Signal to Motion Artifact Ratio
SNR	Signal to Noise Ratio
SPR	Signal to Power Line Ratio
STFT	Short Time Fourier Transform
SVD	Singular Value Decomposition
SVM	Support Vector Machine
TMR	Targeted Muscle Reinnervation
TPR	True Positive Rate
VAD	Voice Activity Detection

Table of Contents

Contents

List of Figures

List of Tables

1 Introduction

Myoelectric, or electromyographic (EMG) signals are electrical signals that occur due to muscle contractions. EMG signals can be measured on the surface of the skin and used to control prostheses. Modern myoelectric forearm (hand) prostheses usually measure the voltage at two surface sites on the forearm: one on a flexor group and one on an extensor group (though as many as six have been used [1]). The Mean of the Absolute Value (MAV) of the voltage is calculated and then used as a direct rate control for the movement. The prosthetic wearer activates the flexor group to close the hand and the extensor group to open it. This control strategy is called Direct Control (DC). The 'pincer' type myoelectric prosthetic claws are an example of a device that uses DC. The first DC myoelectric prosthetic that was used clinically became available in 1964 [2].

The most advanced and expensive prosthetic hands currently on the market have individually articulated fingers that automatically stop when enough grip has been applied. The articulation allows a wider range of gestures to be realised compared with simpler open/close 'claw' models. Unfortunately, the muscle activations required to perform additional gestures do not correspond to the natural muscle activation that would be needed [3]. This is unintuitive, and because of this, not all amputees are able to make full use of the functions available in their prosthesis. The situation is exacerbated by the lack of sensory feedback from current clinical prosthetics [4]. A more intuitive system is needed; one that works based on the interpretation of muscle signals that correspond more closely to the desired gesture, and this is what Pattern Recognition promises.

1.1. Author Publications

[5] Paul McCool, Graham D. Fraser, Adrian D. C. Chan, Lykourgos Petropoulakis, John J. Soraghan, "Identification of Contaminant Type in Surface Electromyography (EMG) Signals", IEEE Transactions on Neural Systems and Rehabilitation Engineering, *in press*.

[6] Paul McCool, Navin Chatlani, Lykourgos Petropoulakis, John J. Soraghan, Radhika Menon, Heba Lakany, "1-D Local Binary Patterns for Onset Detection of

Myoelectric Signals", EUSIPCO 2012, Bucharest, Romania, 27 – 31 August 2012, pp. 499-503.

[7] Paul McCool, Navin Chatlani, Lykourgos Petropoulakis, John J. Soraghan, Radhika Menon, Heba Lakany, "Lower Arm Electromyography (EMG) Activity Detection using Local Binary Patterns", *accepted by* IEEE Transactions on Neural Systems and Rehabilitation Engineering on 5th August 2013, *in press*.

[8] Paul McCool, Lykourgos Petropoulakis, John J. Soraghan, Navin Chatlani, "Improved Pattern Recognition Classification Accuracy for Surface Myoelectric Signals using Spectral Enhancement", *submitted to* Elsevier Biomedical Signal Processing and Control.

1.2. Research Motivation

The aim of this research has been to contribute towards the robustness of pattern recognition and therefore to ultimately improve control strategies for prosthetic hands. The first issue to be addressed is that of muscle activity detection. The pattern recognition system must be able to distinguish between background noise (i.e. the subject is at rest) and muscle activity, to reduce the likelihood of unwanted or incorrect limb movement. There are many onset and activity techniques already in existence, but each has its limitations. The new technique is another tool that performs well with noisy multi-channel data.

The second issue that has been addressed is the issue of noise identification in surface myoelectric signals. Noise is inevitable due to the nature of the measurement scenario: in the case of myoelectric control, a bipolar sensor sits against the skin all day, subject to changes in skin condition, sweat, movement relative to the skin and other noise sources. There are also electrical noise sources such as power line interference or amplifier saturation, and if the sensor is on the torso then there can be ECG interference. The noise must be detected and identified so that the clinician or researcher can decide whether to keep or discard the data, or to attempt some mitigation process.

The final issue to be addressed is noise reduction in EMG. Spectral enhancement has been refined over many decades to enhance single-channel speech signals by

estimating the noise and speech within the signal without a noise reference source, then reducing the noise component. Spectral enhancement was investigated for use with muscle signals to attempt to improve the signal quality and therefore the classification accuracy.

1.3. Aims

A key task in this PhD has been in-depth investigation and implementation of EMG pattern recognition systems that are found in the literature. A few commonly-cited papers have been found to form a standard against which new work is compared [9, 10].

As the research progressed, the potential utility of One-Dimensional Local Binary Patterns and spectral enhancement techniques for use with myoelectric signals became evident. During my placement at Carleton University, Ottawa, Canada, I was working with one of the leading researchers in the field of myoelectric control, Professor Adrian D. C. Chan. The subject of the placement and subsequent journal paper [5] was the automatic identification, using pattern recognition, of contaminant types that are commonly found in myoelectric signals.

The aims were:

- Develop a way of inferring muscle activity in EMG signals by taking advantage of the behaviour of One-Dimensional Local Binary Patterns. Specific histogram bins have been observed to be higher in amplitude during EMG activity and others during inactivity. Our EUSIPCO conference paper [6] demonstrated the potential of this process, and the journal paper [7] described the approach taken, refinements made and results for both real and simulated EMG signals.
- Investigate the feasibility of using Pattern Recognition to detect and identify the types of noise that are commonly found in EMG signals.
- Apply spectral enhancement to EMG signals in an attempt to obtain higher gesture classification accuracy in Pattern Recognition. Algorithms that were designed for voice signal noise reduction were adapted for EMG signals by analysing the assumptions made and modifying them empirically. Results have indicated that a Pattern Recognition (PR) system with the extra Noise Reduction

stage has an improvement in classification accuracy when the signals are contaminated with Additive White Gaussian Noise, and that there is also an improvement in classification accuracy when applied to data sets with a low channel count that are naturally contaminated with noise.

1.4. Summary of original contributions

The contributions are shown in the context of a Pattern Recognition system in Figure 1.1.

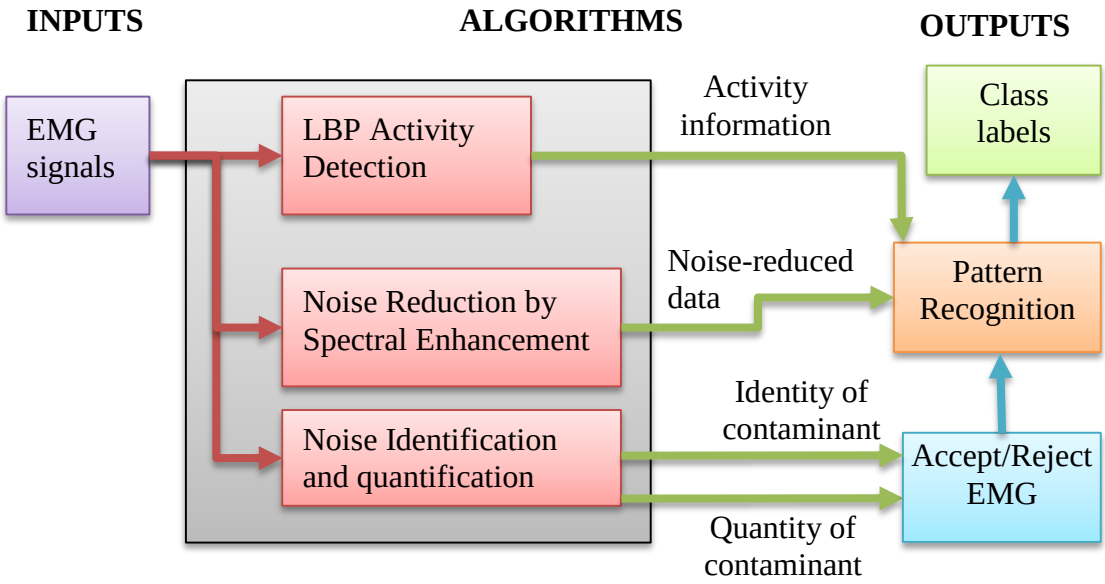

Figure 1.1 – Organisation of novel contributions in the context of a Pattern Recognition system

The Accept/Reject EMG stage in Figure 1.1 is a decision taken by the experimenter for each recording, based on noise type and level, before pattern recognition commences.

The first contribution is a new muscle activity detection algorithm that uses One-Dimensional Local Binary Patterns [6, 7]. The properties of One Dimensional Local Binary Pattern histograms can be used as a means of muscle activity detection when applied to EMG signals. This is useful because the best sensor site for pattern recognition purposes is not necessarily the site with the highest EMG amplitude [11]. A single active/inactive declaration is made across multiple EMG channels without the need for tuning for each channel. Each activity/inactivity decision is made within

a window, without reference to the histogram bin activity in adjacent windows and its performance is tested against two popular methods.

The second contribution a demonstration that Pattern Recognition can be used to identify and distinguish between contaminants that are commonly found in EMG signals [5]. To do this, steady state EMG was artificially contaminated with representative noise types, and then classifiers were trained based on features extracted from the noisy signals. The accuracy of the classification decreased as the SNR increased, where the contaminant has less impact on the usefulness of the EMG for prosthetic control and telehealth.

The final contribution was to show that spectral enhancement techniques designed for speech can be configured for use with myoelectric signals [8]. Spectral enhancement was found to restore signal quality, with a subsequent improvement in classification accuracy, for EMG signals when Additive White Gaussian Noise is present and when real noisy EMG was processed.

1.5. Organisation of thesis

Chapter 1 is this general introduction to the thesis.

Chapter 2 describes myoelectric signals and the issues involved in measurement. Pattern recognition-based EMG control is then introduced, and each step of the pattern recognition process is explained.

Chapter 3 gives a description of Digital Signal Processing as applied to EMG such as onset and activity detection and objective signal quality measures. The tools that will be used in the later chapters are introduced.

Chapter 4 describes One-Dimensional Local Binary Patterns as applied to myoelectric signals for muscle activity detection. EMG activity is detected within recordings by observing the behaviour of the 1-D LBP histogram bins and a technique called LBP-based Activity Detection (LBPAD) is introduced. Muscle activity is inferred from the EMG activity. LBPAD is compared with two popular algorithms and is found to be superior in some circumstances.

Chapter 5 describes noise identification for myoelectric signals. Pattern recognition is shown to be an effective tool for identifying common types of noise that are found

in surface EMG signals. Clean steady-state EMG is artificially contaminated with one of five noise types at several SNR levels, and classification accuracy at low SNRs is high. At higher SNRs, the classifiers confuse the contaminants in particular ways, and this is analysed.

Chapter 6 describes the application of spectral enhancement to surface myoelectric signals for improving PR classification accuracy. The adaptations to the spectral enhancement techniques are discussed, and then the effects of spectral enhancement on EMG signals are explained. Measurements of the change in signal quality are given. The changes in classification accuracy are discussed for real EMG with white noise added artificially and real EMG recordings that have intrinsic noise.

Chapter 7 is a summary chapter, in which areas for future development and issues for future research are discussed.

2 Myoelectric Control

2.1. Introduction

In this chapter, forearm prostheses will be introduced and discussed, and then the myoelectric signal will be described along with the issues that arise when it is used for the purposes of prosthetic control. Human reaction time is explained, then pattern recognition is analysed in the same context. Finally, the types of noise that are commonly found in myoelectric signals are discussed.

2.2. Biosignal-controlled Prostheses

The purpose of prosthetics is to provide some degree of functionality for a missing body part. The simplest type of prosthetic enhances cosmetic appearance by restoring a more 'natural' bodyline. Such prostheses are called 'passive'. Passive prosthetic hands date at least as far back as the Roman Empire: Marcus Sergius had an iron hand made for him after suffering injuries in battle [12].

Body-powered prostheses, which fall under the category of 'functional' prostheses, allow the user to realise mechanical movement of joints on the prosthetic by moving their own body to control them. For example, with a body-powered claw, straps around the user's shoulders allow the user to shrug to open and close the claw. This arrangement gives the wearer a degree of proprioception, which is knowledge of the position of the limb relative to the body (i.e. amount that the claw is open).

The third type of prosthetic functions by reading biological signals (biosignals) from the wearer that are subsequently interpreted into commands for the prosthesis' functions. It is tempting to immediately imagine prosthetic hands that respond directly to brain signals, and indeed a brain-controlled arm has been developed [13]. In [13], sensors are surgically implanted into the brain to read groups of neurons and allow complex and intricate control of an arm and hand. The issues with this approach are the need for brain surgery, the lack of miniaturisation of the control system and the fact that the arm is not yet attached to the patient.

Electroencephalogram (EEG) signals are a measurement of electrical activity from the brain that has the benefit of being non-invasive. The feasibility of EEG as a

control signal has been analysed [14, 15], but at the time of writing, the author was unable to find evidence of research in which EEG is used to directly control a prosthetic hand. EEG signals relate to the movement of the entire body, so careful filtering and signal processing would be required to extract arm and hand control signals.

A myoelectric (or electromyographic – EMG) limb measures voltages that are generated when muscles move, which are called myoelectric signals. The first myoelectric hand was demonstrated at a fair by Reinhold Reiter at an exhibition in 1948 [16]. The first myoelectric limb that was used clinically was introduced by Soviet engineers in 1964 [2]. Each successive model of myoelectric hand has incremental improvements in capability, each of which improves the quality of life for the wearers. For example, the power supply and control unit have been moved from the belt of the wearer to inside the hand or its socket.

If a patient has a shoulder disarticulation, surgery can be performed to have nerves that would have gone to the arm and fingers routed instead to upper torso muscles. This is known as Targeted Muscle Reinnervation (TMR) [17]**.** Surface sensors can be used to read the myoelectric signals, and pattern recognition is performed to identify the gestures that the patient intended for their prosthetic arm.

Though myoelectric and other biosignal-controlled prostheses tend to capture the imagination of the public, they cannot completely replace passive or body-powered prostheses because the nature of each patient's amputation or deformity is different, and therefore the patient may not be able to use a biosignal-controlled prosthesis to its full potential. Bilateral amputees often use a myoelectric prosthesis and one other kind of prosthesis together. In addition, an amputee might own more than one kind of prosthesis for different purposes or even choose not to wear a limb for some tasks.

The more advanced and expensive myoelectric hands currently on the market have individually articulated fingers that automatically stop when enough grip has been applied to the object being held, so that it is not crushed. A microcontroller constantly monitors the currents to the motors that operate the fingers and stalls them once a threshold is exceeded. The iLimb, the first version of which came out in 2007, is a commercial myoelectric limb that has been developed from research on the

Edinburgh Modular Arm System by Touch EMAS (also known as Touch Bionics). The most recent model (at time of writing), the in the Touch Bionics iLimb Ultra Revolution™, has two powered degrees of freedom for its thumb. Thanks to regular incremental updates, the iLimb maintains its reputation as the most advanced myoelectric prosthetic hand on the market, beating the still impressive RSLSteeper BeBionic and Otto Bock Michelangelo limbs in terms of capability.

In all three of these limbs, clever re-use is made of the open-close commands in order to realise more gestures. For example, the limb can be programmed such that a second 'open' command causes a pointing gesture, or a double co-contraction of flexors and extensors together might move a degree of freedom of the thumb. The user can choose which additional gestures he/she would like by programming the limb using their PC or smartphone over Bluetooth. Despite this sophistication, this is still Direct Control, albeit a more functional updated version.

There is a high-profile programme to develop better prosthetics for US veterans, known as Revolutionizing Prosthetics [18], which has produced dextrous robot hands and advanced PR-based control systems, but it has yet to produce prosthetic hands for use outside of the research environment.

Non-amputees have feedback on their actions because their fingers and arm can be seen to move through proprioception. Amputees can see muscles moving on their residual limb, but there is only a feed-forward system for finer controls [4]. Amputees can undergo surgery to restore some sensory feedback. The Krukenberg Procedure crafts a functional pincer from the residual limb [19] and recently the radial and ulnar nerves were stimulated to provide touch sensations from sensors on the fingertips of the prosthetic [20].

2.3. The Myoelectric Signal

2.3.1. Description

When a human wants to move his or her arm, the brain signals the nervous system. Electrical signals are sent down the nerves to the lower arm. The locations at which the muscle fibres are innervated are called Motor Units. The voltage that is generated at the MUAP when the Motor Unit fires is called a Motor Unit Action

Potential (MUAP). It is caused by the movement of ions across cell membranes. Hodgin and Huxley won the 1963 Nobel Prize for their model of this phenomenon [21]. Detailed descriptions of motor unit function can be found in [22, 23].

2.3.1.1. Surface EMG

The myoelectric signal or surface electromyogram (sEMG) is a measure of the attenuated summation of MUAPs within range of an electrode sensor, with additive noise [24] which, during a steady-state contraction, can be represented as:

$$x[n] = \sum_{i=1}^{R} \sum_{l=-\infty}^{+\infty} m_{il}[n - \Phi_{i,l}] + v[n] \quad \textbf{(2.1)}$$

where $x[n]$ is the measured sEMG signal and sample number is *n*, *R* is the number of active motor units, $m[n]$ is *l*th MUAP belonging to motor unit *i*, $\Phi_{i,l}$ is the occurrence time of $m_{il}[n]$ and $v[n]$ is additive noise [25].

The characteristics of EMG, such as its frequency content and amplitude, change depending on its anatomical original. Gait EMG differs from forearm EMG as it has periodicity. Sample rates for surface forearm EMG are usually 2-3kHz. Signals are normally band pass filtered between 6-500Hz, because the majority of the sEMG energy is within this bandwidth [26]. A detailed description of the myoelectric signal can be found in [25]. There is always a small background level of EMG, which is caused by motor units firing to provide muscle tone [22].

The size of a motor unit is determined by the number of muscle fibres that are innervated by a single motoneuron. When a contraction is initiated, the motor units begin firing in order from smaller to larger. To sustain contractions, motor units take turns firing so the individual motor units are not fatigued too quickly [22]. If an individual MUAP is examined, it consists of a repeating and voltage pattern with a distinctive shape ($m[n]$ in equation (2.1)) as cell membranes polarise and depolarise. sEMG is often called 'interference' EMG because it is the interference pattern between the MUAP trains that is being measured, especially at high levels of Maximum Voluntary Contraction (MVC).

It was shown in [27] that the use of interference EMG for prosthetic control gives a 'bigger picture' of muscle activity, which is more useful than looking at the

individual MUAP trains for pattern recognition-based control (PR is discussed in Chapter 3). The shape and spacing of electrodes has a profound effect on measuring process, so to guide EMG researchers, consensus for the recommended configurations for sEMG sensors was reached in the SENIAM project [28-30].

When measuring sEMG on the forearm of non-amputees, it has been found that placing the sensors above specific muscles works no better than simply placing the sensors on a band round the arm in terms of the classification accuracy that can be obtained from a system that uses Pattern Recognition-based control [31].

2.3.1.2. Invasive EMG

Needles can be inserted into the muscle to measure the activity of a few (or even single) motor units within the vicinity of the needle tip. This is called invasive EMG and it is mainly used for diagnosis of myopathies, because the shape of the MUAP can indicate the health of the muscle or nerve for the purposes, for example, of assessing a neuromuscular disease [23]. The bandwidth of invasive EMG is greater than for surface EMG because the low-pass 'tissue filter' effect does not apply [25]. Invasive EMG does not suffer from crosstalk and there is therefore less redundancy between channels, but it is less suitable for control because:

- It is hard to predict whether and when a specific motor unit will fire during a muscle contraction, which makes it unreliable
- MUAPs must be located every time the needles are reinserted, which is time-consuming
- Having needles in the muscle could be uncomfortable, which would impair prosthetic control activities
- The increased possibility of infection due to their percutaneous nature

Implantable sensors can be used to measure EMG for control [32]. Tests on macaque monkeys showed that pattern recognition-based control could be achieved with high accuracy using seven implantable sensors, which were powered through induction. One group showed that there is no improvement in classification accuracy (compared with sEMG) when implanted sensors are used [31], and concluded that clinical factors are more important when deciding on sensor type.

2.3.2. Crosstalk

It has been said that the spatio-temporal information in muscle crosstalk can "implicitly add discriminatory information" [33, 34] for pattern recognition. On the other hand, if closely spaced individual muscles in a residual limb are to be used to control individual prosthetic functions, then it is preferable to minimise crosstalk [35-37].

2.3.3. Frequency distribution

There is a difference in myoelectric signals between people with limb loss and non-amputees [38]. Specifically, there is a wider frequency range and less sharp frequency distribution peak in the power spectral density for amputees and those with congenital limb absence. This is related to the muscle structure, electrode orientation, muscle type, the way the muscle is used based on the type of amputation, type of contraction and the way the muscle developed [38].

2.3.4. Simulated EMG

Simulated EMG is used to make noise-free reference signals with which to test algorithms. The parameters of the simulated EMG can be easily changed, including SNR and frequency content. Once demonstrated on simulated EMG, the algorithms can be tested on real EMG. There are three main types of EMG model: descriptive, phenomenological and structural [25]. An example of a descriptive mode is the presumption of a relationship between EMG amplitude and muscle force. An example of a phenomenological model is an autoregressive model. A structure-based or structural model describes the system in a reductionist manner, for example, individual MUAPs can be modelled and summed to create a simulated signal.

Band-limited Gaussian noise can be used as a simulated EMG signal [39, 40]. In this phenomenological model, unambiguous onset and offset times can be decided by the experimenter, allowing accuracy assessment for onset detection techniques. The SNR can be set by varying the amount of white noise added to the bandpassed signal.

A transfer function can be used to make a phenomenological model to control the frequency content of simulated EMG:

$$H_{EMG}(f) = \frac{jKf_h^2 f}{(f_l + jf)(f_h + jf)^2} \quad \textbf{(2.2)}$$

The parameters f_l and f_h are used to adjust the shape of the EMG spectrum. K can be modified to normalise the energy content of the signal. f is the frequency.

A data set of dynamic simulated EMG was created for use in the activity detection section of this thesis (Chapter 4). To do this, the parameters in (2.2) were changed randomly for each simulated gesture, but kept constant during a gesture to simulate a static contraction. A simulated recording of a 'rest-gesture-rest' was generated of length 15s that has a gesture of length 5±0.5s in duration starting 5-10s into the signal. An onset and offset were generated by 100-sample 'ramps' at either side of the stationary contraction [40], as opposed to the truncated Gaussian used in [39]. Finally, Additive White Gaussian Noise was added to the signal at the required SNR. Figure 2.1 (a) shows a clean EMG gesture, which has AWGN added Figure 2.1 (b) to produce the signal shown in Figure 2.1 (c).

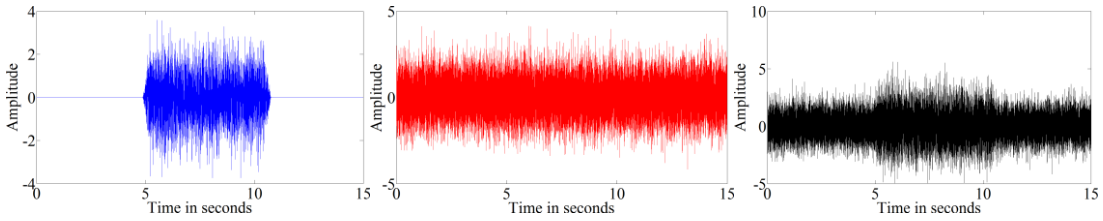

(a) (b) (c)

Figure 2.1 - The creation of simulated recording of an EMG corresponding to a gesture is created.

In Figure 2.1, the clean EMG, which has well-defined onset, steady state and offset locations (a) has noise (b) added to it (c). In this example, f_l = 59, f_h = 129, fs = 2000, SNR = 0dB.

2.3.5. EMG recordings used in this work

2.3.5.1. Data Set 1

This data set consists of four gesture classes (tripod, pinch, point, and lateral grip) recorded from three volunteers with full limbs who performed thirty sessions, each consisting of five gestures, as shown in Figure 2.2.

Figure 2.2 - Gestures in Data Set 1

The gestures were formed by isotonic muscle contractions and held as isometric contractions for five seconds, with five seconds of rest between each gesture. The gestures were recorded in random sequences. The data set, also used in [6], was recorded in the Department of Biomedical Engineering, University of Strathclyde, UK. All protocols were ethically approved. Technical details are given in Table 2.1.

Sample rate	2000Hz
Pass band	500Hz Low Pass
Power line filter details	Notch @ 50Hz
Number of channels	2
Number of fully-limbed subjects	3
Number of amputee subjects	0
Number of trials per subject	30
Number of gestures per trial	5
Electrode type	Dry bipolar
Gestures	Tripod Pinch Point Lateral Grip

Table 2.1 - Details of Data Set 1

Two channels were recorded because most contemporary commercial myoelectric prostheses use two channels. Dry bipolar electrodes (Figure 2.3) were placed on the volunteers' forearms at sites corresponding to the *extensor digitorum* and the *flexor carpi radialis*, which were located using palpation [41, 42]. The experiments were conducted with the elbow flexed and forearm in mid-pronation, rested comfortably

on a table, with the arm stationary and only the fingers moving to form the gestures. The sensors had the same form factor as those used in modern myoelectric limbs, with which conducting gel is not used. The amplifiers, built-in to the sensors, had a high Common Mode Rejection Ratio and a low-pass filter with a cut-off frequency of 500 Hz and a 50Hz notch filter to eliminate power line interference.

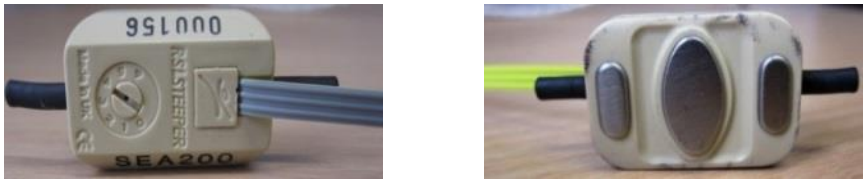

Figure 2.3 - Bipolar sensor of the kind used to collect Data Set 1

The movement onset was controlled by displaying visual cues on a screen, and recording the muscle activity. The volunteers responded to these visual cues, which stated the name and the image of the gesture to adopt (or a 'rest' instruction). In total, about 50% of the data is activity and 50% is rest. The timestamps of the movement cues were logged.

2.3.5.2. Data Set 2

The data set was recorded from thirty volunteers, with eight channels recorded using bipolar sensors; shown in Figure 2.4 [43], with a reference 3M™ Red-Dot electrode on the wrist as ground reference.

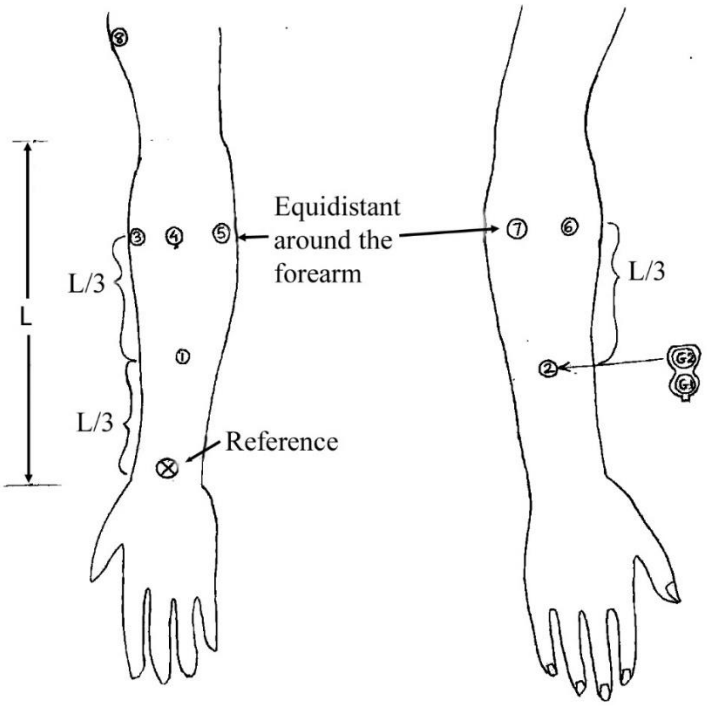

Figure 2.4 - Locations of sensors for Data Set 2 taken from [43]

The timestamps of the movement cues had been logged. Details of the data set are shown in Table 2.2.

Sample rate	3000Hz
Pass band	1Hz-1kHz
Power line filter details	Notch @ 60Hz
Number of channels	8
Number of fully-limbed subjects	30
Number of amputee subjects	0
Number of trials per subject	4 sessions of 6 trials = 24
Electrode type	Wet bipolar with common reference
Gestures	Hand open Hand close Wrist Pronation Wrist Supination Wrist Flexion Wrist Extension

Table 2.2 - Details of Data Set 2

Details of the amplifier and electrodes can be found in [43]. Seven movement classes (shown in Figure 2.5), wrist pronation/supination, wrist flexion/extension and rest) were recorded. The gestures were performed either from the previous gesture or from rest and then held, corresponding to isotonic followed by isometric muscle contractions, in three second intervals, with five seconds of rest at the start and end of each recording.

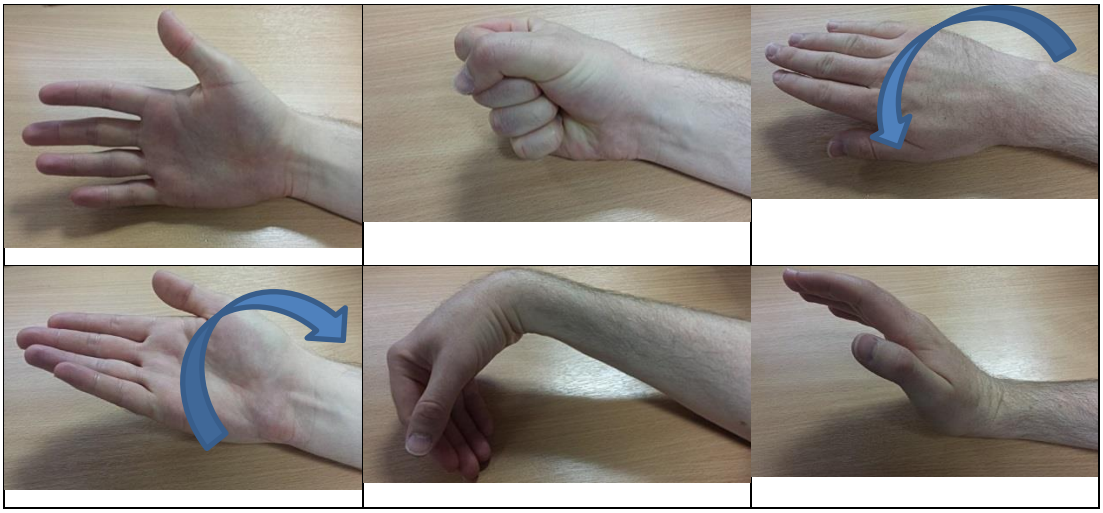

Figure 2.5 - Depictions of gestures in Data Set 2

Each gesture was performed four times per trial in randomized order. The recordings include transitions between gestures, as opposed to returning to rest between every gesture, such that 14.1% of the time between the first and last gestures is rest.

2.3.5.3. Data Set 3

Data Set 3 was recorded at Carleton University, Ottawa [44]. A single recording consisted of 10s of EMG during an isometric, isotonic contraction. Five trials were performed for each subject, with a trial consisting of three contraction levels for each muscle: 20%, 40% and 60% Maximum Voluntary Contraction (MVC). There were 225 recordings (5 subjects × 5 trials × 3 muscles × 3 contraction levels). Each recording of the real data set was assessed manually to exclude EMG recordings that appeared to be contaminated; 113 EMG recordings were found to have negligible contamination and were therefore retained for this research. More details on the EMG data acquisition and assessment are given Table 2.3 and in [44].

Sample rate	3003Hz
Pass band	0.3-1000Hz
Power line filter details	None
Number of channels	*biceps brachii* *quadriceps femoris* (*rectus femoris*) *tibialis anterior*
Number of fully-limbed subjects	5
Number of amputee subjects	0
Number of trials per subject	5
Number of gestures per trial	3
Electrode type	Wet AgCl (MVAP-II, MVAP Medical Supplies Inc., Newbury Park, CA, USA)
Gestures	20% MVC 40% MVC 60% MVC

Table 2.3 - Details of Data Set 3

A pair of Ag-AgCl surface electrodes (MVAP-II, MVAP Medical Supplies Inc., Newbury Park, CA, USA) was positioned above the muscle of interest, according to SENIAM guidelines [28-30]. The signals were amplified (Model 15A54 Grass amplifier, Grass Telefactor, West Warwick, RI, USA) and sampled at 3000 Hz (12-bit, PCI-6071E, National Instruments, Austin, TX, USA). The amplifier was programmed with a bandwidth of 0.3 Hz – 1000 Hz and a gain of 2000 (or 5000 if the EMG amplitude was low).

Table 2.4 shows the number of 5s recording segments that were kept for each subject. Note that there were no data retained for Subject 5 as they were all deemed to have excessive contamination.

		Number of recordings per subject				
	Subject number	**1**	**2**	**3**	**4**	**5**
Muscles	*biceps brachii*	24	30	26	0	0
	quadriceps femoris (*rectus femoris*)	12	24	0	16	0
	tibialis anterior	24	26	26	24	0
	Total	226				

Table 2.4 – Number of clean 10-second recordings per subject and per muscle from Data Set 3

Stationarity of the signals was verified by calculating the CCN across 5s windows of the signals (CCN is described in section 3.5). It changed little as the recordings progressed: The mean value for the first and the second windows was 0.9935 (standard deviation 0.0065) and 0.994 (standard deviation 0.0062), respectively. The mean change in CCN between the first and last 5s windows was therefore less than half a standard deviation. The same test was done across 1-second windows and no discernable trend was observed.

2.3.5.4. Data Set 4

This data set was created by Dr Christian Cipriani of ARTS Lab, Italy. Due to uncertainty during recording, it is unclear which channel corresponds to which surface location on the arm. Details are shown in Table 2.5.

Sample rate	1600Hz
Pass band	
Power line filter details	None
Number of channels	16
Number of fully-limbed subjects	5
Number of amputee subjects	0
Number of trials per subject	2
Number of gestures per trial	60
Electrode type	Wet AgCl 3M™ Red Dot
Gestures	1. Thumb flexion 2. Thumb opposition 3. Index finger flexion 4. Middle finger flexion 5. Ring finger flexion 6. Little finger flexion 7. Thumb extension 8. Thumb "antiopposition" (radial abduction) 9. Index finger extension 10. Middle finger extension 11. Ring finger flexion 12. Little finger flexion

Table 2.5 - Details of Data Set 4

The advantage of Data Set 4 is the presence of real noise, which means that it can be used to test the effects of noise reduction on classification accuracy (Chapter 6).

2.4. Human Reaction Time

For the purposes of real-time pattern recognition control systems for prosthetics, human reaction time is one of the most important limitations. If a prosthetic takes too long to respond to the wearer's command then sluggishness is experienced, which is fatiguing as it requires more concentration. The wearer might even stop using their prosthesis. Human reaction time for myoelectric control has been found to be around 200-300ms [9, 45, 46]. Another study found that the best compromise between classification error and controller delay was 150-250ms [47]. 220ms was used in [46] to assess whether motion discrimination was successful. The use of overlapping windows helps to compensate for longer windows.

Usually the window length from which the features are calculated is as long as possible to allow for more stable features [4], however a shorter window length gives a denser stream of training points with which to train classifiers (which are discussed

in the next section). It is common to use overlapping windows to obtain a denser stream of class labels for longer windows. Modern microcontrollers would otherwise be idle for much of a long window [4].

2.5. Pattern Recognition

There are two main kinds of myoelectric control: Direct Control (DC) and Pattern Recognition. For DC, a sensor is placed on the flexor group and one on the extensor group, and then level-coded control is implemented in which the averaged and rectified voltage of the myoelectric signal is used: The group with the highest level causes the limb to move in that direction. If only one muscle group is available, the hand can be made to close when lower amplitude is present and open when it is at a higher level [25]. The main limitation of DC is the difficulty in controlling more than two or three functions. A detailed discussion about myoelectric control strategies is given in [25].

The simplest definition of Pattern Recognition is that it takes an input or set of inputs and assigns a label to them based on their values. It can be said to be the demodulation of control commands that are encoded in features extracted from the signals [48]. Classification is an example of Pattern Recognition, where input(s) are assigned to one of a set of classes. In the case of prosthetic control, the inputs are voltage readings from sEMG sensors on the forearm or residual limb, and the classes can be finger movements, gestures or contraction levels.

The aim of pattern recognition for myoelectric control is to enable to user to command their prosthesis using muscle movements that correspond more naturally to the intended movement, so that more functions can be implemented and accessed. To be able to do this, the PR controller must be trained in such a way that it will correctly respond to patterns that it has not seen before. The type of training is called *supervised learning* and the ability to respond to previously unseen patterns is called *generalisation*.

These challenges are more easily addressed in a controlled laboratory environment, and for this reason, there is an armoury of research papers into Pattern Recognition on myoelectric signals for prosthetic control. High classification accuracies have

been achieved in laboratory conditions with few (or even single [49]) channels and for many gestures [50], but until recently, no pattern recognition systems have yet been robust enough for clinical use. The feasibility of PR-based prosthetic control from surface EMG was demonstrated in [9], but there was insufficient mobile computational power at the time for mobile implementation on a prosthetic.

The developments in low-powered, high-performance microcontrollers mean that implementing pattern recognition on a prosthetic hand is now feasible. At present, the control systems used for Targeted Muscle Reinnervation (TMR) prosthetics already use Pattern Recognition to interpret the myoelectric signals from the torso into arm and finger commands for the prosthetic arm [17]. This fundamental change in control strategy will lead to more accurate and reliable control for prosthetic hands. Figure 2.6 shows a block diagram of the typical components of a pattern recognition system for EMG analysis.

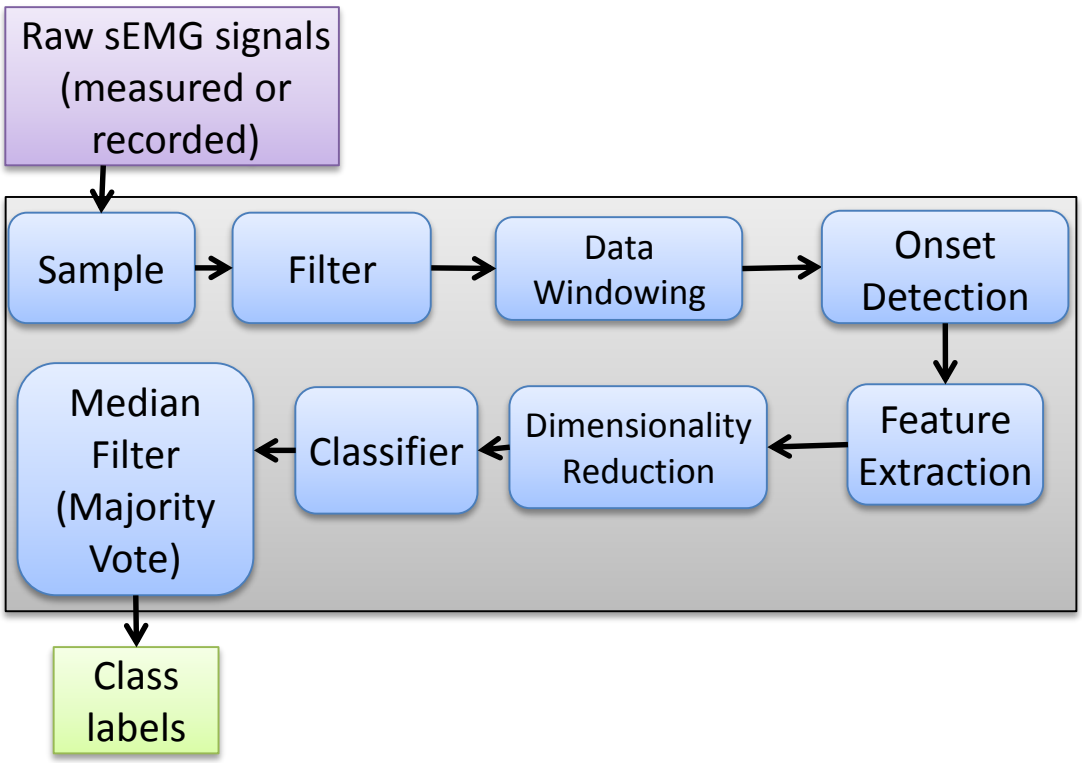

Figure 2.6 - Diagram of pattern recognition system for EMG

When classifying, inputs are always assigned to one of the gesture types: there is usually no 'unknown' gesture type. One way to achieve this is to use a series of classifiers, each trained to recognise a single gesture or 'something else'. If all of the

classifiers produce ‘something else’, then the input the decision could either be made that the input was unknown or ‘suspended’ [51].

Sampling takes the continuous EMG signal and produces a discrete signal that is suitable for processing by a digital system. The sampling of EMG signals is at a rate of 2-3kHz and normally of a resolution of between 8 and 12 bits. EMG is then band-pass filtered before use to remove motion artifacts (below 20Hz) and higher frequencies within which there is little EMG energy (above 500Hz) [26].

2.5.1. Feature extraction

The raw voltages from the EMG electrodes are time sequences of numbers (i.e. samples) which, if fed into a classifier as such, would present a difficult challenge for the classifier [4]. Multiple channels of EMG represent a multi-dimensional space, which exacerbates the problem. Due to the stochastic nature of EMG, it is impossible to exactly repeat a signal voltage pattern [9]. For these reasons, it is common to infer the characteristics of the EMG by extracting mathematical representations of the signals from the concurrent EMG channels over a finite duration (a window). These are called *features*, and several different features are often combined into a *feature set*. The classifier in Figure 2.6 is presented with the features. Figure 2.7 depicts several features being extracted from each channel of the signal (concurrently). The features are concatenated into a single feature vector, along with a class label, for presentation to the classifier.

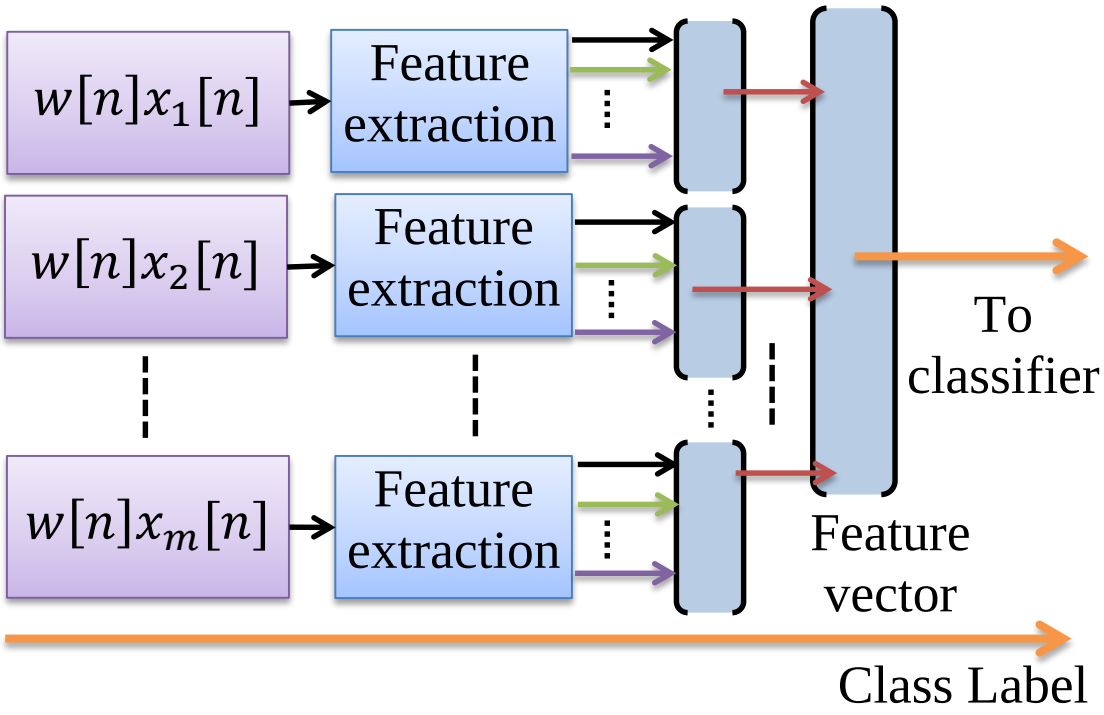

Figure 2.7 - Feature extraction for concurrent window $w[n]$ of *m* channels of EMG signals labelled $x_1[n]$ to $x_m[n]$

In Figure 2.7, the *m* feature vectors are combined into a single feature vector and used with the class label for the supervised learning of the classifier.

2.5.2. Onset and Activity Detection

For any type of myoelectric control, it is common to infer muscle movement by using an onset or activity detection algorithm. This is done by measuring when some property of the signal changes enough to cross a threshold. Feature extraction and classification can then be performed to interpret the myoelectric signal into finger or hand movement commands for the prosthesis.

The simplest EMG activity detection technique is visual inspection of myoelectric signals by a trained expert. This is considered to have poor reproducibility and is affected by the subjectivity of the operator [52]. It is also very time-intensive if a large data set has been recorded.

A distinction is made in this thesis between onset detection and activity detection. Onset detection senses the transition in a signal from 'rest' state to EMG activity. Activity detection identifies and distinguishes between the transitions from rest to EMG activity and then back to rest; as such, EMG activity duration is detected. This

is useful for control because the prosthesis must respond to muscle activity for as long as it continues.

The effectiveness of onset and activity detectors is measured in three ways: overall accuracy, True Positive Rate (TPR) and False Positive Rate (FPR). Overall accuracy is simply a measure of how often the algorithm correctly identifies activity as activity and rest as rest.

Consider a vector the same length (in samples) as an EMG signal, which contains only ones and zeroes. The ones indicate that the algorithm detected activity at that sample in the signal, and zeroes indicate inactivity. True Positive (TP) is a measure of the number of times that activity was correctly identified and is also known as the Probability of Detection. False Negative (FN) is a measure of the number of times that an activity was incorrectly identified as inactivity. The TPR is then defined as:

$$\boldsymbol{TPR = \frac{TP}{TP + FN}} \tag{2.3}$$

The False Positive (FP) is a measure of the number of times that inactivity was incorrectly identified as activity. The true Negative (TN) is a measure of the number of times that inactivity was correctly identified. The FPR is then defined as:

$$FPR = \frac{FP}{FP + TN} \tag{2.4}$$

The FPR can also be called the False Alarm Rate. There are two main types of onset/activity detection: single threshold and double threshold. Single threshold allows FPR to be adjusted and double threshold allows FPR and Probability of Detection to be controlled separately. Examples will be discussed in detail in section 3.2.

A Receiver Operating Characteristic (ROC) curve is a graph of the change in TPR as the FPR is swept between 0 and 1. This is achieved by changing the thresholds between two extremes:

- So high that no activity is detected (0% TPR and 0% FPR) to
- So low that 100% of the signal is detected as activity (100% TPR and 100% FPR).

The behaviour of interest is between these two extremes. ROC curves will be used in Chapter 4 to compare the performance of activity detection methods.

The presence of noise in EMG affects the accuracy of all onset and activity detection methods. In all of the data sets used in this work, it is assumed that the subject has correctly responded to all of the gesture/MVC instructions.

2.5.3. Dimensionality Reduction

Each feature used in the feature set can be thought of as a dimension in a feature space. One of the problems of classification is the *curse of dimensionality* [53], where there is exponential growth in the complexity of the functions needed to describe a feature space as the number of features is increased. The purpose of dimensionality reduction is to condense the most salient discriminatory information from the feature space into fewer dimensions to allow the data to be described by a simpler function, and therefore to improve the classifier's generalisation.

Principal Components Analysis (PCA) identifies the direction (axis) in the feature space that has the highest variance between the feature vectors. This is designated as the first of the new dimensions. A second axis orthogonal to the first is then calculated with second-highest variances. The dimensions with the lower variances can then be ignored, leaving lower-dimensional data that should be easier to classify.

The problem with PCA is that it treats all the feature vectors without taking the individual statistics of the classes into consideration. Individual Principal Components Analysis (iPCA) was applied to the raw EMG signals in [33]. Each feature vector is translated into a separate feature space depending on its class label in an attempt to spatially de-correlate the data before feature extraction. An improvement in classification accuracy was obtained. PCA was also used in [54], where two independent control signals were obtained from the first two significant principal components (which accounted for 90% of the data variance), which were used to perform three prehensile gestures.

2.5.4. Blind Source Separation

The purpose of Blind Source Separation (BSS) is to separate signal sources from signals that contain mixtures of each of the sources. For example, it is possible to isolate the voices of two people speaking simultaneously in a room when provided

with a stereo audio recording. BSS is only capable of separating the sources if there the number of mixtures is greater than or equal to the number of sources. Such a limitation was highlighted in [55], where BSS was used to isolate five 'synchronies' from five EMG recordings made from the hand and forearm. Independent Components Analysis (ICA) has also been tested on EMG where convolved mixtures of the EMG signals at 10% MVC were decomposed into MUAPs [56].

2.5.5. Classification

A classifier has feature vectors as inputs and class labels as outputs. Its class label decisions are based on prior training using labelled feature vectors. When it comes to choosing a classifier, the 'no free lunch' theorem applies. This states that no classifier is inherently superior, but some classifiers are more suitable than others for specific tasks [57].

Another consideration is the 'hot coffee' problem [58]. The classifier might correctly instruct a prosthetic hand to hold a cup of hot coffee 99.9% of the time, but of course dropping hot coffee even once in the real world would be dangerous and unacceptable. This highlights the practical difference between laboratory performance and real-world expectations.

Classification of individual finger movements on amputees using only surface EMG was demonstrated in [59-61], thus showing the rich information that is available in sEMG.

In the case of EMG, it has been shown that Linear Discriminant Analysis (LDA) has been shown to be as effective as several other classifiers that are more complicated to implement [9, 10]. The aim of Linear Discriminant Analysis is to find a linear combination of features to separate one or more classes [57]. Between-class distance is maximised within-class distance is minimised by taking the class means and variances into account. Several types of hyperplanes can be used, including linear and polynomial.

Neural networks are classifiers that take inspiration for their designs from biological brains [9, 53]. Each neuron in the network outputs a level based on the sum of weighted inputs and a bias term. A neural network is a connected network of such neurons. It usually consists of three layers: an input, hidden and output layer of

multiple neurons. It is trained by adjusting the weights and biases to produce a desired output based on training inputs. The performance is then tested by using separate validation data points and the generalisation is tested using cross-validation and a previously untested portion of the data set. The inputs to the input layer are the features and the outputs of the output layer are the class labels. The output layer can be linear, a step threshold or some nonlinear function (e.g. a *tanh* function).

The aim of a Support Vector Machine is to distinguish between two classes by calculating the best possible separating hyperplane in feature space [53]. The feature vectors can be projected into a higher (possibly infinite) dimensional space in order to find a hyperplane that linearly separates the classes. In calculating the hyperplane, support vectors are calculated from the input training data. The support vectors that are closest to the hyperplane are by definition the hardest to classify. SVMs were compared against LDA and neural networks in [62] where they were found to match or exceed their performance (with non-amputee data), and with a low computational load.

To be able to discriminate between more than two classes, it is necessary to use multiple SVMs. This can take the form of 1 versus 1 [53], in which the labelled feature vectors from a class are classified against each of the other class labelled feature vectors. The alternative is 1 versus Rest, the feature vectors of a single class are compared against all the other classes' feature vectors in one go. Each vector is labelled by the classifier as 'belonging to this class' or 'belonging to another class'.

Support Vector Machines can be kernel-based, such as the Radial Basis Function (RBF) kernel, which allows mapping to a higher-dimensional feature space without the need for explicit computation of the data points in the new feature space. Instead, dot products between the feature vectors can be computed in the original space. This greatly reduces the computational burden, and it is called the *kernel trick* [53]. LibSVM [63] is a toolbox that includes a Matlab component. It allows multi-class Support Vector Machine classifiers to be implemented easily.

A Hidden Markov Model (HMM) is a system whose state can only be inferred from outputs of the system. It is completely defined by three parameters:

1. Initial state probability vector π

2. State transition probability matrix **A**
3. State observation probability matrix **B**

The previous states of the HMM have no influence on the future states. HMMs were used in [64] to discriminate six movement classes without the requirement for segmentation of the incoming data and with a lower computational burden than neural networks. In [65], the state of the HMM is used determine the best autoregressive sub-model for reaching movements.

Fuzzy C-Means Clustering is used in [58] on signal mean and standard deviation to achieve a high classification accuracy for three and four separate patterns with amputees and non-amputees respectively.

Kato *et al* developed a continuous online training method [46] where learning data (feature vectors) for the classifier were automatically added or removed through Automatic Addition, Automatic Elimination and Selective Addition. These processes depend on the 'strength' of the gesture decision and the nearby decisions in the class label stream. The paper concludes that the system did not perform as well on data from an amputee.

In this thesis, LDA, SVMs and NNs are used for comparison against activity detection methods. In Chapter 4, SVMs are used for contaminant identification in Chapter 5 and SVMs are used for gesture classification in Chapter 6. Each choice is justified in the respective chapters.

2.5.5.1. Post-processing

When a classifier is well trained and generalised, misclassifications can still occur. These can take the form of spurious class labels within a larger stream of homogenous class labels, especially when a transition between gestures (or between rest and gesture) occur. The isolated labels are unlikely to represent an intention on the part of the limb user to change gesture for the duration of a single window/overlap period: It is more likely a misclassification has occurred. To address this, a majority vote mechanism is often used [43]. Class labels are not considered in isolation. Instead, a group of class labels are considered from the stream at the same time, and the class label that occurs the most within the group is

declared as the most likely label for a given time slot. This helps to address the 'hot coffee problem', but it does introduce controller delay [66].

A velocity ramp was used in [66] to mitigate the effects of misclassifications. The rate of movement of the limb ramps up from zero while a gesture is performed and held by the user, but there is a trade-off between improvement in controllability and the responsiveness.

A maximum likelihood post-processor is used in [67]. The mean global muscle activity levels are used alongside LDA gesture classifications. Better performance than velocity ramp and majority vote were observed, though their method was only tested with offline data.

2.5.6. Mathematical Tools

2.5.6.1. Short Time Fourier Transform (STFT)

The spectrum of a signal provides detailed frequency information, but the times of the occurrences of the frequencies are lost. For example, a high-pitched sound could be present at the start of a recording and low-pitched sound at the end, but the spectrum indicates only the presence of high frequency and low frequency content. To address this, the Short Time Fourier Transform (STFT) of a signal takes the Discrete Fourier Transform (DFT) of windows of the signal at regular intervals across it [68]. This leads to a trade-off: There can be high frequency resolution or high time resolution, but not both at the same time. This can be assuaged by using overlapping STFT windows, where the spectrum at the overlaps is averaged. The STFT of the noisy signal can be thought of as the STFT of the signal plus the STFT of the noise:

$$X(k,l) = S(k,l) + D(k,l) \tag{2.5}$$

X is signal plus noise, S is STFT of signal, D is STFT of noise for frequency bin k and time frame l. STFT is used in spectral subtraction, Minimum Statistics and IMCRA, which are discussed in Chapter 6.

2.5.6.2. Empirical Mode Decomposition (EMD)

Empirical Mode Decomposition (EMD), which is also called the Hilbert-Huang Transform [69], is a non-linearly breaks down a signal into orthogonal functions that are based on the properties of the signal itself rather than of some basis function,

such as those used in wavelet analysis. The orthogonal functions that are generated by the process are called Intrinsic Mode Functions (IMFs), which are generated as follows [69]:

1. Calculate extrema of the signal
2. Form the upper and lower envelopes of the signal
3. Compute the mean between the upper and lower envelopes across the signal
4. Extract the detail signal
5. Determine whether the Zero Mean stopping criteria is met. If not, go back to 1. If so, go to 6
6. Assign the detail signal as an IMF
7. Assign whatever is left as the residual
8. Determine whether the number of zero crossings is less than two

The EMD can be expressed as the sum of its *N* IMFs and the residual, as shown in (2.6).

$$x[n] = \sum_{j=1}^{N} IMF_j[n] + r[n] \tag{2.6}$$

$IMF_j[n]$ is the *n*th IMF.

The IMFs, considered together, have behaviour similar to a filter bank [70]. Higher frequencies tend to be present in the lower-numbered IMFs, and lower frequencies tend to be present in the high-numbered IMFs.

The way the IMFs are used to reconstruct the signal determines the type of noise reduction that is to be performed. *Detrending* is the removal of IMFs with greater low-frequency content. *Denoising* is the removal of IMFs with higher frequency content [71].

2.5.6.3. IMFs as features

The means and variances of IMFs have been used as features for pattern recognition-based control [49]. Several properties can be extracted as features from the IMFs:

- Energy
- Singular Value Decomposition (SVD) coefficients
- Standard Deviation
- Variance

Each of these feature types were tested as a feature set. For all of them, no particular advantage was found when used in place of the Hudgins time domain feature set, which will be discussed in section 3.3. In [72], time domain features were taken of

the EMG data as well as of the IMFs. An improvement in classification accuracy was shown.

2.6. Noise types in EMG

EMG usually contains several distinct types of noise [73], which obscures the useful information in the EMG. Noise types include:

- Motion artifact from cable movement and the movement of sensors relative to the skin
- ECG, in particular when TMR is used
- Additive White Gaussian Noise (AWGN) from the electronic components and measurement noise
- Amplifier Saturation, quantisation noise and clipping when the measuring apparatus has been improperly configured or if the conditions change (e.g. sensor slippage)
- Power Line interference, which is 50Hz in most countries and 60Hz in North America
- Baseline wander

As discussed in section 2.3.1, a little EMG activity is still present when the subject is relaxed, which maintains muscle tone. The only other energy content at rest is noise. When muscles are active, the energy content in the sEMG signal that is not caused by motor unit activity is considered to be noise.

2.6.1. Types of noise in surface myoelectric signals

Several types of contaminant can be commonly found in EMG signals. Figure 2.8 (top) shows a recording of clean, real, steady state EMG from Data Set 3 and its power spectral density (bottom).

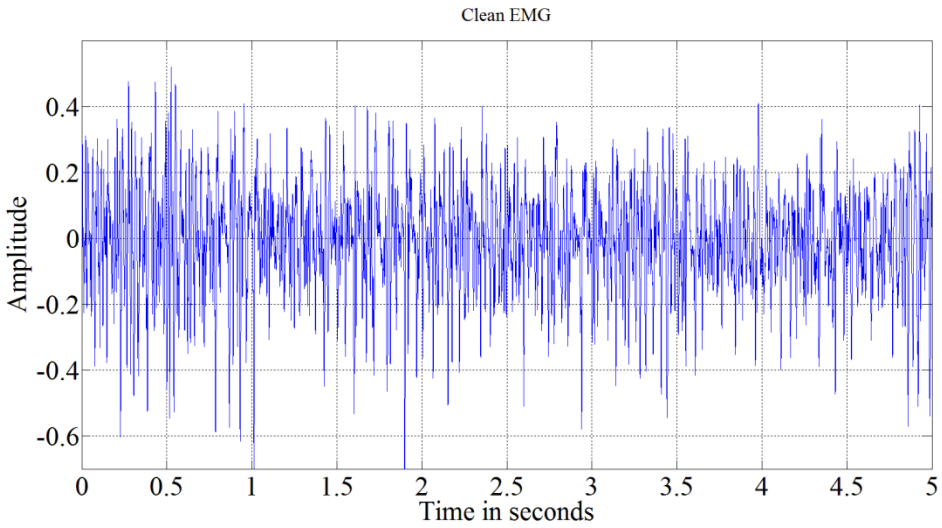

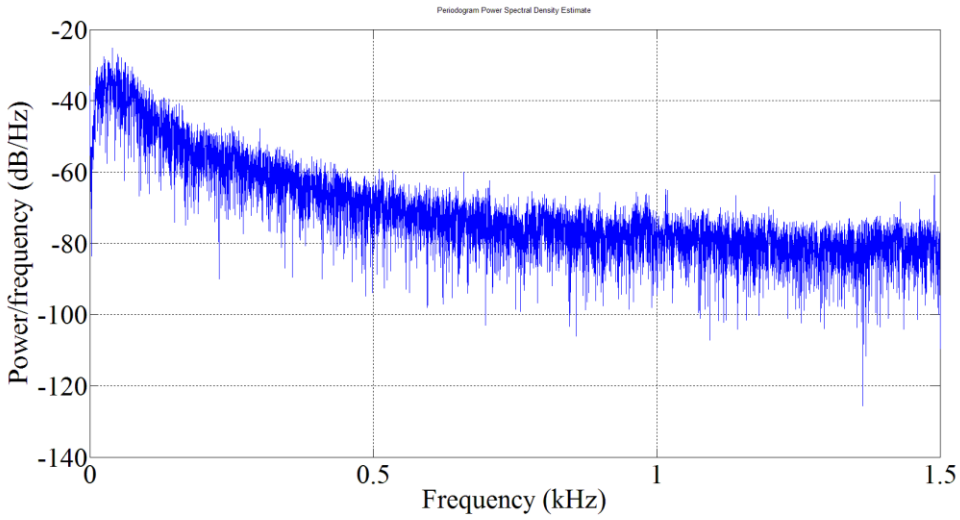

Figure 2.8 - Clean real steady state EMG from Data Set 3 (top) and PSD (bottom)

In the following sections, several types of noise will be added to the example shown in Figure 2.8 by way of demonstration. Methods of simulating or adding the noise to EMG will also be explained.

2.6.1.1. Motion Artifact

Motion artifact noise is caused by the movement of the sensor relative to the skin [74] and by cable movement relative to the sensor. The frequency band within which motion artifacts reside is 0-20Hz [26]. The example steady state EMG shown in Figure 2.8 is artificially contaminated with motion artifact at 0dB SNR and is shown in Figure 2.9.

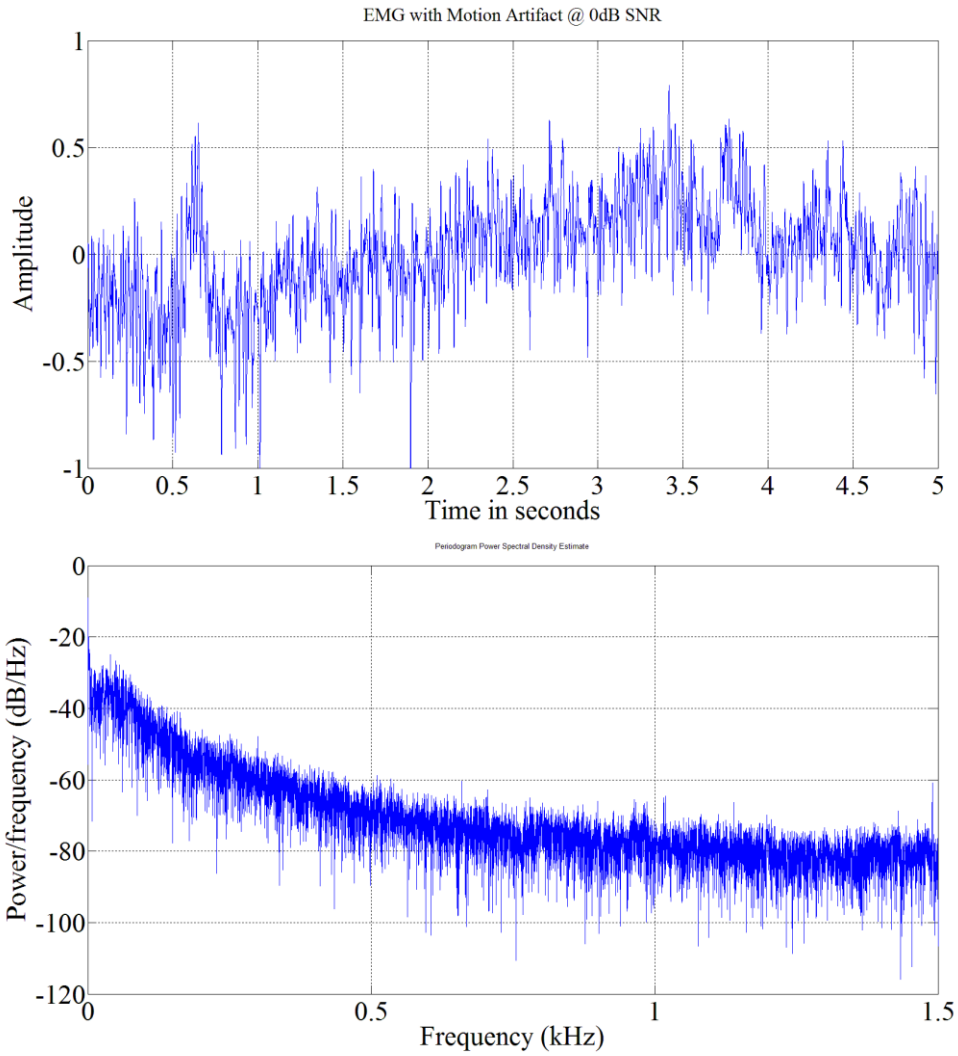

Figure 2.9 - Steady-state EMG contaminated with Motion Artifact at 0dB SNR (top) and PSD (bottom)

Motion artifact is eliminated, in accordance with SENIAM guidelines, by using a high pass filter on the EMG. This also removes any EMG information in the spectrum below 20Hz, which is assumed to have a "fairly linear" distribution between 0-20Hz in clean EMG [75].

In this work, recordings of motion artifacts that were recorded for [44, 76] were used. The recordings were made by measuring inactive parts of the body under ambulatory conditions. The recordings were resampled and added to the EMG at the required SNRs.

2.6.1.2. ECG

The electrocardiogram is the electrical signal from the muscles of the heart during beating [77]. It has a distinct and regular shape and consists mainly of low frequency

components. For EMG measurement purposes, ECG can be problematic when measuring on or near the torso, such as when TMR is used [78]. The example EMG recording has been artificially contaminated with ECG at 0dB SNR in Figure 2.10.

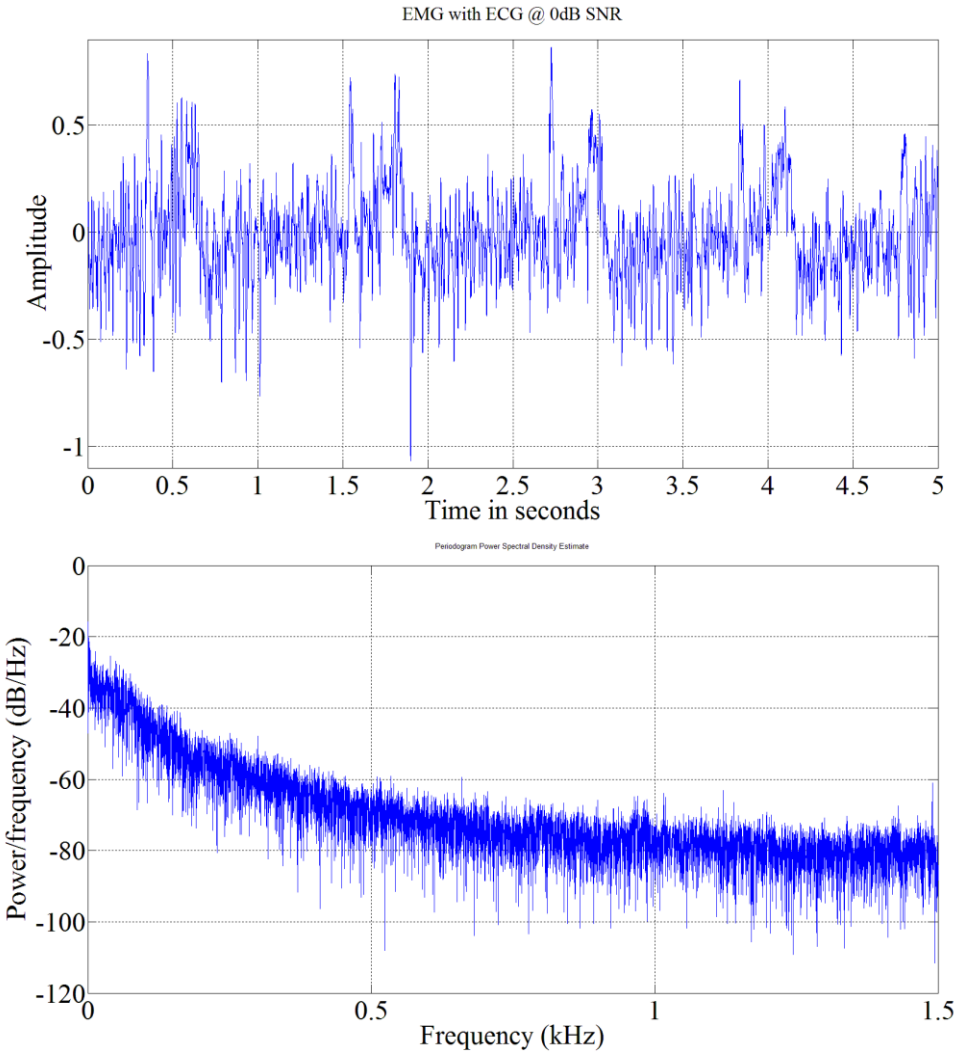

Figure 2.10 - Steady-state EMG contaminated with ECG at 0dB SNR (top) and PSD (bottom)

For ECG interference, recordings of real ECG from one subject were used as a source of contamination, following the procedure described in [5, 44]. To contaminate signals, an ECG vector was chosen randomly from four recordings, and multiplied by amplitude scaling to produce the required SNR. The ECG recording was resampled, repeated and truncated as necessary to match the sample rate and length of the EMG recordings.

2.6.1.3. Additive White Gaussian Noise

AWGN occurs across the frequency range. It can be the result of noise from the electronic components or from measurement noise. It is common to add AWGN to signals to test noise reduction techniques. In the case of EMG, AWGN has been used to test the noise reduction performance of wavelets [79] [80]. The sample EMG recording, artificially contaminated with AWGN at 0dB SNR, is shown in Figure 2.11.

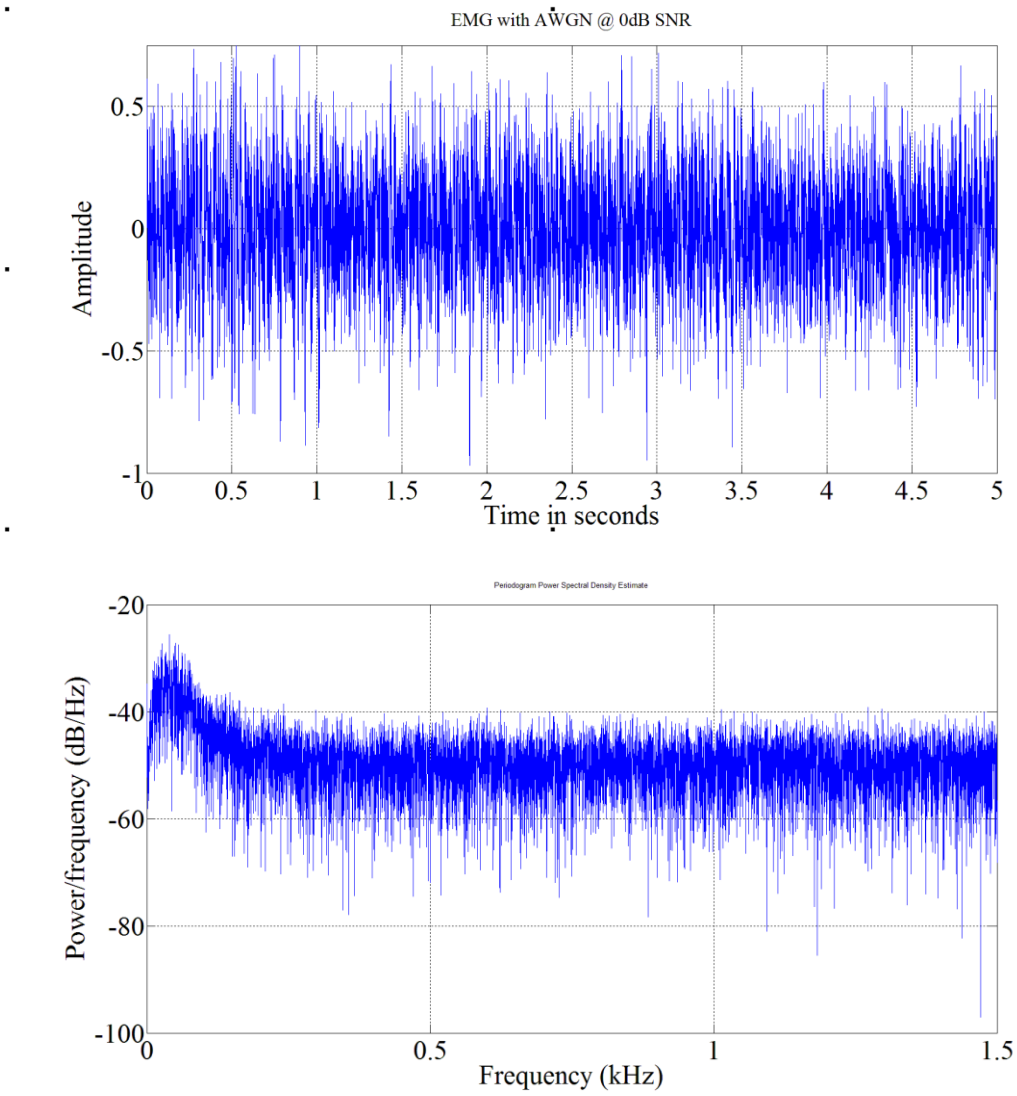

Figure 2.11 - Steady-state EMG contaminated with AWGN at 0dB SNR (top) and PSD (bottom)

To add AWGN artificially, it is simply generated in Matlab with a flat power spectrum and added at the required SNR to the EMG signal.

2.6.1.4. Amplifier saturation

Amplifier saturation occurs when the amplifier starts to operate outside of its linear zone. The result is that the higher EMG values are attenuated in a nonlinear manner towards the maximum saturation level. Amplifier saturation can be simulated using (2.7) [73]. SNR is set by calculating the distortion with reference to a signal that is linearly amplified to the same gain:

$$x[n] = Amp_{max}\left(\frac{2}{1 + e^{\frac{-2G}{Amp_{max}}}} - 1\right) \quad \textbf{(2.7)}$$

The nonlinear range of the signal is defined by the following criterion:

$$\frac{|s[n]|G}{Amp_{max}} > 0.4 \quad \textbf{(2.8)}$$

Amp_{max} = 10V. G is the artificial amplifier gain. The same nonlinear range of operation was used as in [73]; that is, (2.8) had to be satisfied for a sample to be considered in the nonlinear range of the amplifier. The example EMG recording, artificially subjected to amplifier saturation, is shown in Figure 2.12.

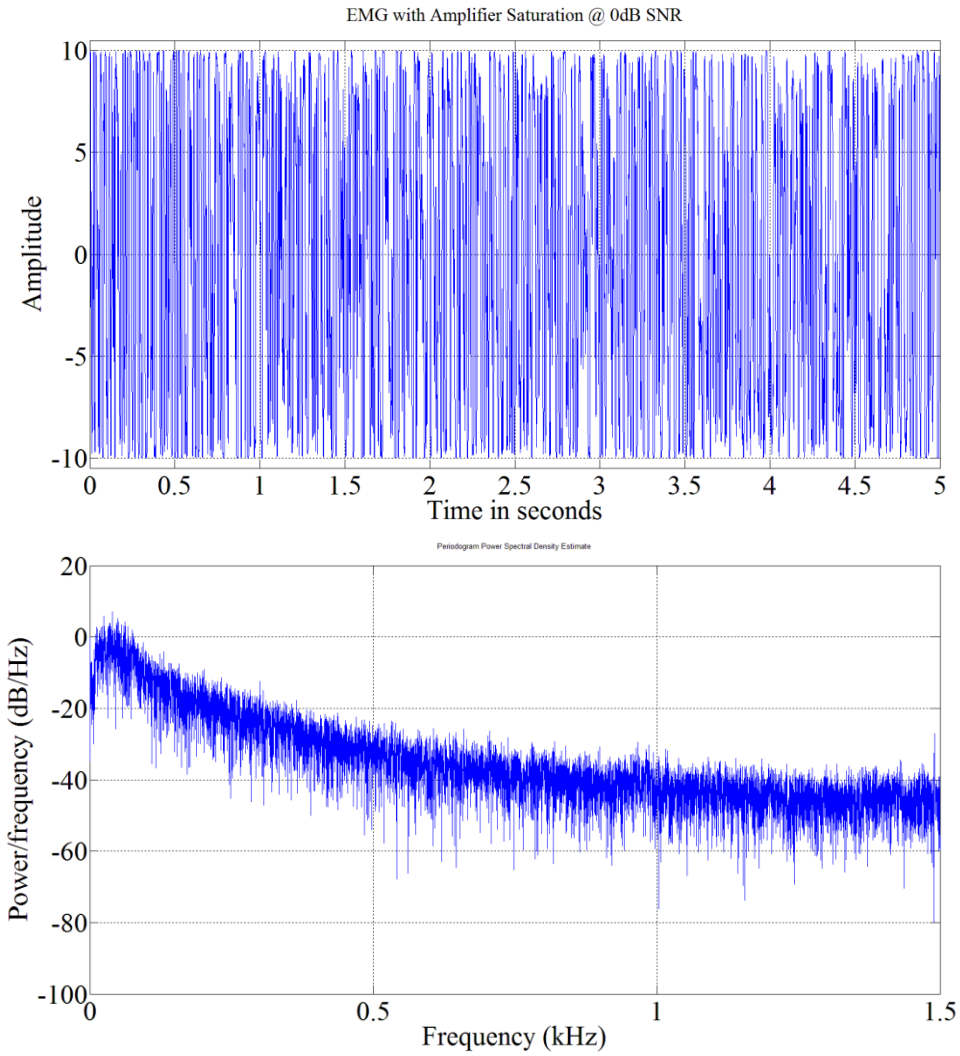

Figure 2.12 - Steady-state EMG processed with amplifier saturation at 0dB SNR (top) and its PSD (bottom)

2.6.1.5. Power line interference

Power line interference is ubiquitous in electronic equipment. It is either 50Hz or 60Hz, depending on the country, and happens to occur in the peak frequency range within which EMG can be found. This means that filtering it using a notch filter also removes a lot of EMG power. An example of steady state EMG that has been artificially contaminated with power line interference at 60Hz at 0dB SNR is shown in Figure 2.13.

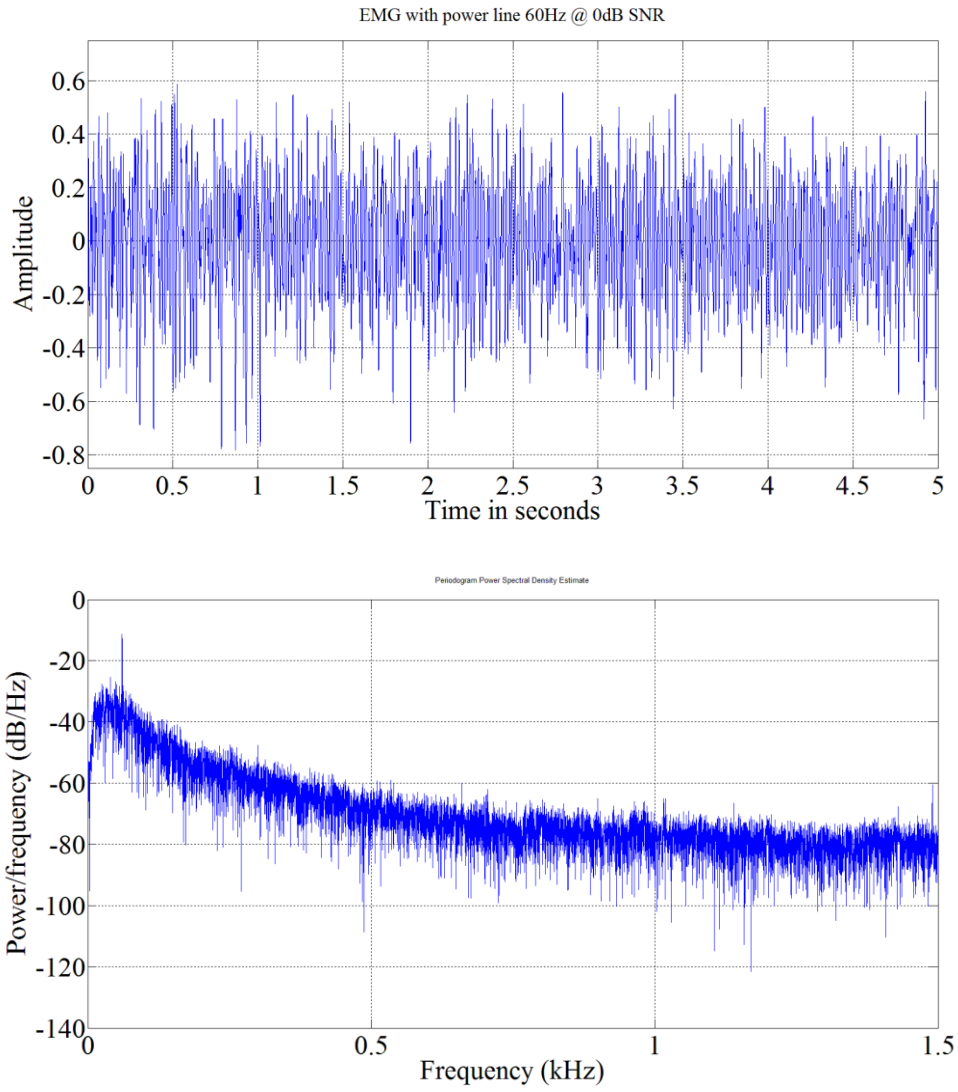

Figure 2.13 - Steady-state EMG contaminated with power line interference at 0dB SNR

In this work, a sine wave with a random phase (without harmonics) was added to the signals to the required SNR level to simulate power line interference. Its frequency was set randomly between 59.5 Hz and 60.5 Hz (in 0.25 Hz increments).

2.7. Conclusion

In this chapter, an introduction to myoelectric control was given. Myoelectric signals were described along with the issues relating to the measurement of EMG for control of forearm prostheses. Pattern Recognition for EMG-based control was described, which will be used in later chapters. Finally, the noise types commonly found in EMG were discussed. The presence of any of these noise types in EMG

would degrade gesture classification accuracy when Pattern Recognition is performed, and render the EMG less useful for telehealth. In the next chapter, tools to address the issues of activity detection, noise identification and noise reduction will be examined.

3 Digital Signal Processing for Myoelectric Signals

3.1. Introduction

In this chapter, an overview of DSP as applied to myoelectric signals is given, with a particular focus on pattern recognition and the tools that will be used in the subsequent chapters. Onset and activity detection techniques are introduced and discussed, and then the feature types that are commonly used with myoelectric signals are described. Several objective measures of EMG signal quality will be explained. Finally, Spectral Enhancement and One-Dimensional Local Binary Patterns are introduced.

For more information, thorough coverage of myoelectric control is given in [25], and a survey of myoelectric control papers up until 2007 is given in [4]. Since 2007, EMG noise detection has been developed [44], sensory feedback has been successfully tested [20] (though with the need for surgery), novel features such as wavelets have been tested [81] and wavelets have also been used for de-noising (discussed in this chapter). The first iLimb (by Touch EMAS) came out in 2007, and its hardware and software has been steadily refined in a series of new models since then.

3.2. Onset and Activity Detection

Onset detection is crucial for DSP, whether it be musical note detection [82], Voice Activity Detection [83] or earthquake onset detection [84]. The methods shown in Table 3.1 have been used with myoelectric signals.

Technique	Reference(s)	Threshold type	Mechanism and Comments
SD + RMS	[58]	Single	Absolute value of the signal must be greater than standard deviation plus several times RMS. Sensitive to noise
Mean Value Comparison	[85]	Single	MAV of signal must be greater than a threshold. Sensitive to noise
Energy	[9]	Single	Energy content of window of signal must be greater than a threshold **or** difference in energy content between windows must be greater than a threshold. Sensitive to noise
Sliding Window Average	[85]	Single	Phase shift in frequency domain Group delay in time domain 50-150ms response
Marple-Horvat Gilbey	[85, 86]	Single	Maximum difference in mean values of signal between windows Sensitive to noise and motion artifact
Difference of Magnitude	[87]	Single	Difference in magnitude of signal envelope between two time slots Slow to respond
Surf	[87]	Single	Slope of signal envelope Extra computational time needed Slow to respond
Fractional Power Envelope	[87]	Single	Convolution of fractional power of the signal envelope with an LTI filter then threshold the convolved result
High Frequency Content	[87, 88]	Single	Detect increase in HF content at onsets Detects onsets only
Maximum Value Detection	[85]	Double	Count peaks in a window of the signal. Segment length is based on electrode distance and tissue conduction speed
Bonato	[39]	Double	Count number of times that a threshold is exceeded in a window Designed for gait analysis
Trained Classifier	[89]	N/A	Train a classifier to recognise between activity and rest Requires classifier training

Table 3.1 – Onset and Activity Detection methods that have been used with myoelectric signals

The techniques listed in Table 3.1 will now be discussed in more detail.

3.2.1. Single threshold techniques

One of the simplest onset detection methods, although sensitive to noise, is to measure when the absolute value of the signal is greater than the Root Mean Square plus several standard deviations of a quiescent period of the signal [58]. Mean Value Comparison [85] compares the mean of absolute value of windows of the signal to a threshold. Activity is declared for a window if the threshold is exceeded.

The energy of the signal can be used to detect onset and activity. In the Short Term Energy, either the absolute value of the energy in a window must be above a threshold, or the difference in energy between two adjacent windows of the signal must be above a threshold for onset to be declared [9]. This is also simple to implement and can be effective but is sensitive to noise.

In the sliding window average [85], the Mean Absolute Value (MAV) of the signal within a window is calculated. Onset is declared at a sample if the MAV goes above a threshold. The Marple-Horvat and Gilbey algorithm [85, 86] detects EMG activity: two adjacent windows are used and the MAV is calculated within each. If the difference of values exceeds or goes below a positive or negative threshold, onset or offset is declared respectively.

Many single-channel onset detection methods are based on the properties of the signal envelope. The simplest of these is Difference of Magnitude, which uses the difference in maximum envelope magnitudes between signal windows [87]. The Surf Method detects onset based on the slope of the envelope [87] and is more resilient to noise. Fractional Power Envelope [87] also considers the background noise. However, as stated in [39], the results for envelope methods depend strongly on the choice of envelope detection technique and threshold. In addition, the response time of envelope methods can be high [39].

High frequency content [87, 88] is based on the observation that the high frequency content of myoelectric signals is higher during onset. It detects onsets only but is said to be sensitive to background noise.

3.2.2. Double Threshold

Double threshold activity detection allows probability to be controlled, in addition to FPR. This is usually achieved by specifying that a first threshold must be exceeded by a specified number of times (the second threshold) within a window. In Maximum Value Detection (MVD) [85], the peaks in a window of the signal are counted and onset is declared if the number of peaks exceeds a threshold. Movement can also be detected by measuring the joints of the forearm using sensors such as accelerometers or goniometers. This is more suitable if measuring sEMG from an intact forearm or if there are useable joints on the residual limb of an amputee. Such information can be used to assist the classifier through sensor fusion [90].

The widely-cited technique introduced by Bonato [4] is a double-threshold onset detection technique designed for gait analysis using surface EMG [39]. An active and a quiescent period are identified so that the characteristics of the detector can be calculated. The signal is first whitened (see section 3.4 for details of whitening), and then the sum of squares of consecutive odd and even samples is calculated and used as an auxiliary time series. Onset is declared if this goes above a threshold for a specified number of consecutive times within a window. In this way, the TPR and FPR (as discussed in section 2.5.2) can be separately controlled, but there is a processing overhead when the signal is whitened. Bonato's method includes a postprocessor to remove events of duration ≤30ms. The steps are as follows [39]:

1. Select length of observation window – longer observation windows are preferable, but this impairs the reaction time of the detector
2. Select second threshold – the second threshold is the number of times that the first threshold must be exceeded within a window before onset is declared
3. Feasibility of the detector - It must be determined whether the desired P_d and P_{fa} are feasible with the parameters chosen in the previous steps. This can be done by referring to the ROC curves in [39].
4. Selection of first threshold – this is chosen to obtain the desired detection rate

3.2.3. Trained Classifier

Another approach to activity detection is to train a classifier to recognise 'no motion' as a class in the pattern recognition process [89]. If used in a real-time scenario, the classifier is then continuously active and producing class labels, once trained. A disadvantage is the need for training of the classifier, which requires a training data set.

3.3. Features

Englehart *et al* demonstrated that the choice of feature set is more important than the choice of classifier [10]. It was also shown that time domain features give the best results for myoelectric pattern recognition. The Hudgins Time Domain feature set is a commonly used standard in the field of myoelectric research against which other features are tested. It consists of five features (taken from [9]):

Mean of Absolute Value	The mean value of the absolute of the signal	$\overline{X}_i = \frac{1}{N}\sum_{k=0}^{N}\lvert x[k]\rvert$ for i=1,…,I
Zero Crossings	Number of times that the signal crosses the time axis. A threshold can be set to compensate for noise	$ZC = \sum_{n=0}^{L} f(x)$ where $f(x) = \begin{cases} 1 \; if \; (x[k] > 0 \; AND \; x[k+1] < 0) \\ OR \; (x[k] < 0 \; AND \; x[k+1] > 0) \\ 0 \; otherwise \end{cases}$
Waveform Length	Sum of Absolute Differences between samples	$WL = \sum_{k=1}^{L-1}(\lvert\Delta x[k]\rvert)$
Slope Sign Change	Number of times that the slope of the signal changes	$f(x) = \begin{cases} 1 \; if (x_k < x_{k+1} \; AND \; x_k < x_{k-1} \\ OR (x_k > x_{k+1} \; AND \; x_k > x_{k-1} \\ 0 \; otherwise \end{cases}$
Mean of Absolute Value Slope	Number of times that the slope of the Mean of Absolute Value changes	$\Delta\overline{X}_i = \overline{X}_{i+1} - \overline{X}_i$ for i = 1,…,I-1

Table 3.2 – Hudgins Time Domain features taken from [9]

Table 3.3 shows other features that have been used with EMG signals.

Name	Reference	Comment
Autoregressive	[91]	Prior values of the EMG in a signal can be used to predict future values with autoregressive prediction
Cepstrum	[4]	Rate of change in the bands of the spectrum
Constraint Sample Entropy	[92]	Constrained measure of entropy of the EMG
EMG Histogram	[91]	Measures "the frequency at which the EMG signal reaches multiple amplitude levels"
Energy	[4]	Sum of squares of absolute values of all the samples in a window of the signal
Kurtosis	[38]	Third moment of the PSD of the EMG
Sample Entropy	[93]	Measure of entropy of the EMG
Skew	[38]	Fourth moment of the PSD of the EMG
Wavelet coefficients	[94]	Properties of wavelet coefficients are used as features
Willison Amplitude	[95]	Number of times that the difference between successive samples of the EMG cross a threshold

Table 3.3 – Other features used with EMG

For *autoregressive* coefficients, prior values of the EMG in a signal can be used to predict future values with autoregressive prediction [96]. A multi-tap filter is created to try to predict the next sample, and the coefficient values of the taps are calculated using a least squares approach. These coefficients can be used as features. The order of AR ranges from 3, 4 in [50] [43, 91] to 6 in [49] and 11 in [97]. The order must be large enough to take noise into account [91].

Hudgins' feature set has been used as a reference throughout the literature. Therefore, in this thesis, gesture classification using pattern recognition will be obtained using this feature set.

3.4. Whitening

Whitening is performed on EMG to improve signal amplitude estimation. The EMG is assumed to be the output of a linear filter that has white noise as an input, so inverting the filter produces the original white noise [98]. In [98], the whitening improved amplitude estimation, but calibration difficulties arose. In [99], an adaptive whitening filter is introduced that improves MVC estimation at levels below 10%, where whitening normally does not help because of the overwhelming measurement noise.

3.5. EMG signal quality measurements

In [44] four steps were identified for dealing with noise in EMG signals:
Detection - The fact that noise exists in the signal can be established without necessarily knowing what it is. That it can be detected at all might mean that it is strong enough to render EMG readings unusable.

Identification allows the type(s) of contaminant to be distinguished. This helps in deciding whether steps should be taken to either discard the data or mitigate the noise.

Quantification can allow a decision on whether the noise is of a level that will cause problems for the intended use of the data.

Mitigation might be, for example, to not use contaminated channels, which is an option with high density EMG recording. The type of mitigation depends on whether the data is real-time or recorded. Depending on the type of contamination, mitigation can be straightforward. For example, high pass filtering can reduce or eliminate motion artifact noise, though this is at the expense of any EMG that was present in the lowest frequency bands (usually below 20Hz).

Not all of these steps need be applied all the time. For example, detection of noise can be sufficient to justify discarding an EMG recording.

Objective measurements of EMG quality can be used to help decide whether to discard EMG or process it to improve the SNR. Some of them detect the presence of noise, while others provide information about the identity and quantity of the noise.

Signal to Noise Ratio (SNR) - The signal to noise ratio is simply a measure of the ratio of the signal power (i.e. power during a gesture) to the noise power.

$$SNR = 10log_{10}\left(\frac{P_{EMG}}{P_{noise}}\right) \quad \textbf{(3.1)}$$

This assumes a high SNR. If not, then the assumption that the noise is negligible during a gesture may not be valid, so the noise power might need to be subtracted from the EMG power thus:

$$SNR = 10log_{10}\left(\frac{P_{EMG} - P_{noise}}{P_{noise}}\right) \quad \textbf{(3.2)}$$

Equation (3.2), of course, assumes that the location at which EMG and noise start and end in the signal are known.

Signal to ECG Ratio (SER) - For Signal to ECG Ratio (SER), the ECG is estimated by computing a moving average of the recorded EMG. In [77], ECG interference was mitigated by estimating the ECG using a combination of a 10ms and 50ms moving average of the recorded EMG. The 10ms moving average was used during QRS complexes because of their high frequency components, and the 50ms moving average was used everywhere else, because it suppresses the EMG more in the ECG estimate. Switching between the two moving averages was based upon QRS detection. In the work presented in Chapter 5, a 20ms moving average filter is used to obtain the ECG estimate, which is a compromise between suppressing the EMG and over-smoothing the QRS complexes. The use of a single moving average eliminates the need for QRS detection, which would be difficult or impossible when the level of ECG contamination is low. The ECG moving average estimate is computed as:

$$\hat{s}_{ECG}[n] = \frac{\sum_{n-m}^{n+m} r[n]}{1+2m} \text{ where } m = \left\lceil \frac{f_s}{100} \right\rceil \quad \textbf{(3.3)}$$

$r[n]$ is the recorded EMG signal and $\hat{s}_{ECG}[n]$ is the estimated ECG signal, which is subtracted from the recorded EMG. The signal power is then estimated from the resulting signal. The SER is the ratio of the estimate of the EMG signal power and is defined as

$$SER = 10log_{10}\left(\frac{P_{EMG}}{\hat{P}_{ECG}}\right) \quad \textbf{(3.4)}$$

where $\hat{P}_{EMG}$ is the estimated EMG power, and the estimated ECG power is $\hat{P}_{ECG}$ [77]:

Signal to Power Line Ratio (SPR) - The Signal to Power line Ratio (SPR) is a measure of the ratio of the estimated EMG power to estimated power line power [100] in a signal. The power line noise is estimated using an iterative steepest descent, least squares method described in [100]. The amplitude (*A*), phase and frequency of the power line interference are estimated. The power of the power line interference is computed using the amplitude estimate:

$$P_{powerline} = \frac{A^2}{2} \quad (3.5)$$

SPR is expressed in Decibels.

SN Ratio - The SN Ratio is a type of SNR that takes the shape of the EMG spectrum in the high frequency range into account in its calculation [75]. It is based on the assumption that there is no EMG activity in the upper 20% of the frequency range. This makes it liable to give falsely high values if ECG or motion artifact noise are present in the signal because the frequency content is then distorted, which causes falsely high SN Ratios.

DP Ratio - The DP Ratio is a measure of the ratio to "the higher mean power density of the spectrum to the lowest mean power density" [75] of thirteen points between 35 and 600Hz. Its purpose is to determine whether "the power spectrum is adequately peaked in the frequency range" where EMG is present.

Ω Ratio - The Ω Ratio is an "index of spectral deformation" [75].

$$\Omega = \frac{(M_1/M_2)^{1/2}}{(M_1/M_0)} \quad (3.6)$$

where M_0 is , M_1 is and M_2 are spectral moments calculated using this equation from [75]:

$$M_n = \sum_{i=0}^{i_{max}} power\ density_i \,.\, f_n^i \quad (3.7)$$

Moments are therefore weighting functions for the power spectrum. The Ω Ratio is sensitive to changes in the symmetry and peaking of the power spectrum and additive disturbances in the high frequency and low frequency regions [75].

Signal to Motion Artifact Ratio (SMR) - The SMR is a measure of the ratio of power estimate of the signal to a power estimate of the motion artifact content of the signal [75]. It was designed with respiratory motion artifacts in mind, but it is also useful for cable motion artifacts. There are two assumptions made when SMR is calculated [75]: that motion artifacts occur below 20Hz and that power distribution of the spectrum of uncontaminated EMG is "fairly linear" between 0 and 20Hz.

Anything that deviates from the straight line is assumed to be energy caused by motion artifact. The 'highest mean power density' is also calculated: the mean power density of thirteen consecutive points is calculated in a window that is slid between 35 and 600Hz, and the highest of these means is taken. The SMR is the ratio of this highest mean to the motion artifact power.

Classification Accuracy - The presence of noise in EMG signals affects the classification accuracy of any pattern recognition systems that have been trained to recognise gesture by using features derived from noisy data. It is therefore asserted in this thesis that, other parameters being equal, the change in classification accuracy can be used as a measure of the effectiveness of noise reduction algorithms. If a noise reduction method is effective, then a classifier trained and tested with the processed data should have a higher classification accuracy compared with a classifier that was trained and tested with features extracted from the original, unprocessed data.

Correlation Coefficient Test for Normality (CCN) - The Pearson Correlation Coefficient Test for Normality was originally developed to identify amplifier saturation. It is a measure of how closely the distribution of a histogram matches a Gaussian distribution. In [73],the CCN was measured between a 10-bin histogram of the recorded EMG amplitude distribution and a normal probability density function (PDF) with equal mean and variance [101]. Contaminant-free EMG has a high CCN, whereas the CCN value decreases as the level of contamination increases [73, 101].

CCN was demonstrated to be also applicable to power line interference, ECG interference and motion artifact in [73]. The correlation coefficient decreased with decreasing signal-to-noise ratio (SNR) for all contaminants. However, it was noted that the rate of decrease differed between contaminant types. This permitted contaminant detection and the potential for quantification.

Single-class SVMs - Single-class SVMs were used in [44] to detect the presence of contamination in steady-state real and simulated EMG. A single contaminant was added artificially to the clean EMG recordings/simulations at SNRs between -20dB and +20dB in increments of 5dB.The contaminated data then was split into training and test data at each SNR. This was performed for all of the contaminants: power

line interference, ECG interference, motion artifact, quantisation noise, clipping and amplifier saturation. It states in [44] that it was possible to detect contamination using trained single-class SVMs, and that the effectiveness varied depended on the contaminant and the SNR.

3.5.1. Noise Reduction in myoelectric signals

In this section, recent EMG noise reduction research is described and discussed.

LTI Filtering - It is common to use Linear Time Invariant (LTI) filters to filter EMG signals. In accordance with SENIAM guidelines [28-30], a simple band pass filter is normally applied to surface myoelectric signals to restrict the frequency range to that in which most of the energy of sEMG signals can usually be found.

Low-pass filtering is performed to remove frequency bands in which there is little, if any, EMG activity. High-pass filtering is performed to remove motion artifact and ECG interference. Band pass filtering removes some of the sEMG signal.

EMD-Based De-noising - The application of EMD to EMG signals was first discussed in [102], where its potential utility was compared with FFT. The first three IMFs were summed in [65] , purportedly to reduce noise, though the mechanism by which noise reduction was to be achieved is not explained in the paper. The same kind of thresholding as applied to wavelet Detail signals is performed on the IMFs [103, 104].

EMD-based Filtering (EMDF) was developed to remove low-frequency noise from speech signals [105]. It works by examining the variances of the IMFs and comparing with the IMF variances that could be expected for clean signals. Specifically, there should be a single ‘peak’ in the variance graph, as shown in Figure 3.1 (left).

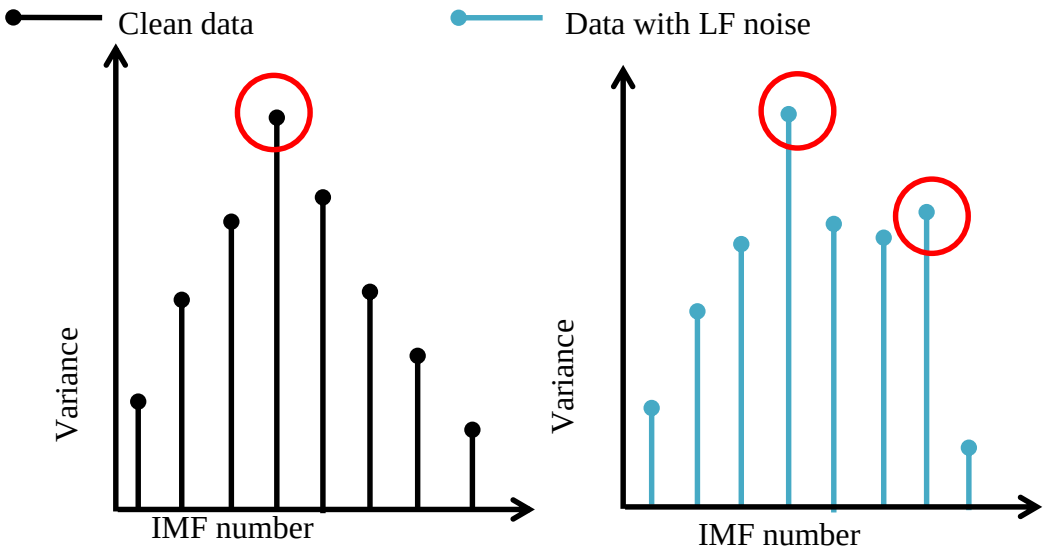

Figure 3.1 – Illustration of a comparison between the variances of IMFs of clean data (left) and data contaminated (right) with Low Frequency noise.

In Figure 3.1, the 'peaks' are circled. Note the extra 'peak' in the variances for the contaminated data. An extra 'peak' is present in the variances of the IMFs in Figure 3.1 (right). This is caused by low-frequency noise, which increases the energy content of the higher-numbered IMFs due to the filter bank-like behaviour [70]. Now that the IMFs with the noise content have been identified, they can be filtered. The sum of the filtered IMFs should result in a cleaner signal.

When LTI high-pass filtering is performed on EMG, 5-10% of the signal energy is lost [25]. It was hoped that EMD could be applied to the EMG to remove the low-frequency noise while keeping the low-frequency components of the EMG relatively intact. This should lead to an improvement in classification accuracy due to the retained information. This will be discussed in section 6.7.

Wavelet Analysis and de-noising - Wavelet and Wavelet Packet analysis are methods of signal decomposition, and are normally used for image analysis and compression (e.g. JPEG2000). In wavelet analysis, the signal is decomposed into Approximation and Detail components. Each Approximation is then further decomposed to produce a decomposition tree. Unlike STFT, which has a fixed time-frequency 'tiling', the time-frequency scaling can be adjusted as necessary by changing the wavelet type and depth [4]. For example, smaller 'tiles' can be used in the higher frequency range to extract more detail. This has led to wavelet analysis

being described as a 'mathematical microscope' [106]. In Wavelet Packet analysis, both Approximation and Detail components are further decomposed. Figure 3.2 shows a wavelet decomposition into three Approximation and three Detail signals.

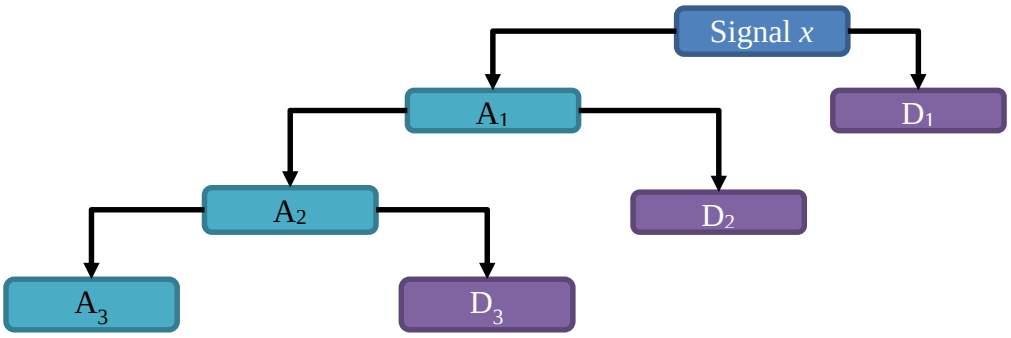

Figure 3.2 - Wavelet decomposition tree to three levels

Features have been extracted from wavelets for pattern recognition and, after dimensionality reduction such as Principal Components Analysis (PCA), classification accuracy superior to time domain features was claimed in [94, 107].

Noise has been reduced in EMG by using wavelets [80, 108], and ECG noise in EMG has been reduced by processing the coefficients that corresponded to low frequency components [78]. A careful choice of wavelet, threshold and level of decomposition is needed: The choice of wavelet is not a solved problem, though some have been suggested [108]. In this work, the Daubechies db2 with four levels of decomposition from [108] was used with a hard threshold. The wavelet transform assumes that the signal is stationary. To address the problem of the dynamic nature of the EMG, the transform is performed in windows for a time scale within which the EMG can be assumed to have stationary characteristics. Therefore, like EMD, this method is applied to windows of the signal just prior to feature extraction, in contrast to the other methods where the filtering is applied to the entire signal before the signal is divided into windows for feature extraction.

Filtering for ECG reduction - Simple high pass filtering of ECG removes some useful EMG information [78], so other techniques are used to attempt to minimise the distortion of the EMG. Spike Clipping, Template Subtraction, Wavelet Transform and Adaptive Filtering [78] are options.

Reducing power line interference - A notch filter is the simplest method of reducing power line interference. A third order Butterworth filter was used in this

work. The problem with a notch filter is that the exact frequency of the power line interference can be slightly different from the country's official frequency, meaning that some residual interference is present. As notch filters cannot be perfect 'brick wall' filters, energy from frequencies next to the mains supply frequency are also removed, which happens to be in the middle of where much of the EMG energy is present [26].

Adaptive filtering addresses these two problems. The power and exact frequency of the interference are estimated using a least squares method. A sine wave of the same power, frequency and phase [100] is generated then subtracted from the original signal to leave a cleaned signal. The trade-off is an increased processing overhead.

3.6. Spectral Enhancement

3.6.1. Description

Spectral enhancement is used for speech is to estimate and reduce noise when access to only a single microphone (i.e. sensor) is possible [109] and no noise reference is available. It is assumed that the speech and the noise are uncorrelated and that the statistical distributions of the STFT of the speech and the noise are "asymptotically independent and complex Gaussian" [110].

The simplest form of spectral enhancement is Spectral Subtraction. An estimate of speech presence across the signal is calculated in the time-frequency domain, across each of the STFT frequency bins. The noise estimate is then subtracted from the spectrum of the original noisy signal to leave speech that is more intelligible. However, this can cause excessive attenuation of sections of the signal that consist of only noise (i.e. low SNR), which leads to musical-sounding tones called 'musical noise' [111].

Minimum Statistics Noise Estimation (MSNE) is a means of reducing noise in speech whilst also reducing musical noise. This is achieved by smoothing the power spectrum of each STFT frequency bin in the time domain, then estimating the noise based on the minimum level of the frequency bin in between peaks caused by speech. This recursive process is a crucial difference from other noise estimation techniques. Firstly, a perfect Voice Activity Detection (VAD) is normally required in order to be

able to operate properly [109, 112]. Secondly, the sensitivity of the VAD must be adjusted to trade between noise attenuation and loss of weak speech components

Like MSNE, Improved Minima Controlled Recursive Averaging (IMCRA) also uses recursively averaged STFT power spectra to estimate the noise floor without the trade-off discussed above. Unlike MSNE, the noise estimate is updated during speech to compensate for rapid changes in noise level. More information about the structure of IMCRA can be found in Appendix A.

For clarity in this thesis, the noise estimation process is called IMCRA and the spectral subtraction process is called Spectral Enhancement based on IMCRA (IMCRA SE). IMCAR SE has also been called IMCRA/OMLSA in [105]. In Chapter 6 it will be shown that it can be applied to myoelectric signals to improve the classification accuracy of pattern recognition-based control. In a similar way to speech, the estimator excludes the strong myoelectric activity that corresponds to gestures.

IMCRA attempts noise estimation even during long speech segments with few pauses. In the case of EMG, long gestures and pauses are present in the Data Sets used in this work. The applicability of spectral enhancement for EMG signals, specifically Minimum Statistics and IMCRA, will be discussed in Chapter 6.

3.7. Local Binary Patterns

3.7.1. Types of Local Binary Patterns

Two-Dimensional Local Binary Patterns (2-D LBPs) are a texture classification technique [113] that have been widely used to extract features from images for texture classification due to their invariance to monotonic changes and rotation. They were used as part of a facial paralysis quantification system [114]. One-Dimensional Local Binary Patterns (1-D LBPs) are a recent adaptation for one-dimensional signals, in which histograms are generated from data using 1-D LBP codes [115] (histograms are explained in section 3.7.3).

3.7.2. Calculating a 1-D LBP code

A 1-D LBP code is a number that represents the behaviour of the samples surrounding a specific sample. The 1-D LBP code is calculated by comparing the neighbouring samples to sample $x[n]$. This comparison is condensed into (3.8):

$$LBP_P(x[n]) = \sum_{r=0}^{(P/2)-1} \left\{ S\left[x\left[n+r-\frac{P}{2} \right] - x[n] \right] 2^r + S[x[n+r+1] - x[n]] 2^{r+(P/2)} \right\} \quad (3.8)$$

where $S[.]$ is a threshold function:

$$S[f] = \begin{cases} 1 \text{ for } f \geq 0 \\ 0 \text{ for } f < 0 \end{cases} \quad (3.9)$$

P is an even number that determines the number of Local Binary Patterns: There are 2^P possible Local Binary Patterns. From (3.8) and (3.9), a number, called an LBP code, is derived which reflects the local activity of the signal around a sample relative to its value. The LBP code is thus independent of the absolute amplitude of the signal and of any Direct Current present in the signal. Figure 3.3 depicts a discrete signal with a sample number n of value $x[n]$.

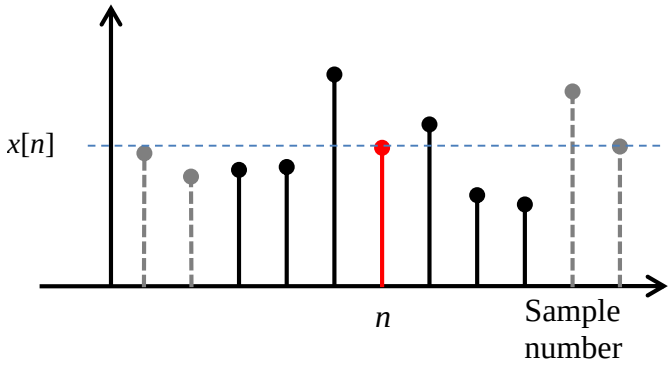

Figure 3.3 - An example of calculation of an LBP code. The six nearest samples (i.e. *P* = 6) to sample *n* in signal *x* are thresholded relative to its value *x*[*n*].

The solid black markers are the six nearest samples to sample n because $P = 6$*. The dashed horizontal line shows the value $x[n]$. Of the six samples nearest to sample n, the two either side of it are greater or equal in value to $x[n]$. Equations (3.8) and (3.9) can now be used to calculate the LBP code for sample n. No threshold calculation is performed on sample n, only on the surrounding samples. A worked

*The value of P is set to 6 throughout this section as an example

example is shown in Figure 3.4. Note that the least significant bit for LBPs is on the left.

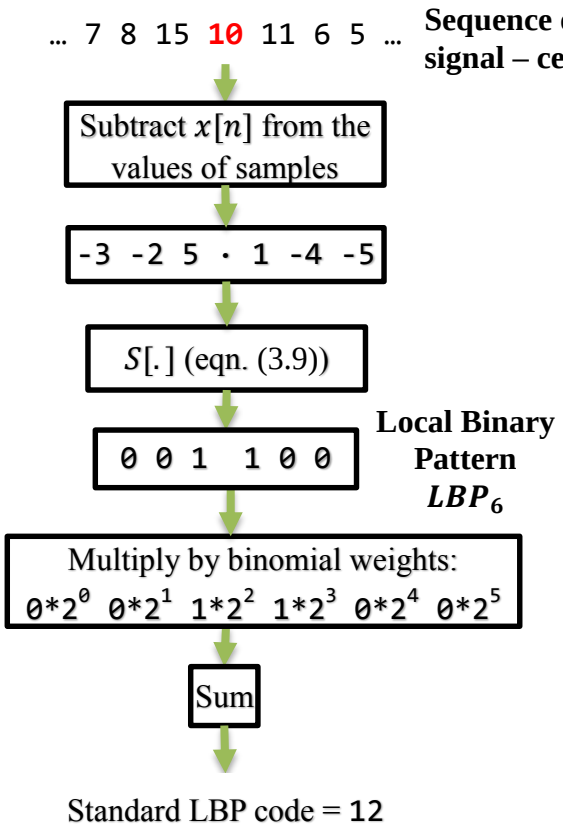

Figure 3.4 - Obtaining a 'standard' 1-D LBP code using equations (3.8) and (3.9), $P = 6$, $x[n] = 10$

There are three other code types that can be used to form histograms: Uniform (U), Rotationally Invariant (RI) and Uniform Rotationally Invariant (URI). These will now be described.

Uniform Code

Uniform histograms have unique bins for each pattern that has at most two 0 to 1 or 1 to 0 transitions. The other patterns are classed as non-uniform and given the same code [113]. Uniform code calculation is shown in Figure 3.5.

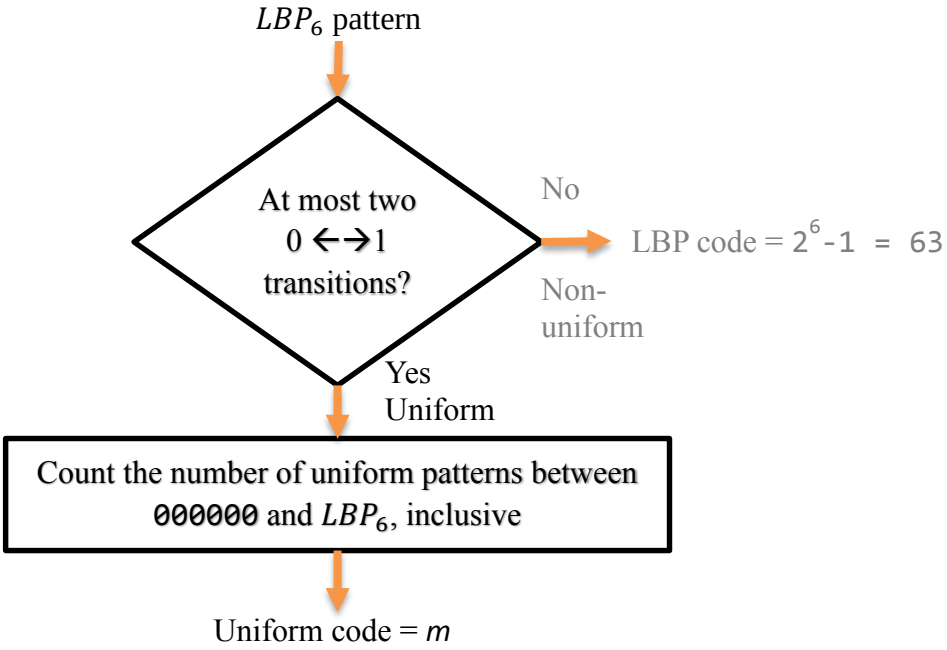

Figure 3.5 Calculation of 'Uniform' 1-D LBP code for *P*=6

The first few uniform binary patterns when $P = 6$ are shown in Table 3.4.

Uniform binary patterns:
000000
100000
010000
110000
001000
~~101000~~ non-uniform
011000
111000
000100
~~100100~~ non-uniform
~~010100~~ non-uniform
~~110100~~ non-uniform
001100
⋮ ⋮
m^{th} uniform pattern

Table 3.4 – The first few uniform binary patterns with $P = 6$

As an example, pattern 001100 (in Figure 3.4) has nine uniform binary patterns between 000000 and itself, so the Uniform LBP code is 8, counting from zero.

Rotationally Invariant Code

To create a Rotationally Invariant LBP, bitwise rotations are performed to minimise the value of the pattern as a binary number, with the least significant bit on the left. This is done using the LBPROT operator, which is adapted from equation (8) in [113] for 1D LBP:

$$LBP_P^{ri} = min\{ROL(LBP_P, i) \mid i = 0,1, \dots, P-1\} \quad \textbf{(3.10)}$$

where ROL is the binary Rotate Left operator. All rotated versions of the binary pattern are compared, and the version that has the minimum value is taken as the rotationally invariant pattern. In this way, a unique code is created for each rotationally minimum pattern. Figure 3.6 shows the process.

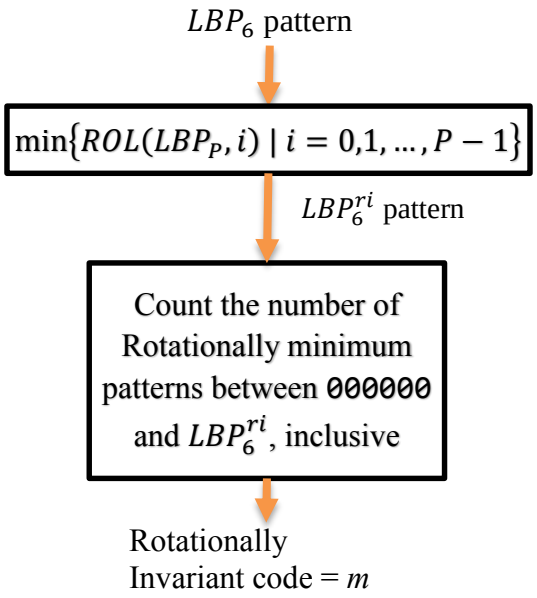

Figure 3.6 Flowchart for the calculation of the 'Rotationally Invariant' 1-D LBP code for *P*=6

Table 3.5 shows the first few RI binary patterns for P=6.

RI binary patterns:
000000
100000
~~010000~~ not rotationally minimum
110000
~~001000~~ not rotationally minimum
101000
~~011000~~ not rotationally minimum

Table 3.5 - The first few RI binary patterns with $P = 6$

As an example, pattern `001100` is rotated to the left twice using (3.10) to become `110000`, giving a Rotationally Invariant code of 2 as it is the third RI pattern counting from all zeroes and counting from 0, inclusive: `000000`, `100000` then `110000`.

Uniform Rotationally Invariant Code

Uniform Rotationally Invariant LBP codes also take into account the transition from the last bit to the first bit when determining uniformity [113]. Figure 3.7 shows the process.

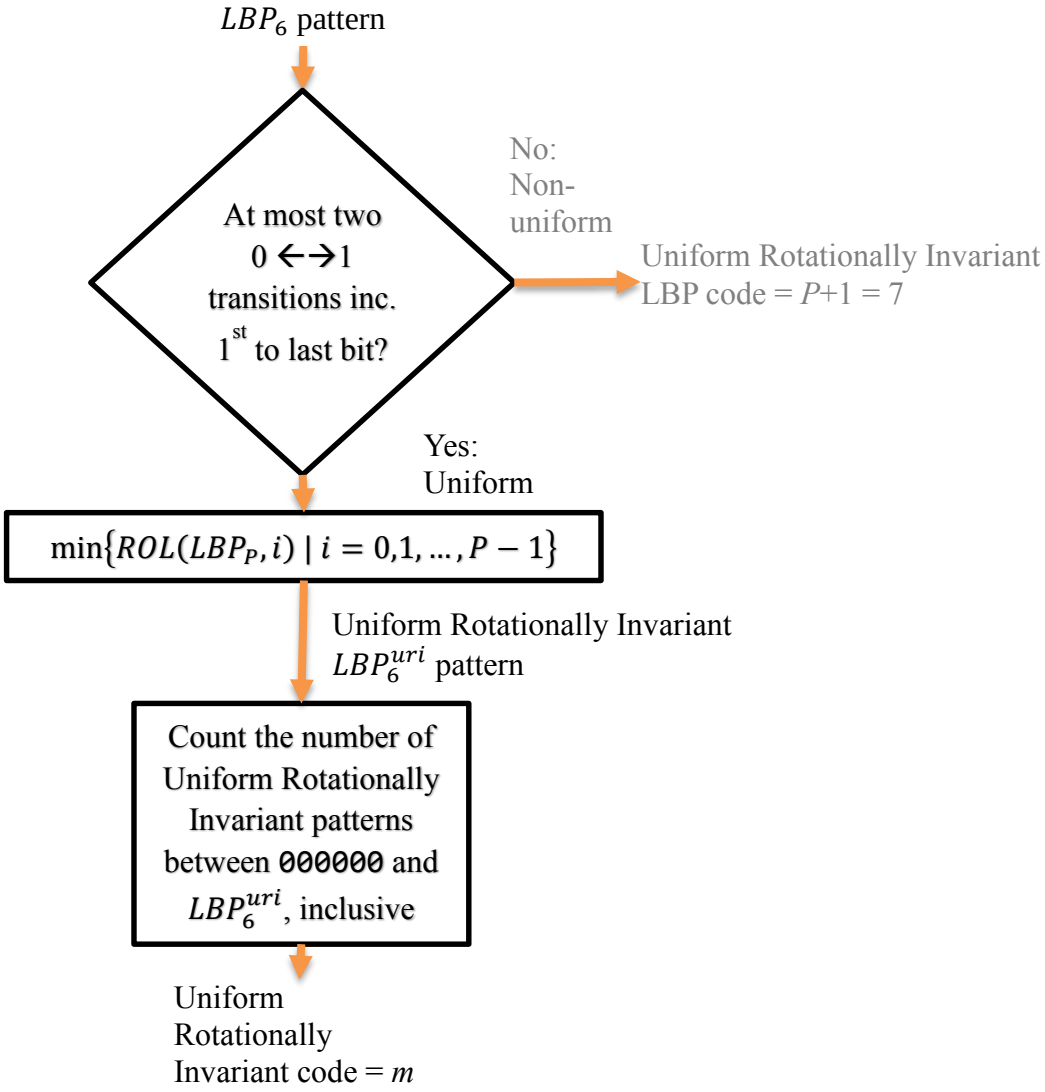

Figure 3.7 - Flow chart for the calculation of the 'Uniform Rotationally Invariant' 1-D LBP code

Table 3.6 shows the first few Uniform Rotationally Invariant binary patterns with P=6.

Uniform RI binary patterns:
`000000`
`100000`
~~`010000`~~ not rotationally minimum
`110000`
~~`001000`~~ not rotationally minimum
~~`101000`~~ not uniform
~~`011000`~~ not rotationally minimum
`111000`
~~`000100`~~ not rotationally minimum
~~`100100`~~ not uniform
⋮ ⋮
m^{th} Uniform RI pattern

Table 3.6 - The first few Uniform RI binary patterns with $P = 6$

As an example, pattern `110001` is rotated left five times to become `111000` giving a Uniform Rotationally Invariant LBP code of 3, counting from zero.

3.7.3. Creating a Histogram

2-D LBP histograms describe the texture of a portion of an image [113]. In a similar way, 1-D LBP histograms effectively describe the 'texture' of a window of a one-dimensional signal. Using one of the methods described above, LBP codes are calculated for the signal or window of length *N* from sample number $\frac{P}{2} + 1$ to sample number $N - (\frac{P}{2} + 1)$. Once the LBP codes are calculated, a histogram is formed from them. The total number of histogram bins equals the number of possible unique LBP codes, which depends on the chosen value of *P* and type of histogram selected.

The distribution of LBP codes within a signal (or within a windowed portion of it) is called the LBP histogram [115] and it is calculated as:

$$H_b = \sum_{\frac{P}{2} \le n \le N - \frac{P}{2}} \delta(LBP_P(x[n]), b) \tag{3.11}$$

where H_b is histogram bin number b (each bin corresponds to an LBP code), the signal or windowed portion is of length N, $b = 0..B-1$, B is the number of histogram bins and $\delta(i, j)$ is the Kronecker Delta. Figure 3.8 shows how the LBP codes are calculated across a window of an example discrete signal.

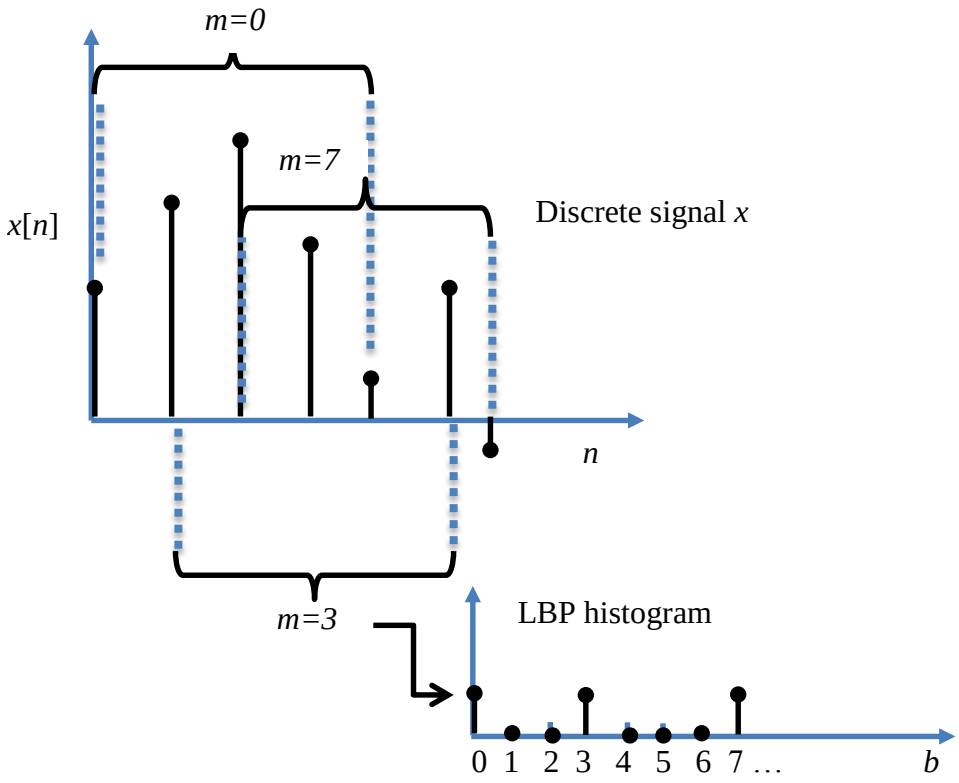

Figure 3.8 – Example of creation of standard 1-D LBP histogram

In Figure 3.8, a Standard 1D LBP histogram (bottom) is calculated from a window of three samples from the discrete time-domain signal with P=4 (top). Once all the codes have been added to the histogram, it is normalised so that:

$$\sum_{b=0}^{B} H_b = 1 \qquad (3.12)$$

The number of bins in a rotationally invariant histogram is equal to the total number of unique binary patterns obtainable when each binary number from 0 to $2^P - 1$ is rotated, by bitwise rotation using (5), to its minimum possible value. The number of bins for each histogram type is shown in Table 3.7.

Histogram type	Total number of bins
Standard	2^P
Uniform	$P(P-1)+3$
Rotationally Invariant	Number of unique RI patterns between 0 and 2^P-1
Uniform Rotationally Invariant	$P+2$

Table 3.7 – Number of bins for each histogram type for a given value of *P*

The algorithm to generate RI histograms first creates a bin for each unique RI binary number between 0 to $2^P - 1$.

3.7.4. Behaviour of 1-D LBP histograms for test signals

To obtain a better understanding of bin behaviour, it is helpful to use test signals. Several test signals are shown in Figure 3.9 and Figure 3.10. The signal (or a portion of it) on the left and the corresponding 1-D LBP histogram is on the right.

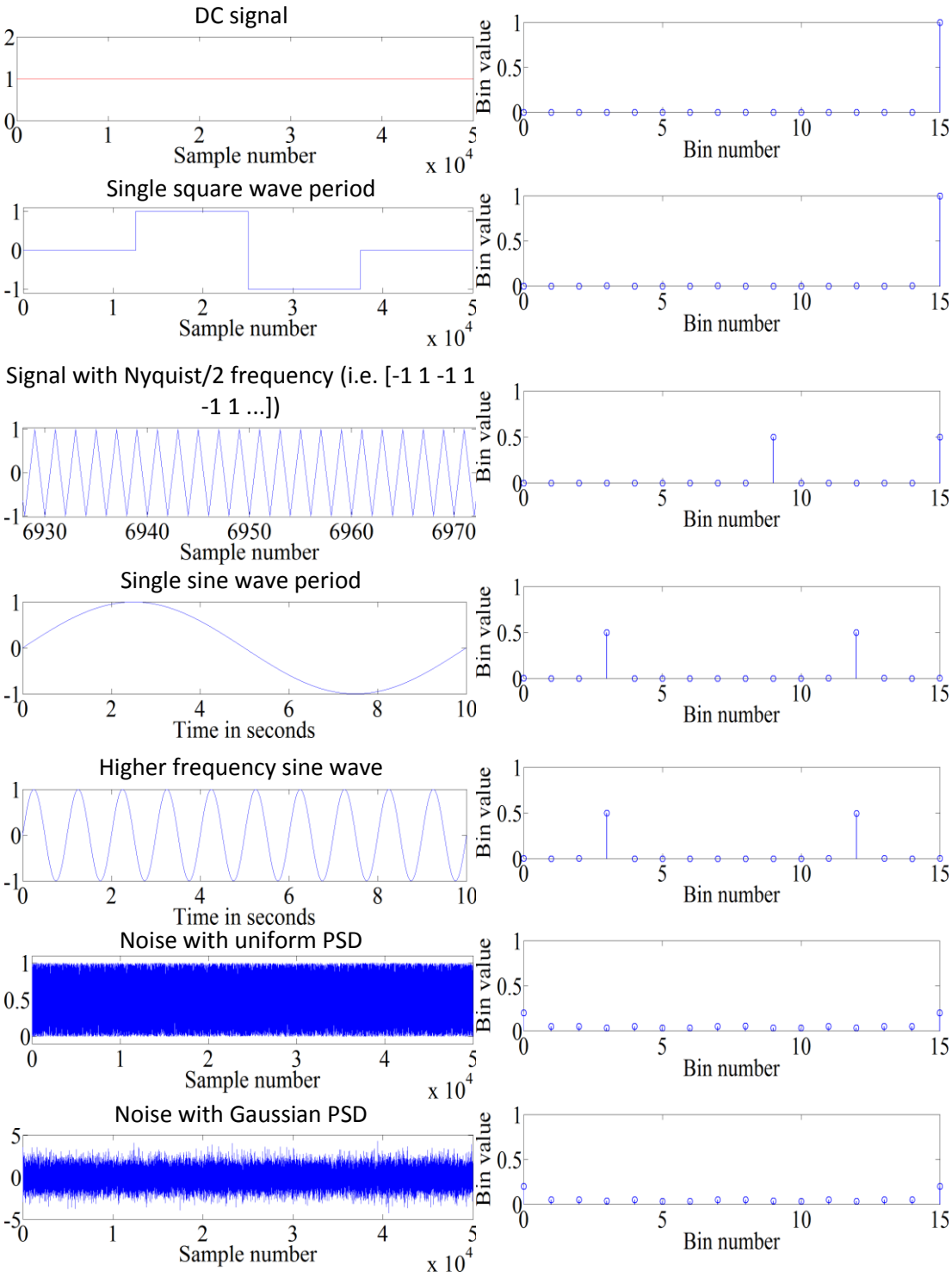

Figure 3.9 - 1-D LBP histograms of test signals or a window thereof (left) and their 'standard' 1-D LBP histograms with *P*=4

More test signals and their corresponding LBP histograms are shown in Figure 3.10.

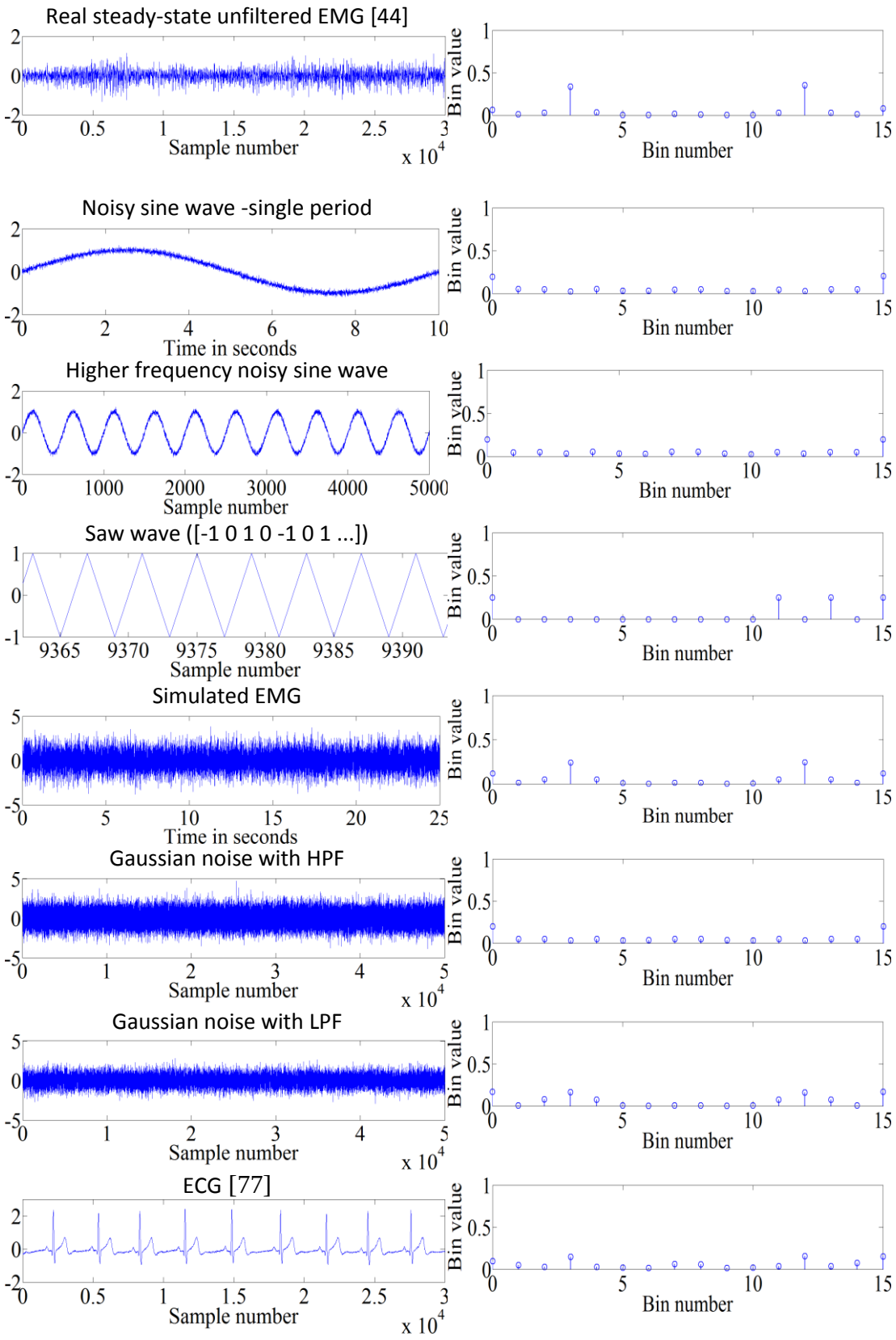

Figure 3.10 – More test signals with corresponding 'standard' 1-D LBP histograms with *P*=4

The histograms of the test signals in Figure 3.9 and Figure 3.10 show that bin behaviour changes in response to trends within the range of *P*. It must be stressed that this is not the same as pure monotonicity, where each successive sample in the chronological order is greater or less than its preceding sample. Distinctive bin behaviour can be seen for each of the signal types, but with limitations: For example, a pure sine wave can be identified by its histogram but its frequency cannot be determined.

Trends within the signal are reinforced by any periodicity and by the presence of more channels that show similar behaviour, because the number of identical LBP codes is then increased. However, it can be seen from the figures that if strong enough noise corrupts a periodic signal, the trend within the range of *P* is obscured and therefore the histogram bin behaviour changes to that of the noise.

3.7.5. Uses for 1-D LBPs

One-dimensional LBPs have been used for Voice Activity Detection of speech signals [115]. Voiced and unvoiced parts of speech signals were distinguished based on histogram behaviour. The Resistor Average Distance (RAD) was used as a metric for assessing the histograms of consecutive windows of the signal, and this was used as a criterion for segmenting the signal. A threshold was set for the RAD, and if this was exceeded between two of the histograms, the start of a new segment of the signal was declared. This is discussed in detail in section 4.2.1. The concept of using 1-D LBP for VAD was further refined by Zhu *et al* [116].

1-D LBPs were used in bone texture characterisation to identify osteoporotic bone structure [117]. It was found that the 1-D LBPs produced superior classification accuracy compared with 2-D LBP histograms of the images of the osteoporotic bones.

1-D LBP histograms have been used in an attempt to improve facial recognition [118], where the face is divided into blocks, then each block is projected into a one-dimensional space. When 1-D LBP was combined with PCA, robust facial recognition was achieved.

3.7.6. Measuring differences between histograms

Histograms can be used to assess characteristics of a signal. They are used to measure the frequency of occurrence of values within the signal or some representation of the signal. For example, a histogram of an image indicates the proportions of light and dark areas. It is often necessary to compare histograms between signals or within parts of the same signal. Several tools exist for this purpose. The Kullback Leibler Divergence [114, 115] is a non-commutative measure, which means that the 'distance' measured from one histogram to another differs depending on which histogram is designated as p and which as q.

$$D_{KL}(p||q) = \sum_{k=1}^{n} p(k)\{\log(p(k)) - \log(q(k))\} \quad \textbf{(3.13)}$$

In (3.13), $p(k)$ and $q(k)$ are probability distributions of discrete random variable k. To overcome this, the resistor average distance uses the FLD in the formulation of a symmetric measure of the difference between two histograms [114, 115]. It is calculated thus:

$$D_{RAD}(p,q) = [(D_{KL}(p||q)^{-1}) + (D_{KL}(q||p)^{-1})]^{-1} \quad \textbf{(3.14)}$$

The Resistor Average Distance will be used in this thesis as a measure between two histograms.

3.8. Conclusion

In this chapter, single- and double- threshold activity detection methods were discussed. It was shown that double thresholds allowed control over TPR and FPR. All of the onset and activity detection algorithms discussed in this chapter require at least one threshold to be adjusted until the best results are achieved. This is exacerbated if methods are combined or if there are concurrent channels, as there are then multiple thresholds to set [85] and co-ordinate. Parameters are calculated and compared against user-defined thresholds, which are decided by comparing characteristics of parts of the signal with and without movement present. A quiescent period of the signal must therefore be identified, which is simple in manual offline analysis but might be difficult to achieve in real-time.

EMG signal quality measures were described and discussed. Each method, though potentially useful for analysing EMG, has limitations and assumptions. EMG noise reduction methods were introduced and discussed, all of which assume that the noise type has been identified in the first place and that the noise is strong enough to justify the processing to remove it. EMD was introduced and EMDF was identified as a method of low-frequency noise identification and reduction. Spectral enhancement was introduced in the context of speech signals. The application of spectral enhancement for EMG will be discussed in Chapter 6. One-Dimensional Local Binary Patterns were introduced, and 1-D LBP histograms were explained. These will be used in the next chapter for EMG activity detection.

4 Activity Detection for EMG using One-Dimensional Local Binary Patterns

4.1. Introduction

This chapter explains how the changing behaviour of 1-D LBP histogram bins between windows of activity and windows of rest can be used as a means of muscle activity detection for myoelectric signals. A new algorithm called One Dimensional Local Binary Pattern Activity Detection (LBPAD) is introduced. The performance of the new method is compared with established methods and the LBPAD is shown to be advantageous in some circumstances. The True Positive Rate (TPR) and False Positive Rate (FPR) can be controlled by changing several parameters.

A myoelectric control system needs to be able to distinguish which part of the sensors' signals are EMG and which are noise. In DC, a threshold is set, below which the limb does not move. In pattern recognition, a threshold can also be used, but the best sensor site for pattern recognition purposes is not necessarily the site with the highest EMG amplitude [11]. The signal could be of low power due to the gesture being performed, or if the movement was slow. In these cases, a trade-off between false alarm rate and detection would be necessary if a threshold method was used. For this reason, it would be advantageous to use some property of the signal other than one related to envelope, amplitude or energy in order to recognise EMG activity.

As discussed in section 3.2.3, a gesture class called 'no motion' can be implemented, such that the classifier outputs 'no motion' labels when it detects only the characteristics of the background noise (i.e. no muscle activity). However, this does not allow control of TPR and FPR, which were discussed in section 2.5.2. To do this, the methods in section 3.2 would need to be used. It is favourable to have zero FPR, even at the expense of TPR. If a low FPR is coupled with a limited TPR, the wearer will have to try harder to activate the limb, and the possibility of unintentional trigger will be lower.

4.2. Histogram Bin Behaviour for Activity Detection

4.2.1. Resistor Average Distance

Here the Resistor Average Distance (3.14) is tested as a method of EMG segmentation to achieve activity detection. A single channel of a single recording from Data Set 1 is shown in Figure 4.1 (a), which has the activity detections based on RADs shown in a lighter shade as 'boxes' around the EMG. The EMG is channel 1 of trial 17 from subject 1 from Data Set 1 was used. P=8 and window length is 60 samples.

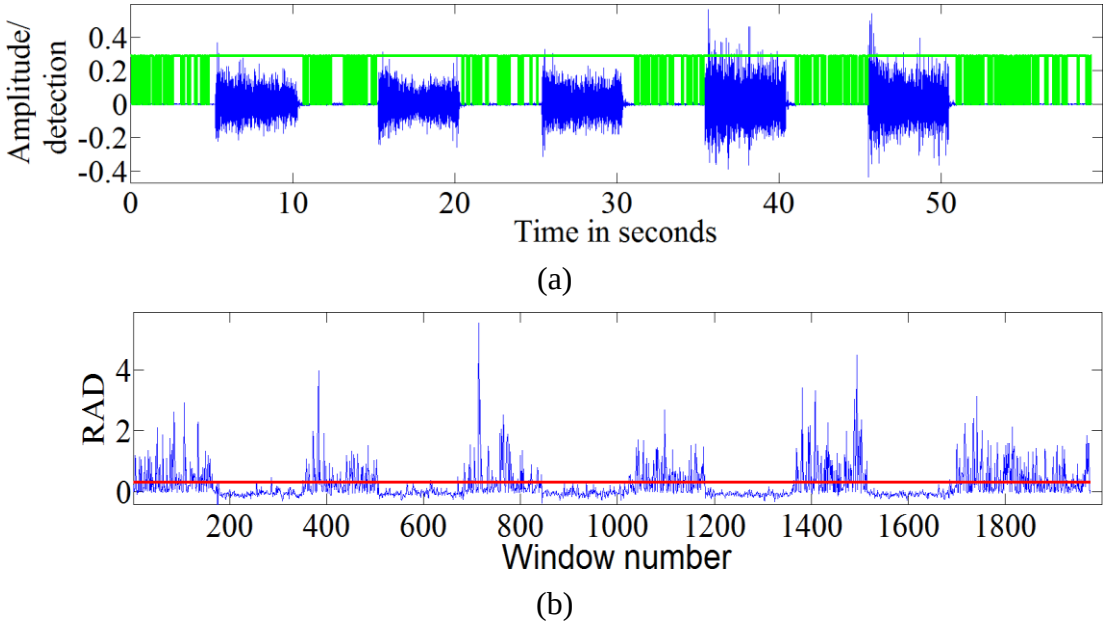

Figure 4.1 - (a) EMG recording with segmentation based on RAD indicated (b) RAD of the 1-D LBP histograms of windows of the signal shown in (a).

In Figure 4.1(b), the RAD between 1-D LBP histograms of successive windows of the signal is shown. The horizontal line is the threshold used to generate the segments. The horizontal line is the threshold, which in this case was chosen empirically to be 0.3. The horizontal lines are tuned to indicate 'activity' where the RAD is similar between windows. The RAD fluctuates greatly during the 'rest' periods, whereas the RAD between windows of a gesture is low and relatively stable. We can refine the detection a little by using an inverted version of the smoothing algorithm described in section 4.4: The 'inactivity' regions are joined together if they occur within 0.5s of each other. The result is shown in Figure 4.2.

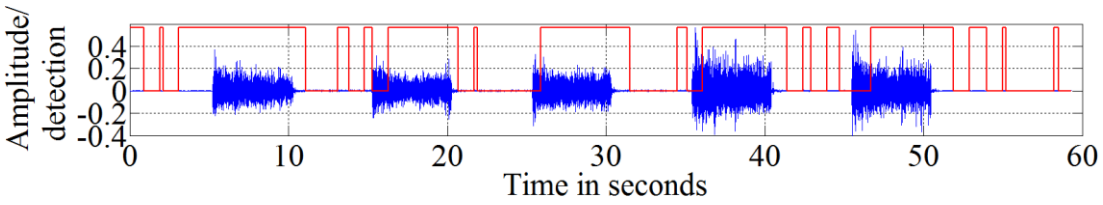

Figure 4.2 - RAD-based activity detection with smoothing filter to join regions of similar RAD

Figure 4.2 shows the potential of 1-D LBP histograms for segmentation of signals between activity and rest. However, a manual threshold had to be chosen and the length of the smoothing filter in this case was too long for real-time use. Most importantly, the segmentation was not very accurate. We will now look at a way in which segmentation can be performed based on the properties of specific histogram bins, as opposed to the properties of the overall histogram.

4.2.2. Standard Deviations of 1-D LBP Histogram Bins

The normalised 1-D LBP histogram is calculated using the method described in Section 3.7.3 for a single channel of a recording (Channel 1 of Subject 1, Trial 1, Data Set 1) in which several different gestures are performed. The recording site is on the skin adjacent to the *extensor digitorum* muscle. This is shown in Figure 4.3. It is clear that the signal consists of five periods of activity interspersed with 'rest', or inactivity, periods.

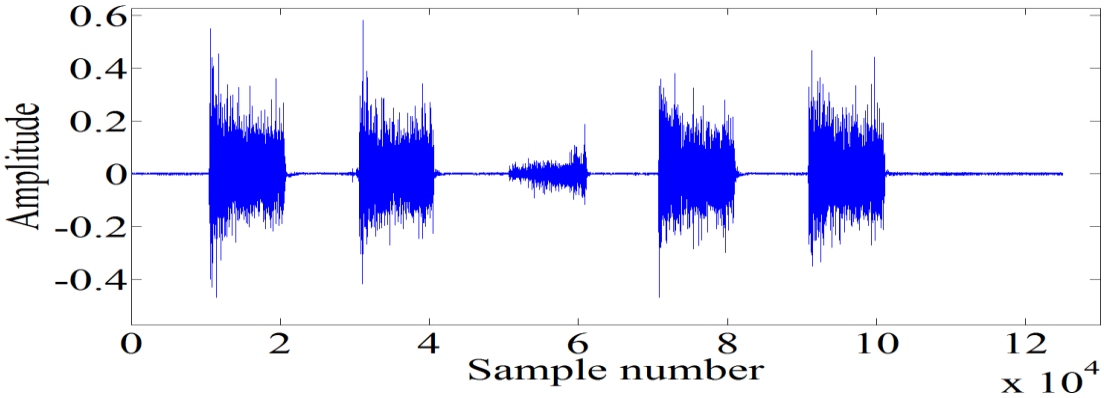

Figure 4.3 - Single channel (*extensor digitorum*) of real unfiltered EMG from channel 1 trial 1 Subject 1 of Data Set 1 – Tripod, Pinch, Point, Tripod, Pinch

A single normalised 1-D LBP histogram is generated for the entire signal with P=6 and a standard histogram type, shown in Figure 4.4.

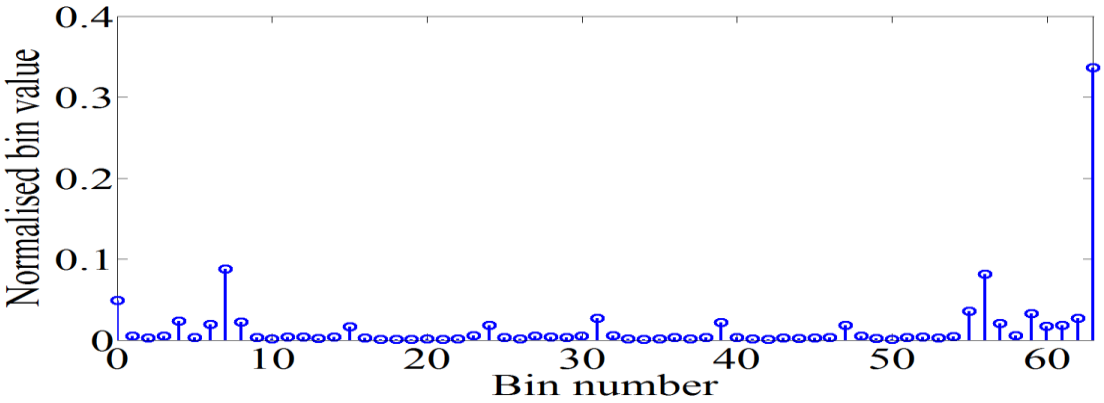

Figure 4.4 - 1-D LBP histogram of signal shown in Figure 7, *P*=6 and standard histogram type

Figure 4.4 indicates that several of the bins have a higher value across the signal than others. If windows of the signal are now taken, the standard deviations of the histogram bins across the windows can be calculated. Histograms of consecutive 300ms windows of the signal were generated, and the standard deviations of the histogram bins were calculated. These are shown in Figure 4.5.

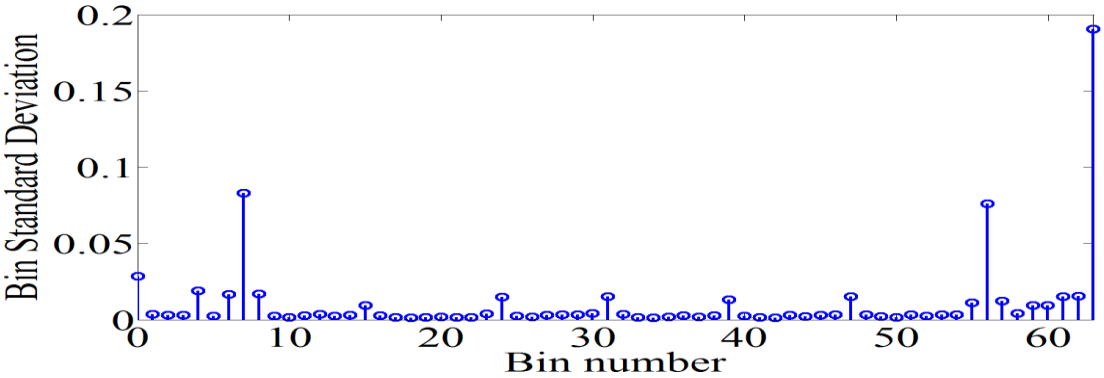

Figure 4.5 - Standard deviations across 300ms windows of the real EMG shown in Figure 4.3. *P*=6 and standard histogram type

Figure 4.5 shows that the three bins that have the highest amplitude also have a much higher standard deviation between the windows than the rest. A distinction will now be made between the rest and activity periods of the signal, and the histogram bin behaviour in each will be examined separately. Histograms are calculated of short windows of rest and activity parts of the signal as shown in Figure 4.6(a). The bins with the highest amplitudes are circled in Figure 4.6(b) and Figure 4.6(c).

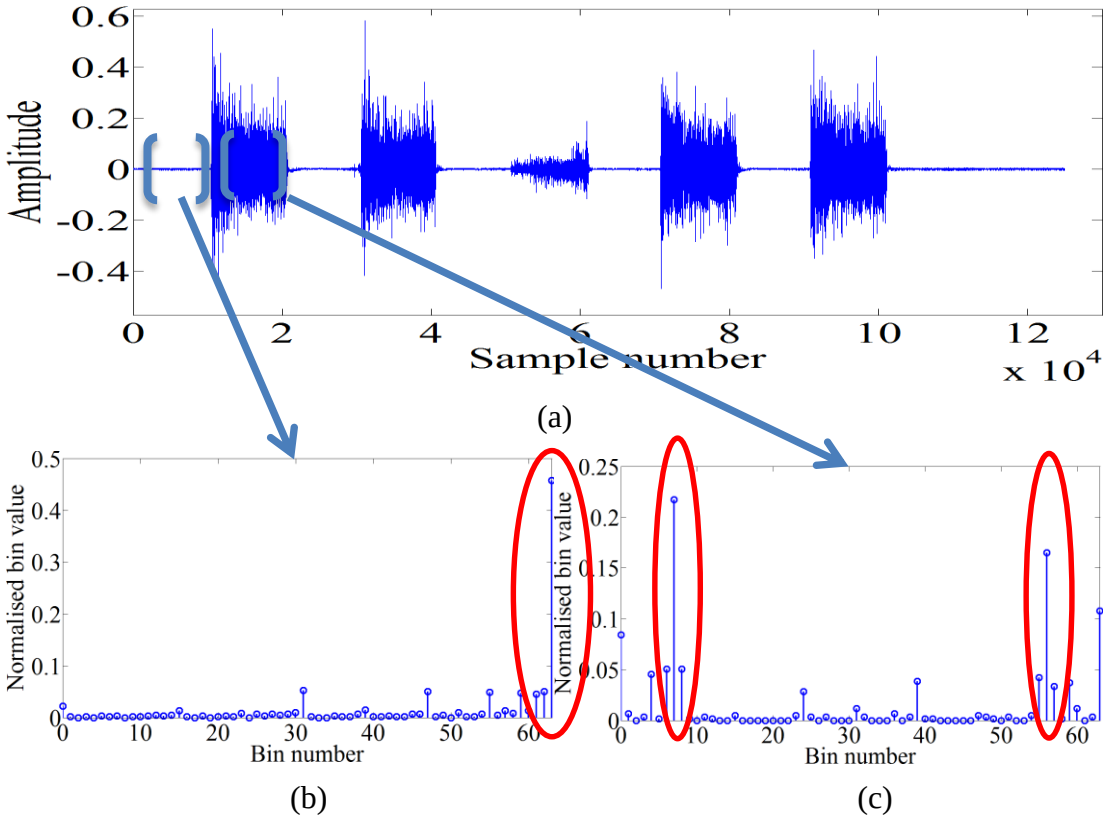

Figure 4.6 - Sketch of a comparison of histograms between a window of activity and a window of rest *P*=6 standard histogram from (a). (b) shows inactivity bin circles and (c) shows activity bins

Figure 4.6(a) shows a single channel of a gesture from a recording of real EMG. 1-D LBP histograms were taken from a rest period and an activity period respectively, as indicated by the two windows. Figure 4.6(b) shows the normalised 1 D LBP histogram from the first window. Figure 4.6(c) the normalised 1 D LBP histogram from the second window. The histograms for the 'noise only' and EMG are similar to the histograms for the corresponding test signals in section 3.7.4 Figure 3.9 and Figure 3.10.

The three bins with the highest amplitudes in each window can now be considered in isolation. A plot can be made of their values across the successive windows of the signal. Bins 7 and 56 from Figure 4.6 (c) are summed and shown in Figure 4.7.

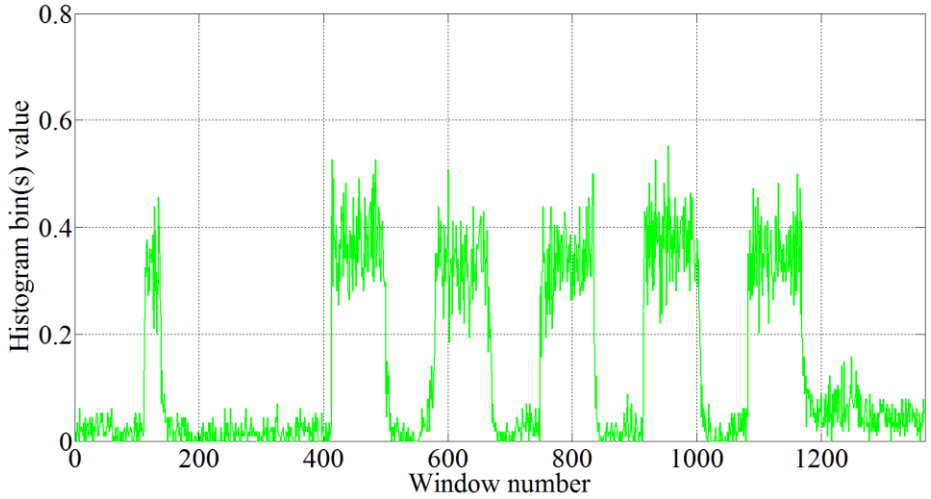

Figure 4.7 – Sum of bins 7 and 56 from 1-D LBP histograms of successive windows of the signal shown in Figure 4.6(a)

Figure 4.7 shows the sum of bins 7 and 56 for successive windows of the signal shown in Figure 4.3. It is clear from Figure 4.7 that a threshold could be set to infer EMG activity for each of the windows. A threshold of around 0.2 would allow this. It is, however, not necessary to set a manual threshold. Instead, the bin values in Figure 4.7 can be compared directly with bin 63, which is the bin with the highest standard deviation shown in Figure 4.6(b). The histograms are normalised, so a direct comparison between their amplitudes can be made. This is shown in Figure 4.8.

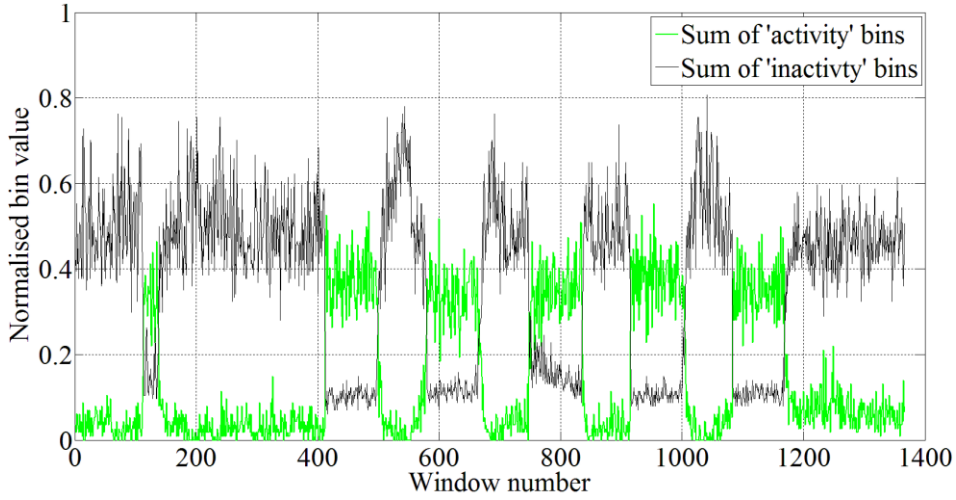

Figure 4.8 - Comparison of normalised (bin 7 + bin 56) with bin 63 from 1-D LBP histograms of successive windows of the signal shown in Figure 4.6(a)

Figure 4.8 shows that bin 63 is higher in value than the sum of the other two bins when there is no EMG activity. The locations where the relative amplitudes change are defined here as 'crossovers'. This can be used to develop an algorithm for automated activity detection. The process can be condensed into a flow chart. Figure 4.9 depicts the stages involved in 1-D LBP Activity Detection (LBPAD).

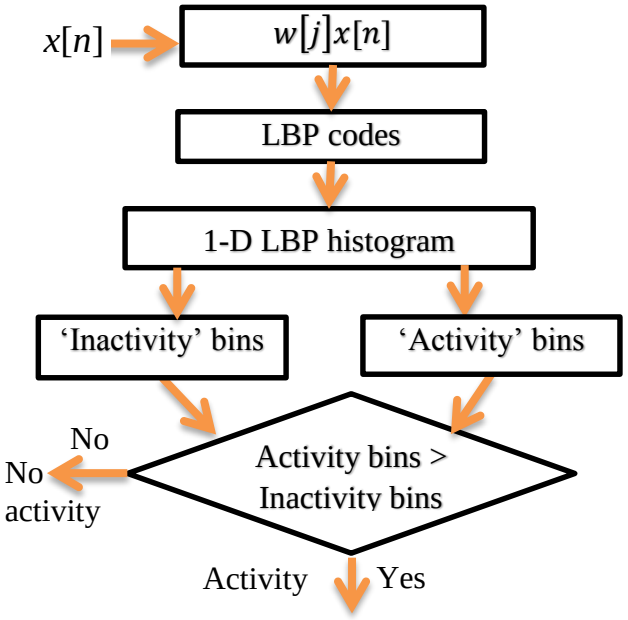

Figure 4.9 Flow chart for the One Dimensional LBP EMG Activity Detection (LBPAD)

LBPAD is described by the following steps:

1. For a single channel, the signal is first split up into windows by applying a window $w[j]$ of length W:

$$x[j] = w[j]x[n] \tag{4.1}$$

2. The 1-D LBP codes of all the samples in each window are calculated using equations (3.8) and (3.9).
3. The Standard LBP histogram for each of the windows is calculated using equation (3.11) and Figure 3.4.
4. The Standard LBP histogram bin values are then mapped to the histogram bins of the chosen histogram type using equation (3.10), Figure 3.5, Figure 3.6 and Figure 3.7.

5. The histogram bins corresponding to ‘activity’ and ‘inactivity’ are then determined based on Table 4.1 below.
6. For each window, determine whether the normalised ‘activity’ bin value(s) is/are higher than the normalised ‘inactivity’ bin value
7. Filter the resulting activity vector such that windows with activity detections that are within human reaction time of each other are considered part of the same activity. Use the smoothing algorithm in section 4.4 for this.

In step 5, the ‘activity’ and ‘inactivity’ bins were identified by observing bin behaviour in real sEMG signals. All of the histogram types were found, by systematic observation, to have specific bins that were higher in amplitude during quiescent periods and other bins that were higher in amplitude during EMG. From these observations, the formulae to determine the bin numbers were calculated, which are listed in Table 4.1.

Histogram type	**Total number of bins**	**Activity bin number(s)**		**Inactivity bin number(s)**
Standard	2^P	$2^{(P/2)}-1$	$2^P-2^{P/2}$	2^P-1
Uniform	$P(P-1)+3$	$\frac{(7P^2-10P+8)}{8}$	$\frac{-1}{48}\frac{-1}{48}P^4+\frac{13}{24}P^3-\frac{115}{24}P^2+\frac{217}{12}P-20$	$P(P-1)+2$
Rotationally Invariant	Number of unique RI patterns between 0 and 2^P-1	$2^{(P/2)-1}$		*B-1*
Uniform Rotationally Invariant	$P+2$	$P+1$		$P/2$

Table 4.1 - List of activity bins and inactivity bins for each histogram type for LBPAD

Note that the 'activity' bin formulae for Uniform histograms in Table 4.1 work as high as $P = 10$, which is adequate for the uses described in this thesis. The equation was obtained by creating a polynomial equation that produced the empirically determined activity bin numbers from each even value of P from 2 to 10. The 'inactivity bin' for all but the Uniform Rotationally Invariant histogram happens to also be the last bin in the histogram. Bin numbering in all cases starts from zero.

Other bins have a little response to activity/inactivity. From Figure 4.6 where P=6 with a standard histogram, bins 0, 4, 6, 8, 15, 24, 31, 39, 47, 55, 57, 59, 60, 61 and 62 also have some degree of response to the presence of EMG. For RI histograms in addition to the second-last bin the first and last bins have increased amplitude in 'inactivity' windows. These were added to activity/inactivity bin calculations too, but in general, the results were less accurate and so the choice of bins was kept to the bins listed in Table 4.1.

4.3. 1-D LBP EMG Activity Detection

4.3.1. Testing on a simulated and real EMG signal

Figure 4.10 (a) shows a dynamic simulated EMG signal created using the method in 2.3.4, with a sampling rate of 2kHz and SNR of 6dB. The vertical markers indicate actual onset and offset markers (with 100 sample 'ramps' after each event [40]), and the horizontal line shows the activity estimation by LBPAD.

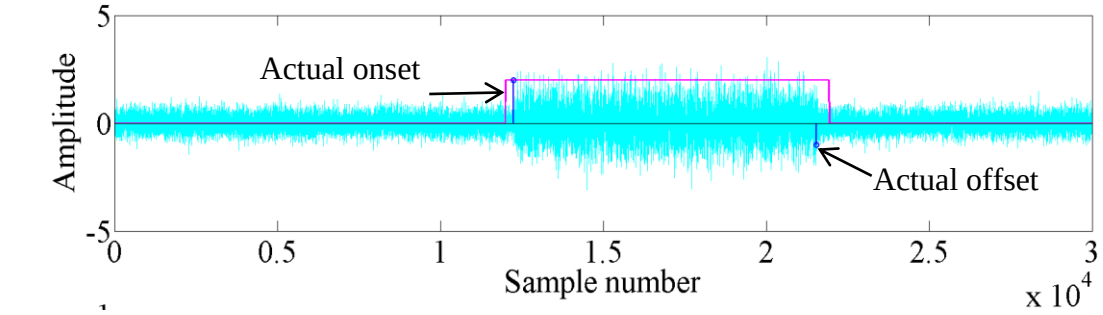

(a)

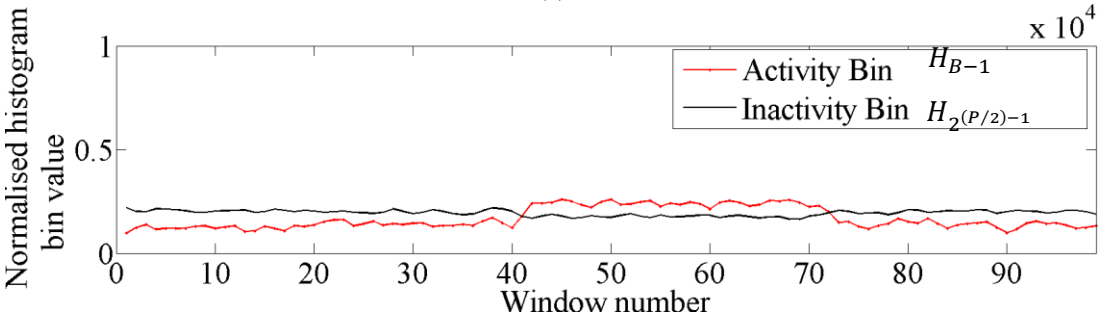

(b)

Figure 4.10 (a) LBPAD applied to a dynamic simulated EMG signal of SNR 6dB. (b) normalised RI histogram bin activity

An example of a 'gesture' of simulated EMG is shown in Figure 4.10. The box indicates the activity detected by LBPAD. Figure 4.10(b) shows normalized histogram bin activity corresponding to the signal in (a). This is the bin behaviour that is used to determine when onset and offset occur for an RI histogram with P = 4, window size of 600 samples with 50% overlap. During EMG activity, the value in the last bin (H_{B-1}) decreases and the value in bin $H_{2^{(P/2)-1}}$ increases.

Figure 4.11 (a) shows LBPAD applied to a single gesture of a real sEMG signal (surface site corresponding to extensor digitorum muscle) from Data Set 1. The vertical markers indicate movement and rest cues that were given to the subject. The dashed horizontal line is the activity detection based on the algorithm above. Figure 4.11 (b) shows the 'active' and 'inactive' Rotationally Invariant histogram bins (P=4) taken from windows of the signal.

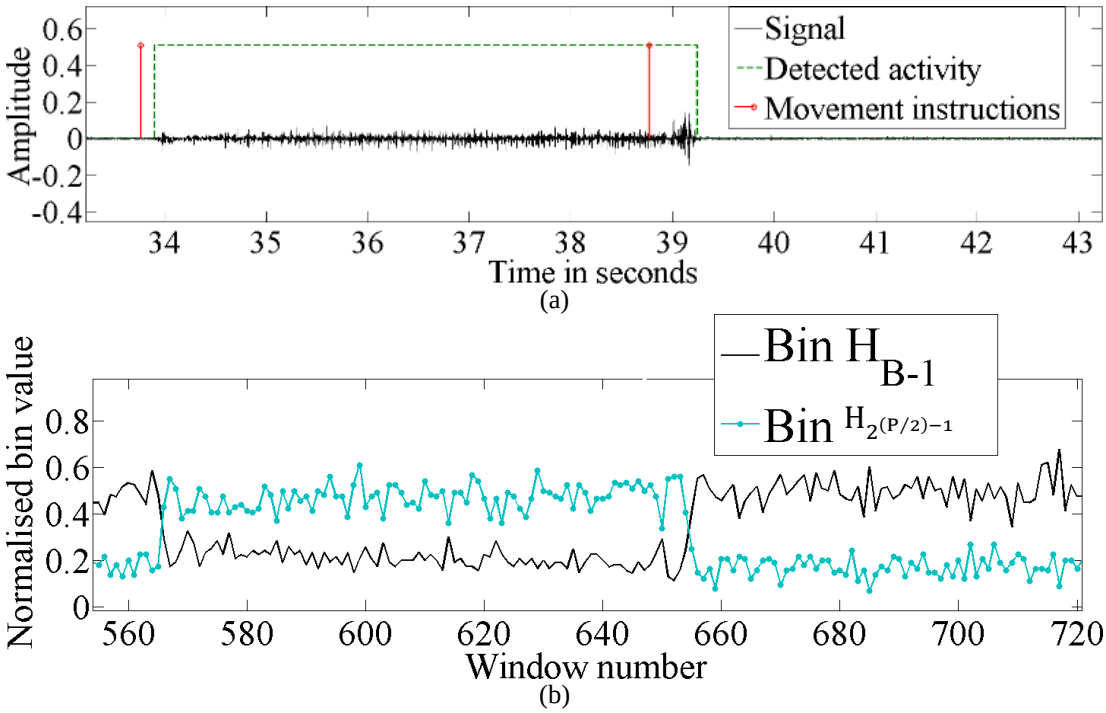

Figure 4.11 (a) Surface myoelectric signal from Data Set 1 (b) Normalized RI histogram bin activity

Figure 4.11(a) shows an example of a surface myoelectric signal from Data Set 1, which has activity detection and movement cues superimposed. Figure 4.11(b) shows the normalised histogram bin activity from the signal in (a). The dark line is RI 'inactivity' bin and the marked line is the RI 'activity' bin. The window length is 120 samples with no overlap.

4.4. Quiescence Detection and Smoothing Filter

The output of onset detection methods is usually an array in computer memory that contains markers at the samples where onsets are detected. Activity detection methods produce an array that contains markers to indicate both onset and subsequent EMG activity. The array is seldom an exact representation of the activity: There can be several markers around an onset and spurious inactivity markers during an active period. To address this, human reaction time period (discussed in section 2.4), which is about 300ms, can be taken into consideration: all markers in the array that are within this period are assumed to form part of the same intentional movement. Activity detection, feature extraction and classification must all be calculated within the aforementioned time. Figure 4.12 shows the smoothing algorithm used in this work.

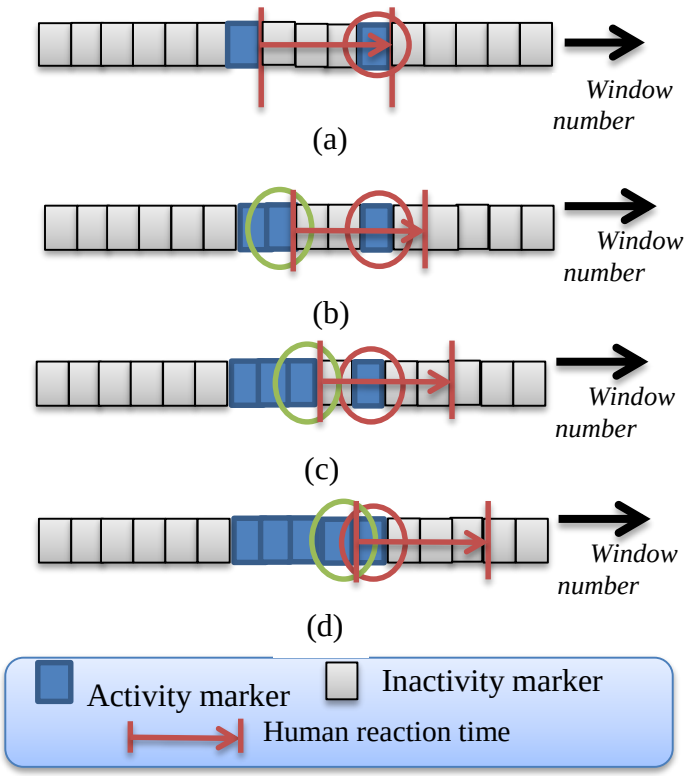

Figure 4.12 - Illustration of the smoothing algorithm

The 'gaps' between activity markers are 'filled in' if they occur within human reaction time of each other:

1. Search sequentially from the start of the array for an activity marker
2. When an activity marker is found, look for at least for one other activity marker within human reaction time of found marker
3. If at least one other marker is found (circled in Figure 4.12(a)), set the next marker to 'active' if it is not already (left circled in Figure 4.12(b)) and look within human reaction time after that marker (right circled in Figure 4.12(b) and (c))
4. If no other 'active' maker is found within human reaction time (Figure 4.12(d)), look sequentially for next 'active' marker and repeat the process

4.5. Performance Evaluation

Data Sets 1 and 2, described in section 2.3.5, were used to evaluate the performance of LBPAD. It was compared to the Energy activity detection method (energy within a window must be above a threshold) and Bonato's method as explained in section

2.5.2. Bonato was configured in accordance with the parameters in [39] with the exceptions of *h*, which was varied to make the Receiver Operating Characteristic (ROC) curve. T_1 was set to 1: changing it to 2, 3 or 4 altered the performance of Bonato's method as shown in Figure 4.13. Several of the methods described in section 3.2 detect onsets only, so were not included in this comparative study.

Both channels of Data Set 1 were used together. Bonato's method was applied separately to each channel and activity was declared if at least one channel was active. For Energy, the sum of the energy of both channels within a window had to be above a threshold for activity to be declared. For LBPAD, a single histogram was created from the sum of the LBP codes of both channels together within a window. The Energy and Bonato thresholds were varied to obtain the ROC curves [119]. All sessions of all subjects were used. Adjacent windows of size 60ms (120 samples) were used, with no overlap. The resulting curves are shown in Figure 4.13. The quiescent period for Bonato's method was taken as the time between the first two markers ('start of trial' marker and first movement cue).

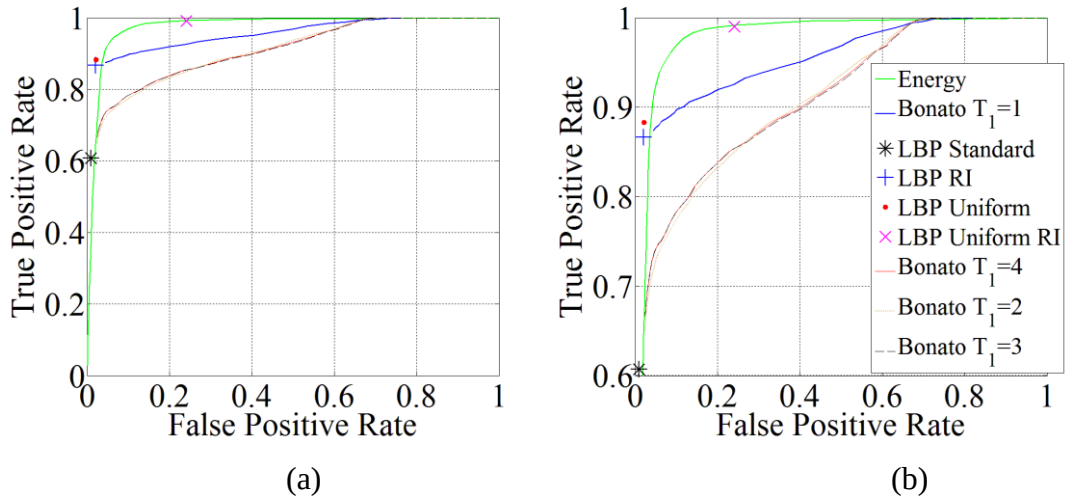

Figure 4.13 – (a) ROC curves and points for activity detection on Data Set 1. (b) The same ROC curves with different axis locations

Figure 4.13 (a) and (b) show ROC curves for Energy, Bonato (T1 = 1) and LBPAD (P = 4) for Data Set 1. The window length was 120 samples (60ms) with no overlap and a 200ms smoothing window for both Energy and LBPAD.

It was observed that the time between a movement cue and EMG activity for all subjects in Data Set 1 was about 200ms. This value was therefore taken as the

reaction time throughout this experiment: EMG onsets and offsets were assumed to be consistently 200ms after the movement and rest cues. All the activity detection methods were compared against this. To investigate the consistency of this standard, different assumptions about the delays were tested: Using 180ms and 220ms assumptions respectively slightly deteriorated the results for all methods. Consequently, a value of 200ms for the reaction time was considered appropriate for Data Set 1.

It is necessary to create a reference template, or 'gold standard', against which activity detection methods can be compared for each trial in the data sets. For this, the movement cues that were recorded with the data sets were used along with the assumption about reaction times discussed above. For an EMG recording session, an 'activity/inactivity' array is made, which is the same length as the recording, where '1' represents activity and '0' represents inactivity' for each sample of the recording. The activity detectors were programmed to produce this same format of output, so that a direct comparison can be made. This way, True Positive Rate (TPR), False Positive Rate (FPR) [119] and accuracy can all be calculated on a sample-by-sample basis.

Figure 4.13 shows ROC curves for the Energy and Bonato methods and symbols to represent the markers for each of the four LBP histogram types, where there are no ROC curves since there are no manual thresholds to sweep. ROC curves are direct indicators of performance (accuracy and robustness). The target for ROC curves is simultaneous maximization of TPR and minimization of FPR values. Figure 4.13 shows that superior TPR and FPR values are possible using LBP with P=4 (chosen experimentally) compared to both Energy and Bonato, for Data Set 1, when using the combined results for all three subjects. For each subject individually, the TPR/FPR achieved was better than or similar to the results for Energy and Bonato's method.

The much noisier Data Set 2 was used for a comparison between the two methods that gave the best results for Data Set 1: Energy and LBPAD. The Bonato method would have required a subjective majority vote system across all eight channels and did not perform as well on Data Set 1.

The results from all thirty subjects were used and the mean values of the combined results were plotted for comparison (Figure 4.14). For LBPAD, the window length was 300ms with 50% overlap for all trials and subjects, with *P* set to 4. The Energy method's performance was better with 60ms windows, which was used. The human reaction time was assumed to be 300ms for this data set (reaction time is discussed in section 2.4), so this was used as the duration of the smoothing filter.

The energy threshold at which 100% False Positive was achieved was first determined. The threshold was then swept between zero and this value in fifty steps logarithmically spaced (i.e. more steps closer to zero) the TPR was calculated at each step. This was done for all 24 trials for each of the 30 subjects, giving 720 ROC curves. The mean TPR at each of the FPR steps was calculated, and the result is shown in Figure 4.14. The markers indicate the results for LBPAD; specifically they are the mean TPRs and FPRs for each of the histogram types. The superior LBPAD performance is evident: the Standard histogram has lower FPR for the same TPR compared to the Energy method.

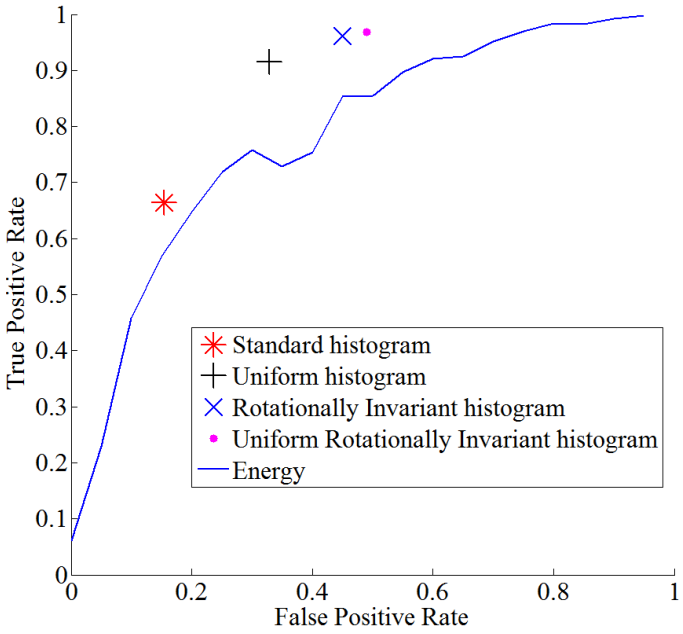

Figure 4.14 - ROC depicting a comparison between Energy and LBPAD combined results from all subjects in Data Set 2.

In Figure 4.14, the ROC curves and points were calculated with $P = 4$, window length 60ms for Energy and 300ms with 50% overlap for LBPAD

4.6. Comparison with classifiers trained to recognize 'no motion' class

LBPAD was also compared with classifiers that were trained to recognize 'motion/no motion' classes. Data Set 1 was used. A Linear Discriminant Analysis (LDA), a Neural Network and a 1v1 Support Vector Machine (SVM) were tested. The mean of the accuracy, TPR and FPR were determined for the three subjects of the data set. The results are shown in Table 4.2.

Method	**Accuracy %**	**SD (σ)**	**TPR**	**FPR**
LBPAD, both channels (RI P=4)	93.9	7.8	0.8829	0.0216
Linear Discriminant	88.2	7.83	0.89	0.08
Linear Support Vector Machine	89.5	6.75	0.83	0.04
NN (3 runs per subject)	92.9	3.21	0.92	0.06
NN with PCA pre-processing (3 runs per subject)	93.2	2.86	0.92	0.05

Table 4.2 Comparison of LBPAD with classifiers

The parameters used in Table 4.2 were as follows: Window length 60 milliseconds using all subjects of Data Set 1, Two channels of Hudgins' Time Domain feature set [9], 40 windows taken 200ms after movement/rest cue, 60ms windows with 30ms overlap, 60/40 training/test ratio.

In this case, the neural network had similar accuracy, better TPR, but worse FPR than LBPAD. In practical prostheses applications, consistency and robustness are important, so superior FPR performance is preferable to avoid unintentional movement. The author's discussions with Touch EMAS[2] have indicated that prosthetic users can compensate for a lower TPR by retrying. Moreover, the statistical nature of neural network training means that the results were not consistent between runs, unlike LBPAD.

[2] Touch EMAS, also known as Touch Bionics, design and manufacture the iLimb, as discussed in chapter 2

4.6.1. Additional test

A separate test was also performed in which the entire Data Set 1 was used. Hudgins Time Domain features were calculated for the EMG signals for windows of the signals the first index marker of each session for each subject, except for 200ms transitional periods that occur between gestures and rest. Assign 'active' or 'rest' labels were assigned to each feature vector as appropriate. SVM, NN and LDA were then trained with identical training data and test with identical validation and test data. These results were compared with the accuracy, TPR and FPR obtained with all of the LBP histograms types and for several values of *P*. Results are shown in Table 4.3.

Accuracies **Histogram Type**	*P*=2	*P*=4	*P*=6	*P*=8
Standard	94.26	93.72	91.89	88.85
RI	94.24	94.28	92.73	90
Uniform		93.72	91.9	88.85
Uniform RI	61.9	83.49	90.48	93.16

TPRs **Histogram Type**	*P*=2	*P*=4	*P*=6	*P*=8
Standard	0.93	0.9234	0.9117	0.8482
RI	0.92	0.9242	0.9202	0.8618
Uniform		0.9234	0.9117	0.8418
Uniform RI	0	0.9977	0.9952	0.9801

FPRs **Histogram Type**	*P*=2	*P*=4	*P*=6	*P*=8
Standard	0.019	0.019	0.017	0.016
RI	0.019	0.02	0.018	0.016
Uniform		0.019	0.017	0.016
Uniform RI	0	0.11	0.065	0.053

Classifier **Classifier Type**	**Accuracy**	**TPR**	**FPR**
LBP (RI *P*=8)	90	0.8618	0.016
SVM	95.89	0.941	0.0261
LDA	92.2	88.35	0.0458
NN	93.4	0.9069	0.0433

Table 4.3 – Results for additional comparison test

It was found that higher overall classification accuracies are gained when NN and SVMs are used. However, it is possible to get a lower FPR at the expense of some TPR and accuracy when LBP is used.

4.7. Comparison between 1-D LBP histogram types for activity detection

The performances of the histogram types were tested across all of Data Set 1 and results are shown in Table 4.4.

Histogram type	Accuracy (%)	TPR	FPR	SD
Standard	83.3	0.6071	0.0098	0.1
Uniform	93.3	0.8661	0.0203	0.0501
Rotationally Invariant	**93.9**	**0.8829**	**0.0216**	**0.0476**
Uniform Rotationally Invariant	85.4	0.9903	0.2414	0.0706

Table 4.4 Comparison between histogram types for activity detection across Data Set 1, *P*=4, window length 60 milliseconds

Table 4.5 shows a comparison of the different histogram types and their performance in LBPAD. The Rotationally Invariant and the Uniform Histograms can be seen to have the best balance between accuracy, TPR and FPR with little difference between them for Data Set 1. The parameters should be chosen experimentally for a given data set and with the SNR taken into consideration.

P	Accuracy (%)	TPR	FPR
2	93.9	0.8852	0.0232
4	93.9	0.8829	0.0216
6	92.2	0.8374	0.0187
8	89.1	0.7562	0.0159
10	83	0.6042	0.0124

Table 4.5 Comparison between values of *P* for Rotationally Invariant histogram across Data Set 1, window length 60 milliseconds

Table 4.5 shows the accuracies, TPR and FPR for different values of *P* across all of Data Set 1. An RI histogram and window length of 60ms (120 samples) were used. The smoothing algorithm was used with length 200ms. *P*=2 and *P*=4 produce similar results with this data set.

4.8. Isolation of transitional periods

The LBPAD algorithm does not detect transitions between non-rest gestures; only transitions to and from rest are identified. As such, all transitions between gestures should be detected as 'activity'. For Data Set 2, the accuracy of detection for these transitional periods between gestures was assessed and the mean was 92-93% for all the histogram types.

4.9. Effects of varying the parameters

4.9.1. Window Length and Overlap

The window length and overlap affect the responsiveness of detection. An activity decision is made for every interval equal in duration to window length minus any overlap. It is generally necessary to use longer windows for lower SNRs, so increasing the overlap improves the responsiveness. However, using very short windows was found experimentally to increase the FPR. Figure 4.15 shows that the accuracy does not vary significantly for window lengths above about 50ms for Data Set 1.

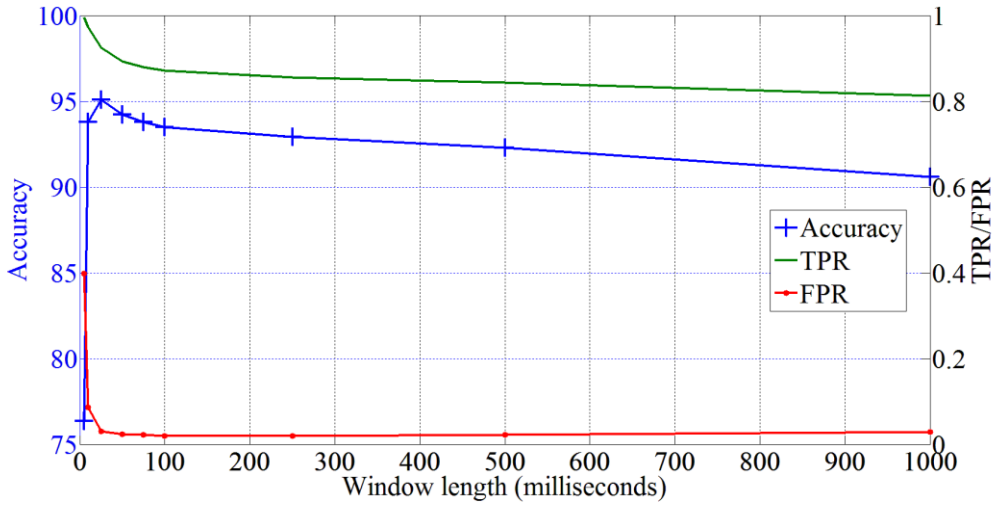

Figure 4.15 - Accuracies obtained by varying the window length across Data Set 1 using LBPAD, Rotationally Invariant histogram, *P*=4

The window length determines the smoothness of the activity detection, but as window length increases, resolution decreases. The use of overlapping windows was found to mitigate this. Degrees of overlap were compared for a fixed window length.

The results in Figure 4.16 indicate that adjusting the overlap improves the FPR slightly but does little to improve the accuracy for Data Set 1.

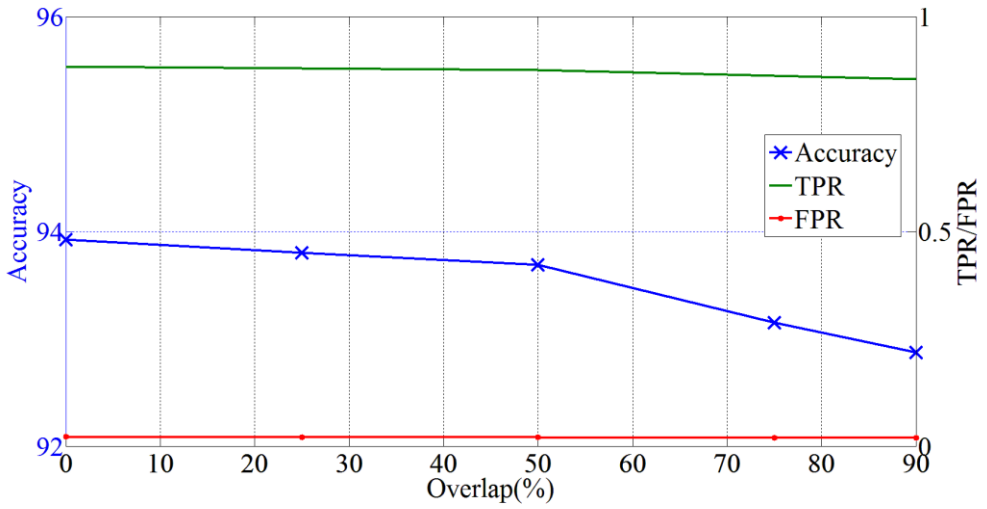

Figure 4.16 - Accuracies obtained by varying the amount of window overlap across Data Set 1 using LBPAD, window length 60 milliseconds, Rotationally Invariant histogram, *P*=4

The length of a window and the overlap are decided by:

- SNR – based on tests with simulated EMG, lower SNRs require longer window lengths
- Desired resolution of activity detection
- Desired smoothness of activity detection
- Value of *P* – typically this was an even value between 4 and 8, inclusive

I can be seen from Figure 4.15 that for Data Set 1, there is little change in TPR or FPR for window lengths longer than about 100ms. There is a steady decline in accuracy as window length approaches 1s in duration, which makes sense as the resolution of LBPAD declines as window length increases. Figure 4.16 shows that window overlap changes the TPR and FPR very little for this data set, but that the accuracy actually declines, and more sharply as it exceeds 50%. The good performance of LPBAD on Data Set 1 and the fact that changing the window parameters has little impact is due to gesture/rest durations being longer than the window lengths tested here. The relatively high SNR is also a factor.

LBPAD does not detect transitions between non-rest gestures; transitions to and from rest are identified.

4.9.2. Histogram type and value of *P*

Specificity and sensitivity can be influenced by the choice of histogram type, as shown in the ROC curve in Figure 4.14. The difference in performance between the histogram types and choice of *P* value can be accounted for by the level of detail that is retained within each window of the signal: The window is described in a different way by each of the histogram types. For example, when the Uniform Rotationally Invariant histogram is used, any local activity that is not uniform and rotationally invariant is placed in the same histogram bin, thus sacrificing any potentially useful discriminatory information that is held within these bins for a higher TPR at the cost of a higher FPR.

The value of *P* sets the number of samples that are used to calculate LBP codes. Changing *P* therefore changes the scope of the observation for the trends that are categorised by the 'activity' bins.

4.9.3. Effects of pre-filtering the signals

It is common to perform noise reduction such as band pass filtering on EMG signals. However, this changes the behaviour of LBPAD. Band passing can reduce the performance of LBPAD. For example, the same signal used in Figure 4.6 was taken, and then the LBPAD was performed. The resulting activity detection is shown in Figure 4.17(a). The distinctive 'crossover' phenomenon of the activity and inactivity bins can be seen in Figure 4.17(b).

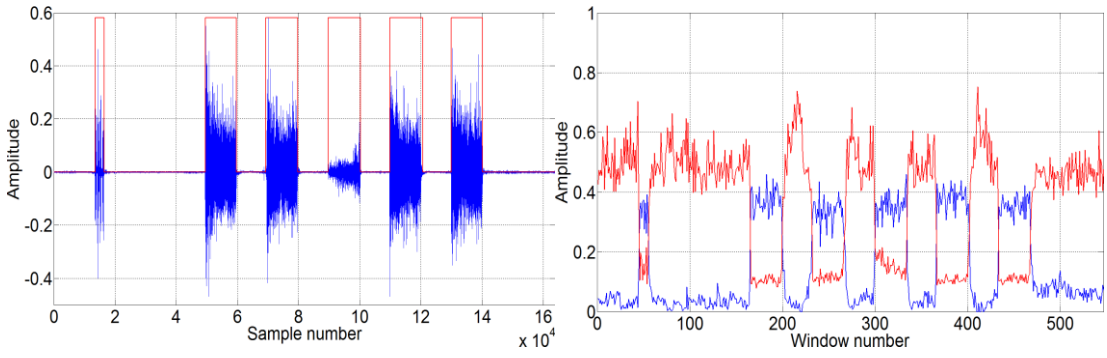

(a) (b)

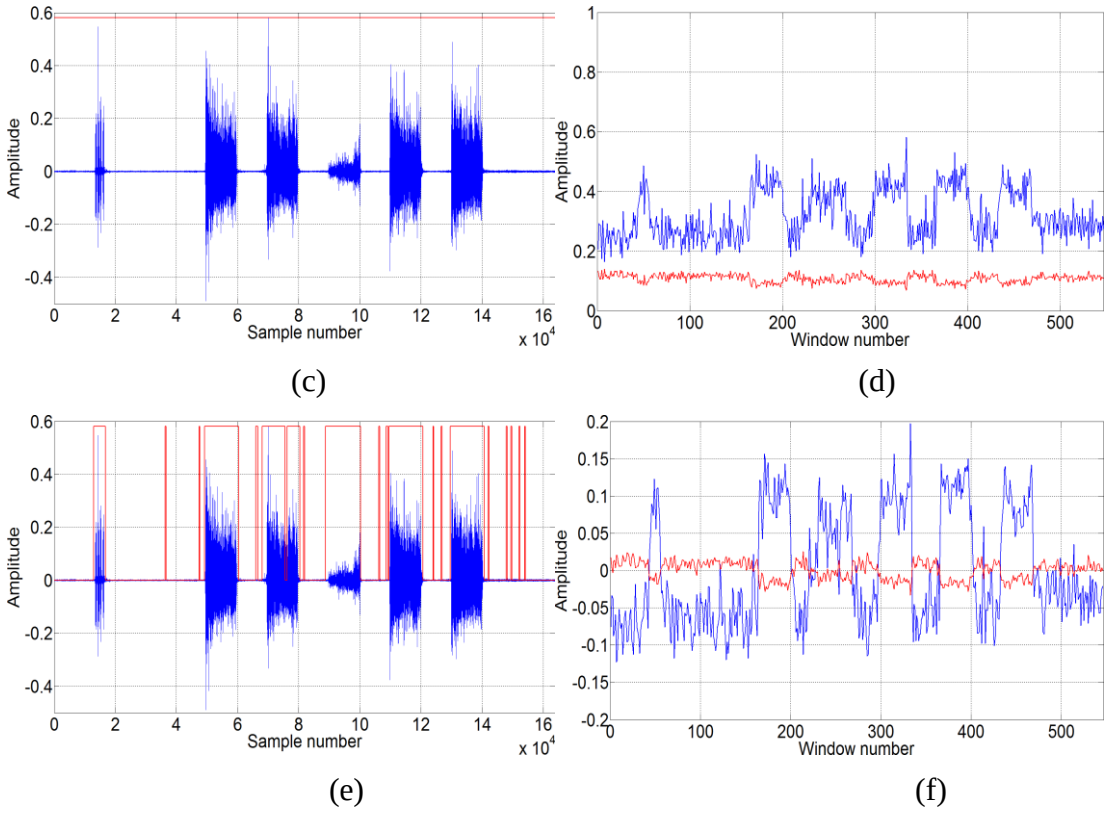

Figure 4.17 – (a) The signal from Figure 4.6 with LBPAD (b) Histogram bin behaviour (c) Signal after band pass filter with LBPAD (d) Histogram bin behaviour (e) Signal after band pass filter with LBPAD with mean removal (f) mean-removed histogram bins

Figure 4.17(c) shows the same signal, but bandpassed, with the activity detected using LBPAD superimposed. It can be seen that the entire signal is detected as activity, and this is because of the loss of bin crossover behaviour in Figure 4.17(d). If the parameters are changed (window length/overlap) and then the mean of both the activity and inactivity bin vectors are subtracted, the bin amplitudes can be directly compared again, as shown in Figure 4.17(f). The resulting activity detection is shown in Figure 4.17(e). The alternative to this 'Mean Removal Trick' would be to apply a manual threshold to the sum of the 'activity' bins. This, however, negates one of the key advantages of LBPAD, i.e. that manual thresholds need not be set.

4.9.3.1. Effect of power line interference

The performance of LBPAD was tested on Data Set 4. It was discovered that pre-filtering the data by notch filtering was necessary to allow LBPAD to perform at all. This indicates that power line interference has a detrimental effect on the performance of LBPAD.

4.10. Discussion

4.10.1. Multiple concurrent EMG channels

As discussed in 3.2, the sum of the energy across all channels within a window must exceed a threshold before activity is declared for that window. This is why energy was chosen for comparison against LBPAD. To get the best possible accuracy for the multi-channel energy method, it was necessary to get the best threshold (and therefore the best results) for each EMG recording in the data set. The window length and overlap were kept at the same values throughout.

For each EMG recording, the energy threshold was swept from 0 (i.e. 100% of the signal detected as 'activity') to the highest maximum energy level in the entire EMG recording (i.e. the value at which none of the recording was detected as activity) in 1000 steps, and the best of these was used for comparison against LBP.

For LBPAD, several values of *P* were tested with each of the four histogram types, and each combination of *P*/histogram type was tested on the entire data set without adjustment. The best combination of *P* and histogram type was then chosen for comparison against the energy method.

Knowledge is not required of the properties (e.g. variance) of a quiescent period or of any thresholds that define such a period. Other approaches rely on the assumption that estimates of the noise can be obtained in this way. Instead, activity/inactivity decisions are made based on the properties of the signal within each window

In the results shown in 4.9.1, the best histogram types for activity detection are Rotationally Invariant and Uniform. The Uniform histogram was also found experimentally to be useful when testing on noisier simulated data. The Uniform Rotationally Invariant method was the most sensitive; it had a higher FPR than the other histogram types, especially if the data was noisy and, therefore, it may not be as useful as an activity detector unless it can be improved by post-processing.

In all the cases studied, choosing window length, *P* (therefore the number of histogram bins) and histogram type to obtain the best accuracy depends on the SNR. For example, for Data Set 1, due to the high SNR, a lower value of *P*, shorter window length and RI histogram were found to be more appropriate. Objective measures of signal quality were discussed in 3.5.

With multiple channel outputs, fair comparisons with methods that are primarily developed for individual channel use, are not easy. In the case of Bonato, a comparison for eight channels would have required a subjective majority vote approach.

Both Energy and LBPAD had lower performance with the noisy Data Set 2, but LBPAD displayed more robustness even though the parameters were not separately adjusted to get the best results for each of the 240 trials that were used.

4.10.2. Refinements

LBPAD gives an activity detection decision for each window of the signal. Some refinements were tested in an attempt to obtain more accurate activity detection locations. The resolution of LBPAD is determined by window length and amount of overlap. A different method was tried:

1. Perform LBPAD
2. Take the two windows where the transition from rest to activity were evaluated
3. Go back halfway between the two windows and calculate another LBP histogram
4. Determine activity/inactivity for this window
5. If ‘active’, go left a quarter window, if ‘inactive’ go right a quarter window
6. Repeat until window size is too small to continue.

The main problem with this approach is that there can be more than one ‘active’ to ‘inactive’ crossover within the two windows. Overall activity detection accuracy was not found to increase when this method was tested.

4.11. Conclusion

In this chapter, the problem of onset and activity detection for EMG was described. Methods were described and discussed. A novel multi-channel EMG activity detection algorithm was presented in this chapter, which uses histograms obtained from the recently developed one-dimensional local binary pattern method. There are a few parameters to set: Window length/overlap, histogram type and P, which determines the number of histogram bins. These are set once for an entire data set, and for the data sets used, results rivalling or improving on those of the Energy and Bonato methods were obtained.

The advantage of the proposed method is that a single activity/inactivity decision is given for multiple channels. The process requires no pre-processing such as whitening. For multiple concurrent EMG channels, the LBP codes, across the concurrent window of each channel, are simply amalgamated into a single histogram, rather than requiring a, usually subjective, Majority Vote mechanism. Increased robustness has also been demonstrated both in terms of lower FPR and in the presence of noise.

4.12. LBP histograms as features for pattern recognition

It was discovered that 1-D LBP histograms extracted from windows of gestures could be used as features for pattern recognition. The results were similar to the Hudgins feature set when higher numbers of channels were available. This leads to the possibility of using the same extracted histogram for LBPAD and as a feature set.

5 Contaminant Identification in Myoelectric Signals

5.1. Introduction

This work was started by the author at Carleton University, Ottawa, Canada. It was carried out under the supervision of Prof Adrian Chan of Department of Systems and Computer Engineering at Carleton University as part of the CleanEMG project. The aim of the CleanEMG project described in [120] is to provide open source, user-friendly methods to automatically assess the quality of EMG signals. Previous research included methods targeted towards the specific contaminant types in EMG recordings that were discussed previously in section 2.3.5.

It is not possible to know in advance what kind of contaminant might be present. Currently, verification of the EMG signal quality during acquisition is performed by human operators using visual inspection, or semi-automated approaches, if it is done at all. In the majority of signal processing algorithms and in pattern recognition, there is an assumption of adequate EMG signal quality, which can lead to invalid results or interpretations if this assumption is incorrect [4, 121, 122].

Quality analysis of biosignals can be organized into the four categories of detection, identification, quantification and mitigation. In [123], it was noted that the "literature base is close to non-existent" with regards to automated biosignal quality analysis. There has recently been a rapid growth in research in this area, which acknowledges a growing need that cannot be met by methods that rely on human involvement, as they are subjective, unreliable or impractical (e.g., time and cost), or simply not feasible (e.g. in real-time prosthetic control). This need is driven by a number of factors including:

1) An increase in monitoring applications
2) The increased use of multichannel systems
3) Continuous monitoring
4) Monitoring in unsupervised environments (e.g., telehealth)
5) Ensuring signal quality in practical implementations (e.g. prosthesis control)

Increased research activity can also be seen in biosignal quality analysis for EMG [44, 75, 100, 101, 120, 124-129].

Biosignal quality analysis provides a link between the signal acquisition and processing by validating the recorded signal to ensure sufficient signal quality prior to subsequent processing. Since the contaminant type would not be known *a priori*, a means of identifying the contaminant in a measurement enables an informed response. For example, automatic identification of the contaminant type could direct an operator how to adjust an acquisition setup to improve the quality of the recording. Identification of the contaminant type could also enable judicious application of signal processing to mitigate contaminants in the recorded signal, possibly paving the way towards real-time contaminant evaluation and mitigation systems.

It was reported in [44] that contaminant *detection* was achieved using a one-class support vector machine (SVM) to determine whether an EMG recording was free of contaminants. In this chapter, several analysis methods are combined for particular contaminants to perform contaminant *identification* (i.e., determine the type or source of contaminant). The outputs from these methods are used as input features to a classifier to evaluate the potential of discerning the contaminant type. The performance of this identification method is evaluated on simulated and real EMG data.

5.2. Methodology

Figure 5.1 shows a block diagram of the pattern classification system. Contaminant identification is performed through pattern classification using Support Vector Machines (SVMs). As indicated in Figure 5.1, the feature extraction process involved quantifying the contamination in the EMG signals using seven of the methods discussed in section 3.3. The outputs of these methods were used as features for a classifier that identified the contaminant type.

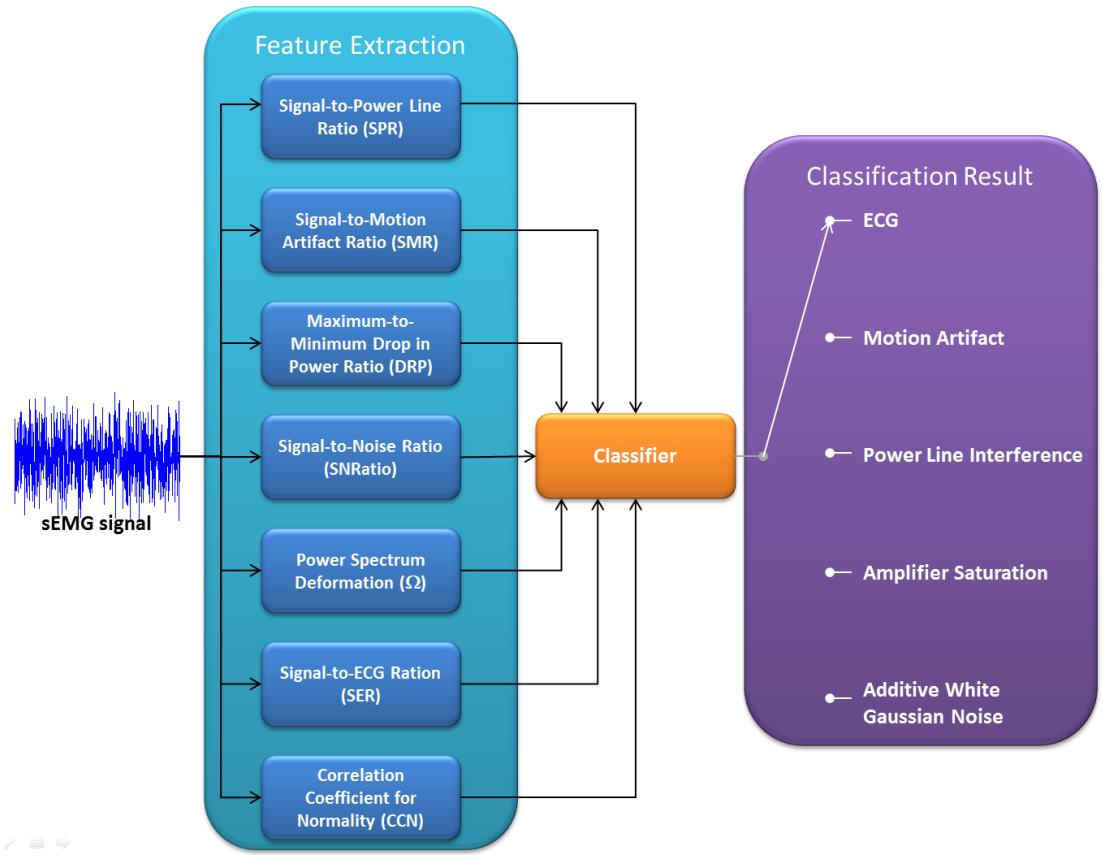

Figure 5.1 - Pattern classification system for identification of the EMG contaminant type

Data Set 3 was used and a simulated EMG data set (see 2.3.4) was made that was the same size and sample rate as Data Set 3.

5.2.1. Artificial Contamination

As shown in Figure 5.1, the contaminants chosen were:

- ECG
- Motion Artifact
- Power Line Interference
- Amplifier Saturation
- Additive White Gaussian Noise

These represent the main contaminant types that can be found in sEMG.

5.3. Classifier Training and Testing

For the simulated EMG data, the dataset was randomly split into four subsets of the same size as the real EMG subsets (as explained next). The classifier training was performed using three of the subsets and testing was carried out on the remaining subset. This process was repeated a total of four times such that each subset was

used as test data on separate neural networks. For the real EMG data, the dataset was split into four subsets based on the four subjects (the number of recordings per subset ranged from 40 to 80).

As shown in Figure 5.1, the features chosen were:

- Signal to Power Line Ratio (SPR)
- Signal to Motion Artifact Ratio (SMR)
- Maximum-to-Minimum Drop in Power Ratio (DPR)
- SNRatio
- Power Spectrum Deformation (Ω)
- Signal to ECG Ratio (SER)
- Correlation Coefficient Test for Normality (CCN)

The EMG data for the training data (Data Set 3) was artificially contaminated with each of the five different contaminants in turn, with an SNR ranging from -20dB to 0dB in steps of 10dB (if the number of EMG signals used in the training dataset was N_{train} then the number of training signals was $N_{train} \times 5$ contaminant types $\times$ 3 noise levels). The EMG data for the testing data was artificially contaminated with each of the five different contaminants, with an SNR ranging from -20dB to 20dB in steps of 5dB (if the number of EMG signals used in the training dataset was N_{test} then the number of test signals was $N_{test} \times 5$ contaminant types $\times$ 9 noise levels). With this setup, only lower levels of SNR were used in the training data, while the testing data uses levels of SNR that are not used for the training data, including high levels of SNR where the contaminant is not visible.

The behaviour of the features is shown in Figure 5.2 to Figure 5.8. Left-hand graphs are for simulated EMG and right-hand graphs are for real EMG.

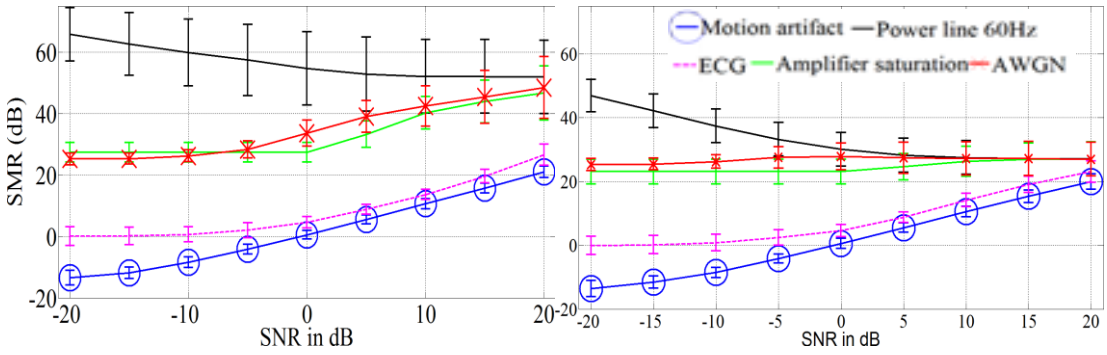

Figure 5.2 – SMR feature behaviour. Left-hand graphs are simulated EMG data set and right-hand graphs are real EMG data set

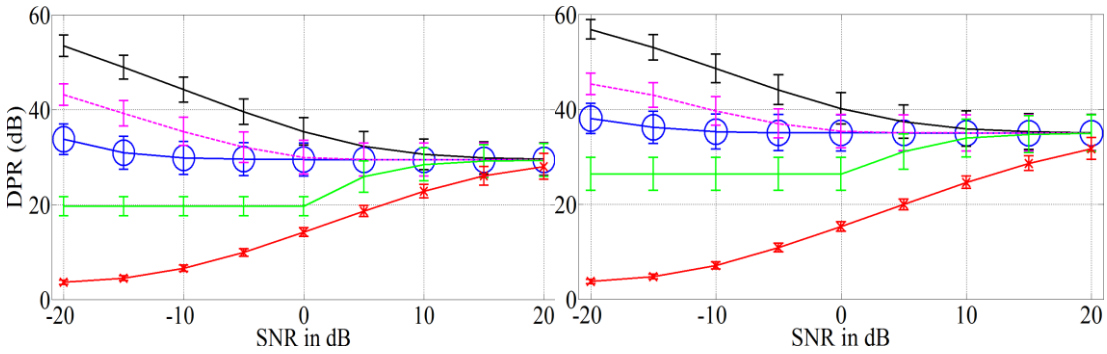

Figure 5.3 – DPR feature behaviour. Left-hand graphs are simulated EMG data set and right-hand graphs are real EMG data set

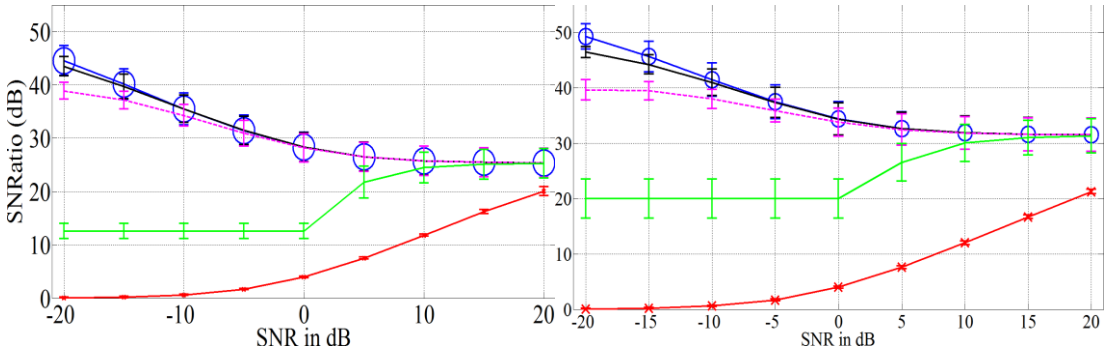

Figure 5.4 – SNRatio feature behaviour. Left-hand graphs are simulated EMG data set and right-hand graphs are real EMG data set

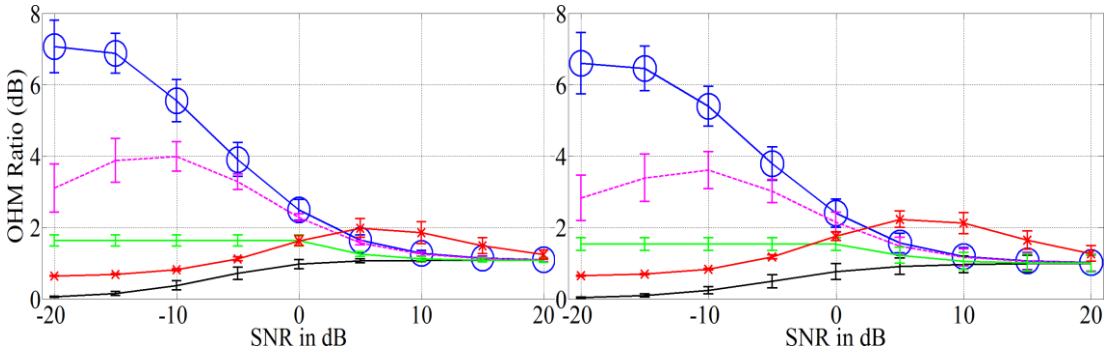

Figure 5.5 - Ω Ratio feature behaviour. Left-hand graphs are simulated EMG data set and right-hand graphs are real EMG data set

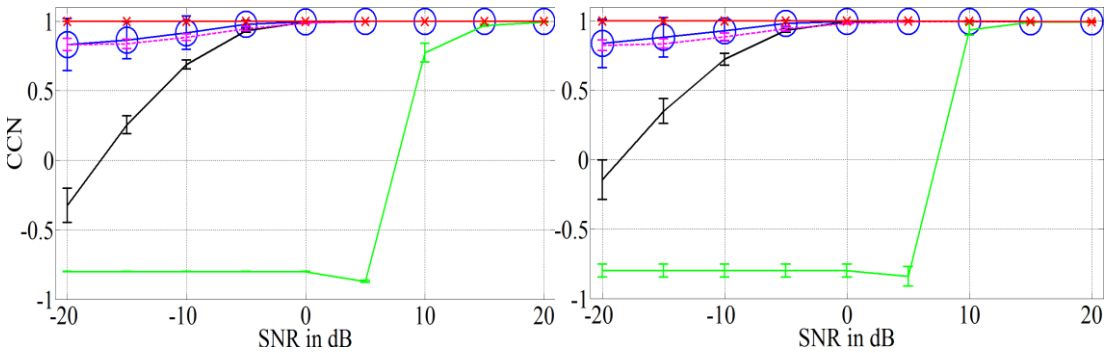

Figure 5.6 – CCN feature behaviour. Left-hand graphs are simulated EMG data set and right-hand graphs are real EMG data set

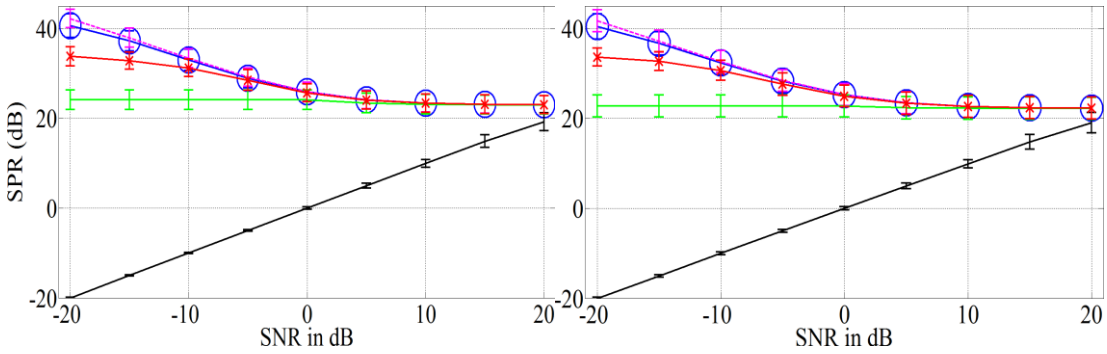

Figure 5.7 – SPR feature behaviour. Left-hand graphs are simulated EMG data set and right-hand graphs are real EMG data set

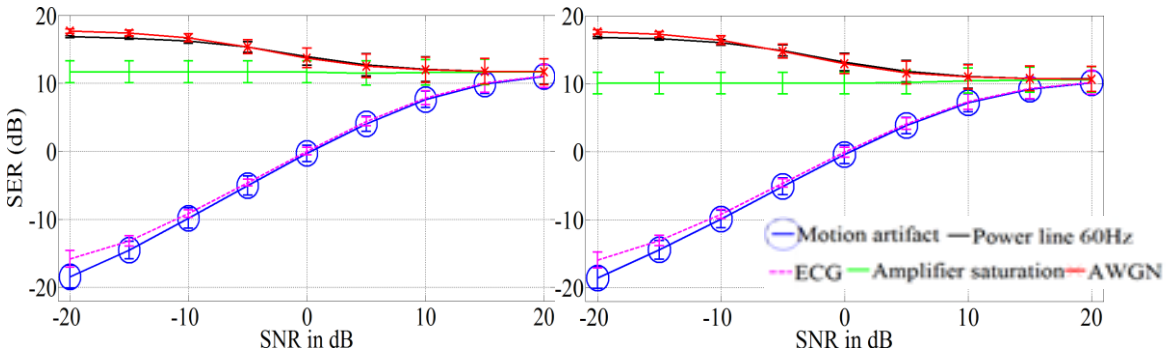

Figure 5.8 – SER feature behaviour. Left-hand graphs are simulated EMG data set and right-hand graphs are real EMG data set

In all graphs in Figure 5.2 to Figure 5.8, the error bars are ±σ (standard deviation) across all recordings. The legend is given above Figure 5.2 applies to all the graphs.

5.4. Results

Accuracies for each contaminant across the range of SNRs are shown in for simulated EMG in Figure 5.9(a) and for real EMG in Figure 5.9(b). As expected, most are misclassified as the SNR increases because the amount of contaminant is low at high SNR, making the contaminant type hard to discern. The type of misclassifications differs between real and simulated EMG.

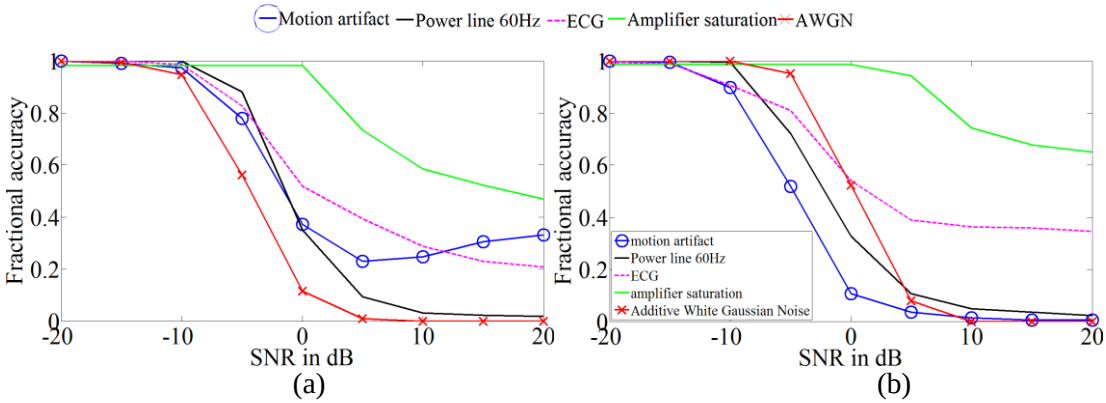

Figure 5.9 - Accuracy of classification for each contaminant as the SNR is changed for simulated EMG (a) and real EMG (b). Classifier is 1v1 Support Vector Machine system with RBF kernels

Figure 5.10 shows confusion matrices for the SNR levels -20 dB to 20 dB in 10 dB steps for (a) simulated EMG and (b) real EMG. The target classes are listed on the horizontal axis and the classifier's output classes are listed on the vertical axis. There were 1130 test vectors at each SNR classified by the SVM. The correctly classified contaminants are on the diagonal running top left to bottom right. For example, in Figure 5.10(a) (top), ECG is in the first vertical column. In Figure 5.10(a) (middle), the second box in the first column indicates that ECG is incorrectly classified as motion artifact for 32.74% of the vectors, at 0dB.

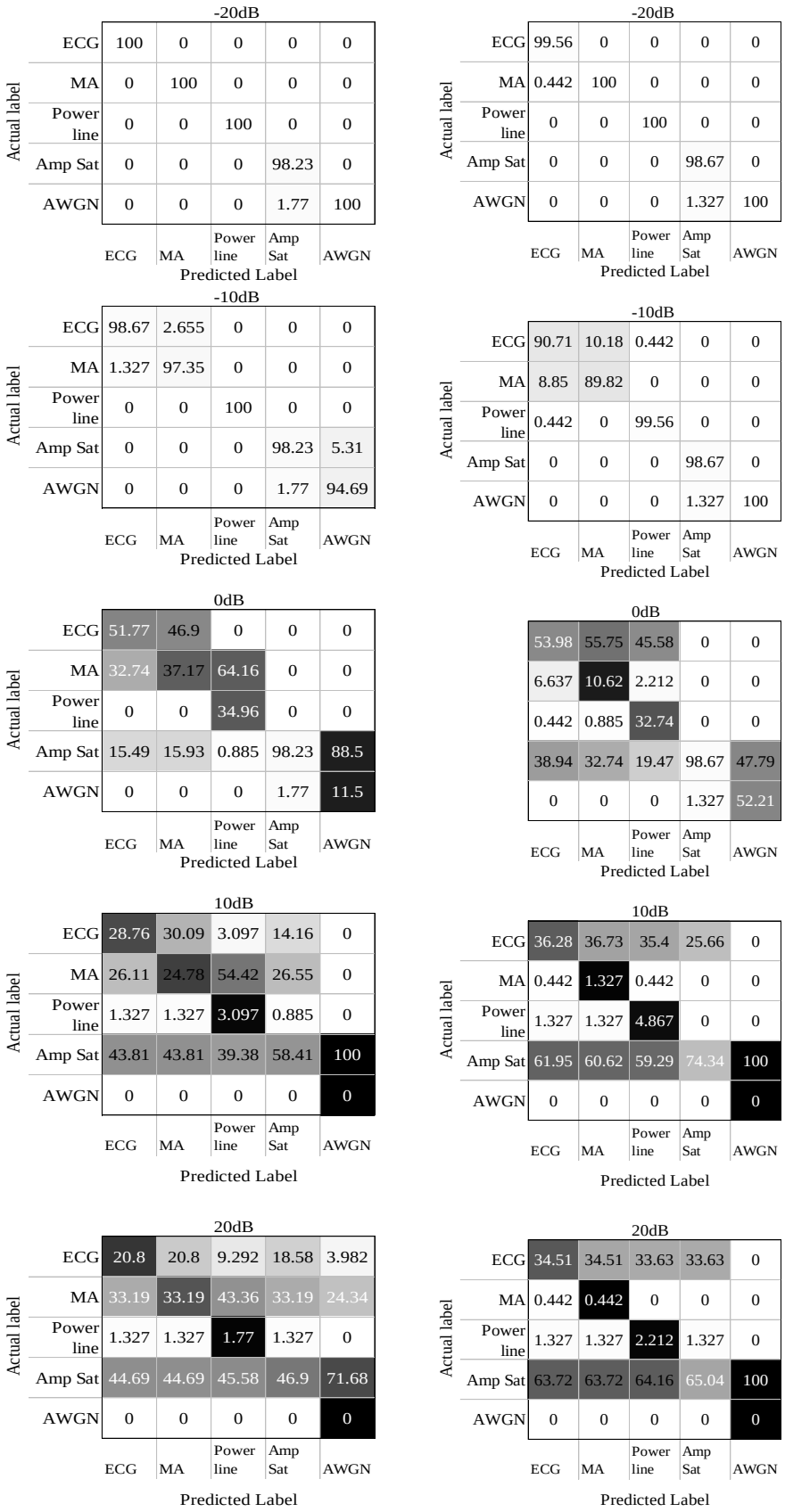

Figure 5.10 - Confusion matrices for different contamination levels simulated EMG (left) and real EMG (right)

Figure 5.10 shows confusion matrices for different contamination levels of simulated EMG (left) and real EMG (right). The darker colours indicate higher errors, so lower values on the top-left to bottom right diagonal have darker shading if accuracy is lower. Higher off-diagonal values have darker shading to show higher confusion.

5.5. Discussion

In Figure 5.10, high classification accuracy was observed at low SNR levels: For simulated EMG, the values for the overall classification accuracies were observed as 100% at -20dB and 97.79% at -10dB. For real EMG, overall classification accuracies were 100% and 95.75% for -20dB and -10dB, respectively. The classification accuracy was around 20% at an SNR of 20 dB, which is equivalent to random chance given that there are five contaminant types. At high levels of SNR, the classifier identifies the contaminants as motion artifact or amplifier saturation for the simulated EMG (Figure 5.10(left) bottom), whereas the classifier seems to favour amplifier saturation and ECG for the real EMG (Figure 5.10(right) bottom).

It is evident from Figure 5.10 that, in general, features in isolation are unable to reliably distinguish between all of the contaminants, especially those with similar characteristics. There is a feature, or combination of features, that can uniquely identify each of the contaminants:

- ECG can be detected by SNRatio, Ω Ratio, SER, although these features are also sensitive to motion artifact.
- SMR, SNRatio, Ω Ratio and SER are sensitive to motion artifact; these features could be used for its detection but there is the potential for confusion with ECG.
- Power line interference is best identified by SPR due to the excellent quantification estimate across the range of SNRs tested and the distinct behaviour of SPR towards the other contaminants.
- CCN can be used to detect, but not quantify, amplifier saturation.
- AWGN is detected by DPR, but DPR is sensitive to changes in all of the contaminants.

At low SNR (-20 dB and -10 dB), the proposed method is successful at identifying the contaminant types with high accuracy. At 0 dB, the contaminants become

difficult to visually discern and, as it would be anticipated, classification accuracy begins to drop (Figure 5.9 (a) and (b)). At high SNR, the classifier performance is equivalent to random chance.

The results obtained in this work are, at this stage, for individual contaminant types but they illustrate the potential which exists for developing methods to identify and mitigate the influence of contamination on acquired EMG signals. This is an important consideration in case of low SNR as it can potentially result in cleaner signal output, whilst preserving a larger frequency spectrum by avoiding indiscriminate signal filtering.

The results also indicate potential issues that need to be resolved by any such methods when applied to signals where there is simultaneous existence of multiple contaminants. Figure 5.10 for example, shows that when misclassification occurs for motion artifact and ECG interference, they are often misclassified as each other. The spectrum of motion artifact completely overlaps that of the ECG and its morphology often resembles that of the P, QRS and T waves [130]. In fact, biosignal quality analysis methods that have attempted to mitigate motion artifact in ECG recordings have noted difficulties due to the similarities of the two signals [130, 131]; therefore, misclassification between motion artifact and ECG interference would be anticipated. Bottom-up approaches that are directed towards a particular contaminant type could be employed to resolve these identification errors; for example, the ECG exhibits characteristics that are near cyclostationary and this could be used to discern it from motion artifact. Other complementary bottom up approaches could similarly be integrated to further increase classification accuracy.

5.5.1. Investigation of fatigue

Due to the length of contractions recorded in the real EMG, there is the possibility that fatigue could affect its frequency spectrum and therefore the features. To test for this, the median frequency of the first 5s of each real EMG recording was compared with the median frequency of the second 5s. No trend was discernable, with some increasing in median frequency and some decreasing. The changes were less than half of a standard deviation. In addition, the similarity in the results between the

simulated EMG, which definitely would not exhibit fatigue, and real EMG indicates that fatigue had little effect on the signals.

As the SNR increases, the impact of the contaminant upon signal usefulness is reduced. A contaminant detection method such as the one in [44] could be used, before the contaminant identification process, to screen out data that is uncontaminated or has high SNR.

To investigate the effect of using shorter windows, the 10-second recordings were split into 1s and 2s analysis windows. The classification accuracies compared against 5s windows are shown in Figure 5.11.

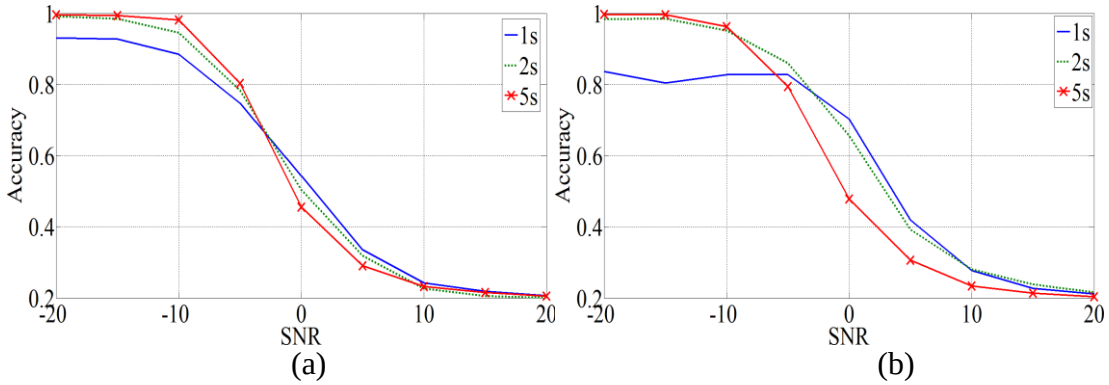

Figure 5.11 - Overall classification accuracies for 1 s, 2s and 5s windows for (a) simulated EMG and (b) real EMG

Figure 5.11 shows that at low SNR levels, the classification accuracy decreased as the length of the analysis window decreased; this would be anticipated as a reduced number of data points would result in an increased variance in the signal features. This decrease was more apparent in the real EMG, perhaps associated with the larger variability that could be expected with real data, relative to the simulated data. At higher SNR levels, the classification accuracy appeared to be better for shorter analysis windows, with a larger difference noted for the real EMG. At the highest SNR level (20dB) the classification accuracies were all around 20% (equivalent to random guessing) but the influence of the contaminant is less significant. This suggests that a minimum useful window length in this case is between 1s and 2s.

The results obtained in this work indicate that automated procedures to detect the presence of contaminants, and even identify the types of contaminants present in signals, are indeed possible, particularly when SNR values are low. Automated

identification of contaminants could trigger bottom-up approaches (e.g. moving average [77]), for quantifying, mitigating or simply rejecting the contaminated signals.

5.6. Classifier Choice

The choice of classifier was Radial Basis Function Support Vector Machines. Linear and Quadratic Discriminant Analysis were tested, but these variants would not converge to a solution when the SNR was high. Fuzzy Logic was considered, but time constraints during the placement precluded their use. Linear SVMs did converge but the RBF SVMs produced better results at higher SNRs. The trade-off was that the grid search for the best RBF parameters took a long time [62].

5.7. Other feature types

Several other feature types were tested in place of (*not* in addition to) the signal quality feature set. The Hudgins Time Domain features were tested in place of the signal quality features. The results were significantly worse because they are not directly designed to respond to the presence of the noise types used in this work. As discussed in section 2.5.6.3, the variances of the IMFs can be used as a means of noise identification. For example, the variance of IMFs of a signal consisting of steady-state simulated EMG are shown in Figure 3.1. The results were encouraging, but no better than the results when the measurements discussed in section 3.5 were used. The applicability of the IMF variance behaviour for noise identification is worthy of further study.

5.8. Conclusion

Several identification methods were combined and used as features for the classification system in this chapter. It has been shown that a classifier can be trained to produce a single decision on the identity of the contaminant. The methodology presented in this chapter expands on previous work where the presence of contaminants was detected [44] by also identifying the type of contaminants. Identification of the contaminant type can validate measurement setups, providing direction to operators for appropriate action if the signal quality is inadequate. The

initial findings for shorter windows indicate that future real-time evaluation and mitigation of contaminants in EMG signals could be possible.

It is encouraging that the results for simulated and real EMG are similar. This shows that the effects of any residual contamination in the real EMG are low to negligible.

6 Spectral Enhancement for EMG

6.1. Introduction

In this chapter, the applicability of Spectral Enhancement for EMG signals will be examined. Minimum Statistics Noise Estimation (MSNE) and Spectral Enhancement based on IMCRA (IMCRA SE, which referred to as IMCRA/OMLSA in [105]) will be investigated as means of improving the classification accuracy of a pattern recognition system that is trained to recognise gestures from noisy multi-channel EMG. It will also be compared against other noise reduction methods.

MSNE and IMCRA SE were developed for single-channel speech where neither a clean reference signal nor a noise reference source are available. Some noise reduction methods such as Wiener Filtering [132] require such a reference. In forearm EMG, there is no clean reference, but there are often multiple surface channels with crosstalk and therefore redundant information between the channels, as discussed in Section 2.3.2.

The only prior instance of the application of spectral enhancement to EMG was spectral subtraction in [81], where the mean spectrum of the noise is calculated across several 'noise only' STFT windows to account for its variation. The mean noise spectrum is then subtracted across the STFT windows of the entire signal.

Figure 6.1 shows spectral enhancement placed in the context of a pattern recognition system that is trained to recognise gestures from featured extracted from EMG.

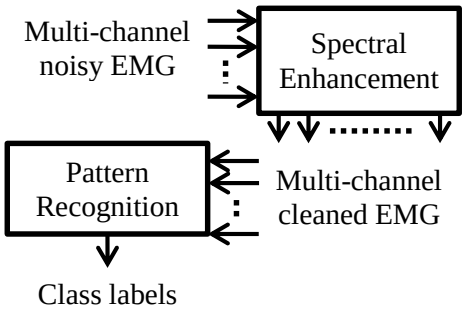

Figure 6.1 - EMG is pre-processed using Spectral Enhancement on each channel individually, and then pattern recognition is performed

In Figure 6.1, the pattern recognition system is trained and validated using features extracted from the spectrally enhanced EMG. As discussed in section 3.6, spectral

enhancement assumes that the signal and noise are uncorrelated, which is the case for white noise in EMG [99]. Dynamic recordings of real EMG were needed, and for this reason, Data Set 2 and Data Set 4 (see Section 2.3.5) were used for the noise reduction research. AWGN was added to Data Set 2, and Data Set 4 was already noisy.

A detailed description of IMCRA and MSNE can be found [109, 133] and an outline of IMCRA is given in Appendix A.

6.2. IMCRA SE applied to EMG

In this section, the behaviour of spectral enhancement upon EMG will be demonstrated. The example in Figure 6.2 below is of a single channel of EMG from Data Set 1 consisting of five five-second recordings separated by five-second inactivity periods. The signal is shown in the time domain in Figure 6.2(a). IMCRA SE was applied to the signal, and the result is shown in a lighter shade on the same graph. In Figure 6.2 (a), (b) and (d), the gesture instructions are shown by thick solid vertical lines and rest instructions by thin dashed vertical lines.

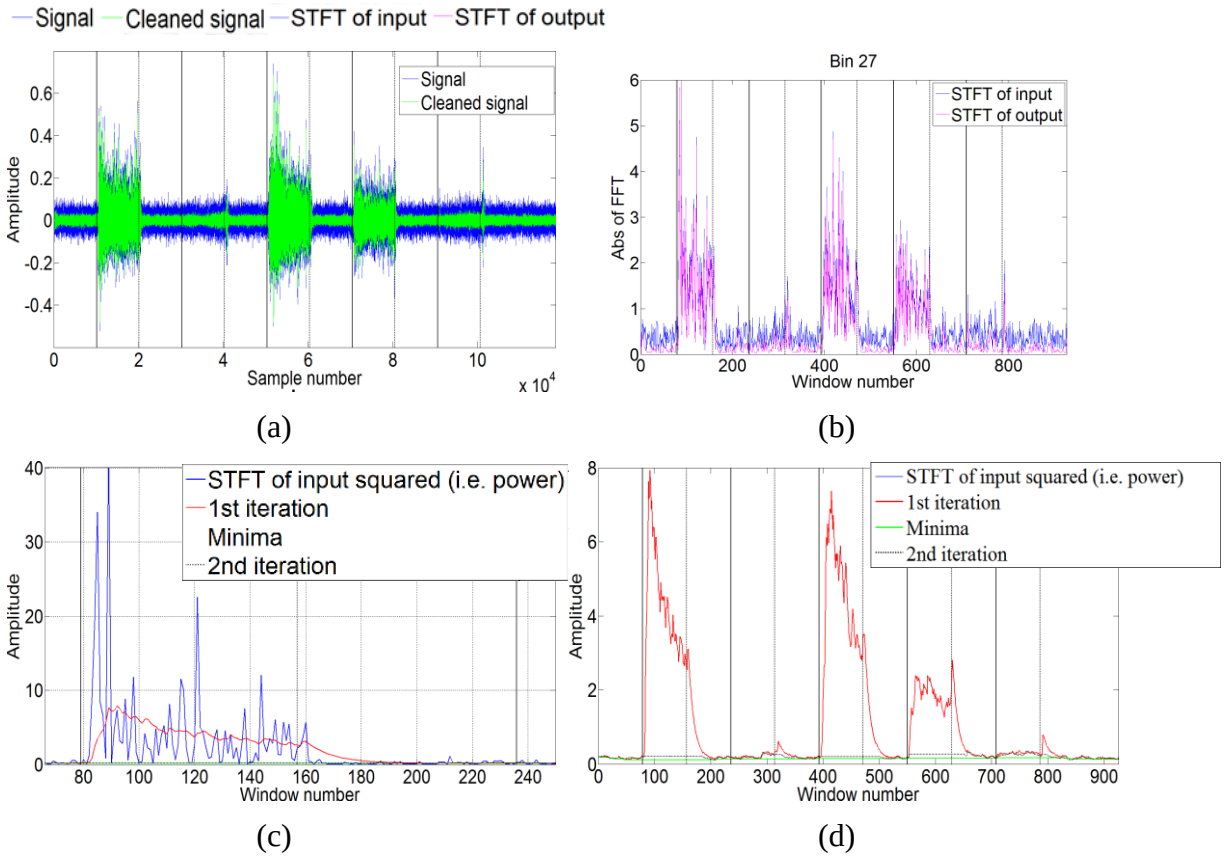

Figure 6.2 (a) Bin 27 from a recording of EMG of five gestures from Data Set 1 (b) magnitude of the STFT of the signal and its cleaned version (c) square of STFT bin and smoothed version of the first gesture (d) smoothed power spectrum

One DFT bin was chosen to demonstrate the behaviour of IMCRA towards EMG. Figure 6.2(b) shows the absolute value of the STFT of bin 27 (centre frequency 158.2Hz) before and after IMCRA SE is applied. It can be seen that the inactivity periods have been attenuated more than the gesture periods. Figure 6.2(c) shows the square of the DFT bin (light) and the smoothed power spectrum (dark) for bin 27. A single gesture is shown for clarity. Figure 6.2(d) shows the first iteration of the smoothed power spectrum (continuous line), the second iteration (dashed line) and the minima tracking (dotted line) for bin 27. The figure indicates that the recursive spectral smoothing in IMCRA SE is effective at omitting the three stronger gestures from the spectral noise estimate.

All the channels of Trial 4 of Session 2 of Subject 11 from Data Set 2 were examined in the time and time-frequency domain. Then the data was band pass filtered and IMCRA SE was applied. The results are shown in Appendix B. The solid vertical

lines represent an instruction to the subject to perform a gesture and the dashed vertical lines represent 'rest' instructions.

AWGN contains noise at all frequencies, so it is useful for assessing the performance of noise reduction algorithms across frequency and time. AWGN was added to channel 6 (a dorsal site near the lateral epicondyle) from a recording from Data Set 2. The result is shown in Figure 6.3.

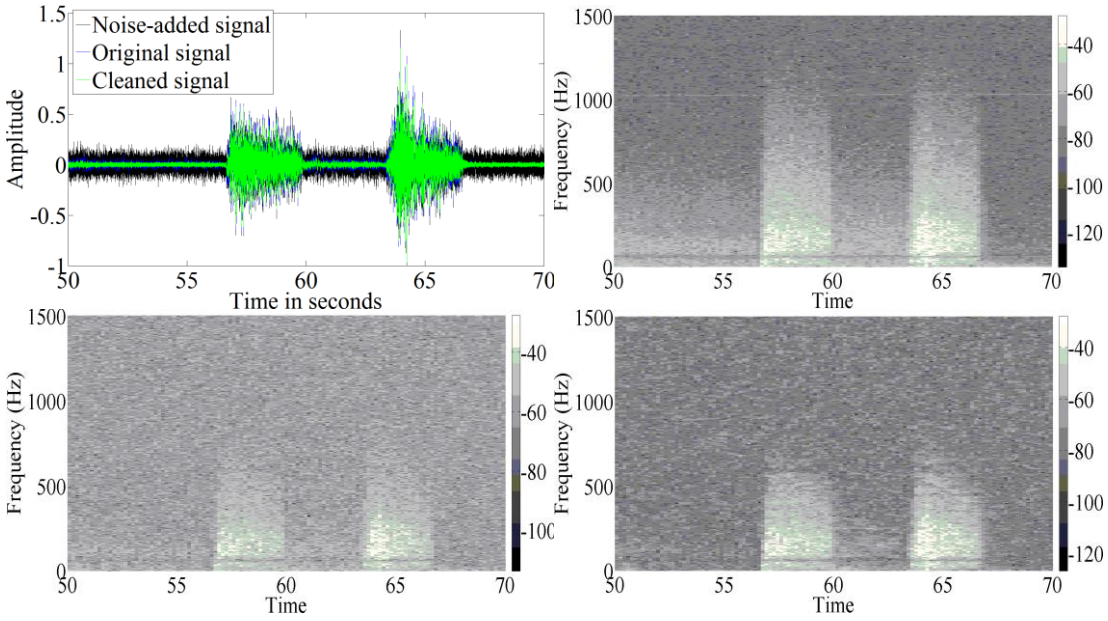

Figure 6.3 - Example of IMCRA SE applied to EMG from Data Set 2 that has AWGN added

Figure 6.3(a) shows time domain representations of the noisy and clean signals. The lighter-coloured de-noised signal is shown superimposed on the signal with added noise. The movement sequence is hand close; wrist extension; wrist flexion; wrist extension; rest. Figure 6.3(b) shows the spectrogram of the original signal. Figure 6.3(c) shows the spectrogram of the signal with AWGN added, and finally Figure 6.3(d) shows the spectrogram of the signal after IMCRA SE has been applied. These spectrograms suggest that the added AWGN is reduced while much of the energy from the stronger gestures remains, which indicates that IMCRA SE is capable of estimating background noise in offline EMG signals.

Three different examples have been given, which indicate that IMCRA is applicable to EMG signals for the purposes of spectral enhancement. In the following section, the parameters will be configured.

6.3. Configuring IMCRA for EMG

In order to get the best possible improvement in classification accuracy when applying IMCRA SE to Data Sets 2 and 4, it was necessary to change the values until the best possible classification accuracy was obtained for the entire data set. The values of many of the parameters given in [109, 133] were optimised for speech sampled at 16kHz, so empirical tests had to be performed to determine the best values of the parameters for EMG. The parameters were changed one at a time and then, if there was an improvement in accuracy, the best value was kept and the other values were then tested. IMCRA SE was applied to each EMG channel independently. IMCRA assumes that the first window of the signal contains only noise, which is true for Data Sets 2 and 4.

The most important parameters were found to be L, V and U. L is the size of the STFT window in IMCRA, which determines (by definition) the number of FFT bins and is therefore a power of two in length. U and V set the number of samples and frames over which the minima are tracked and updated. The values used for IMCRA with Data Sets 2 and 4, which are shown in Table 6.1, were decided with empirical tests in which a range of values for each parameter were systematically tested in turn to assess the effect upon classification accuracy.

Name	Description	Value used Data Set 2	Value used Data Set 4
L	Length of FFT window	256	512
V	Minimum of current sub-window of *V* samples	15	10
U	Number of sub-windows within the *V* samples for minima tracking	4	4
α	Smoothing factor for recursive spectral estimation	0.92	0.92
α_d	Smoothing factor for noise	0.85	0.85
α_s	Smoothing factor for minima spectrum	0.9	0.9

Table 6.1 – Values used for IMCRA Spectral Enhancement for Data Set 2 and Data Set 4

The conditional gain G_h was tested in place of the recursively-smoothed conditional gain *G*, and the classification accuracy was found to consistently improve for Data Set 2. Therefore, G_h was used throughout this work, which means that the presence probability was not used in the recursive smoothing of the spectral gain.

The quantities α, α_d and α_s are smoothing factors, the values of which determine the smoothness of the recursive spectral estimation for the signal, noise and minima spectrum respectively. These were also configured experimentally by assessing the change in classification accuracies.

IMCRA compares the PDF of the STFT coefficient magnitudes with a PDF, in order to estimate the noise content of the signal [73]. This is discussed in Appendix A. A Gaussian PDF was chosen for this work, but a Gamma distribution might also be considered to be appropriate depending on the contraction level in the window [134, 135]. For example, a Gaussian distribution was chosen in [135] based on the assumption of constant-force, constant-angle and non-fatiguing contractions. The short FFT window sizes mean that the EMG can be considered effectively stationary [65].

The purpose of the bias of the minimum noise estimate, B_{min}, is to minimise attenuation of weak speech components. A value was calculated using the inverse of the mean of $S_{min}(k,l)$ in accordance with [109, 133] and found to be 0.04 for Data Set 2. However, using this value in fact reduced the classification accuracy.

6.4. Methodology

Spectral enhancement (MSNE and IMCRA SE) were compared against other noise reduction techniques. Three different approaches were taken. Firstly, the change in signal quality for noisy simulated EMG was tested before and after the application of each noise reduction method. Second, the change in classification accuracy was measured for Data Set 2 with added AWGN added at various levels. Finally, classification accuracy for Data Set 4 was examined for different numbers of channels with and without noise reduction.

Table 6.2 lists the noise reduction methods against which spectral enhancement was compared. Details of these methods were given in section 3.5.

A	EMG with AWGN added	I	EMD: sum of first three IMFs applied to signal A
B	Band pass of A	J	EMD: sum of first three IMFs then band pass applied to signal A
C	IMCRA SE applied to signal A	K	EMD: IMF thresholding [104] applied to signal A
D	IMCRA SE then band pass applied to A	L	EMD: IMF thresholding [104] then band pass applied to signal A
E	Wavelet [81] applied to signal A	M	Band pass of the raw EMG (i.e. EMG with no added AWGN)
F	Wavelet [81] then band pass applied to signal A	N	Wiener applied to signal A
G	MSNE [111] applied to signal A	O	Wiener then band pass applied to signal A
H	MSNE [111] then band pass applied to signal A		

Table 6.2 - Noise reduction methods that were compared

It was necessary to check whether the application of spectral enhancement adversely affected the signal quality. To do this, the objective measures of signal quality discussed in section 3.5 were used. SNR, DP Ratio, Ω Ratio and SNRatio were assessed before and after the application of IMCRA SE for both data sets.

For each of the seven lower-arm channels of each recording in Data Set 2, the mean power of the 'gesture only' parts was calculated. Three contaminated data sets were created by adding AWGN at -10dB, -5dB and 0dB relative to these values for every channel of every trial.

A set of linear Support Vector Machines (SVMs) was used to classify gestures because LDA classifiers failed to converge at the higher noise levels and because the grid method for finding optimum RBF SVM [62] parameters took excessively long to calculate (i.e. several days per subject). For the feature extraction, window length was 300ms with an overlap of 150ms, and ten windows were taken from each gesture. For each subject, half of the data (12 of the trials) were used for training and half for testing. This was done for each trial all thirty subjects. The mean and standard deviations of all of the accuracies across all trials of all subjects was then taken. Classification accuracy from the bandpassed 'clean' data was used as the reference.

For Data Set 4, Linear Discriminant Analysis was used for classification [10]. The gesture classification accuracies for all combinations of two channels out of sixteen were calculated, and then the mean across all combinations for all five subjects was taken. This was repeated for four, six, eight, ten, twelve and fourteen channel combinations for each of the processes tested, to allow a comparison of spectral enhancement against the effectiveness of adding more channels. The mean accuracy across all subjects when all sixteen channels were used was assessed for each process and used as the reference.

6.5. Results

6.5.1. Signal Properties of Simulated EMG

The properties of the simulated EMG that was contaminated with AWGN at 0dB were investigated before and after each of the noise reduction techniques. The results varied greatly depending on whether band pass filtering was also used. For this reason, results both with and without band pass filtering are given below. The SNR, DP Ratio, SN Ratio and Ω Ratio before and after noise reduction were investigated using the methods described in section 3.5. The results are shown in Figure 6.4.

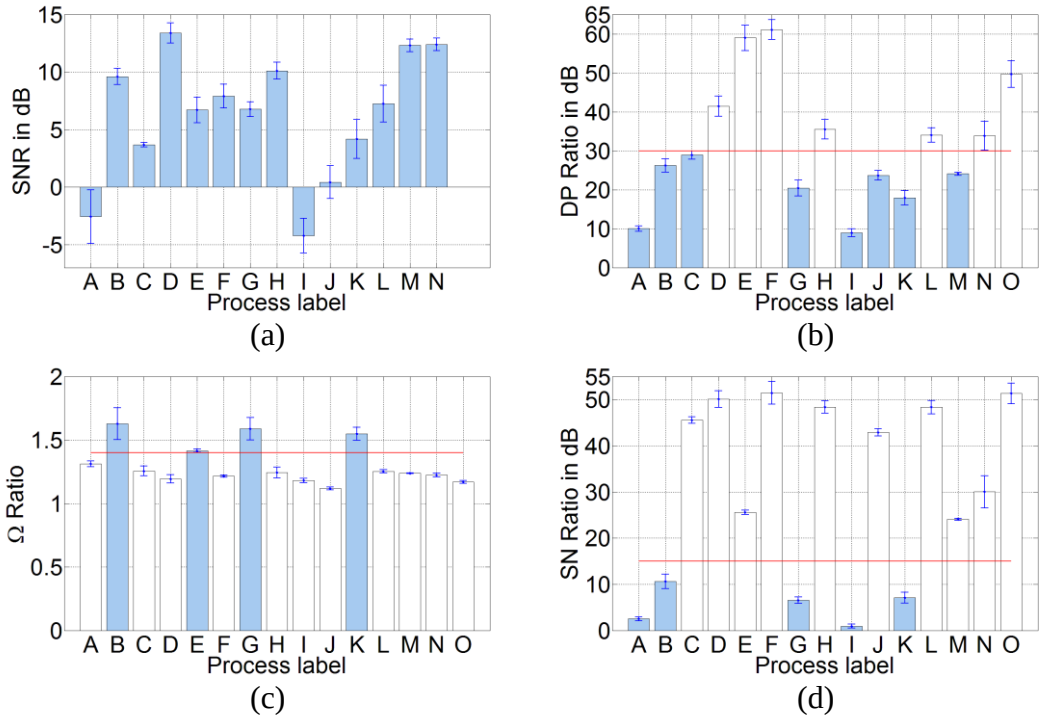

Figure 6.4 - Mean change in signal properties for each of the filtering types with AWGN @ 0dB SNR. (a) SNR, (b) DP ratio, (c) Ω Ratio, (d) SN Ratio.

Some recommended values were given in [75]: maximum Ω Ratio is 1.4 (lower is better), minimum DP Ratio is 30dB, minimum SNRatio is 15dB. Figure 6.4 shows the mean change in the signal properties for each of the filtering types across the 500 simulated gestures with AWGN added at 0dB SNR. In Figure 6.4(b) the horizontal line is minimum DP Ratio. In Figure 6.4(c) the horizontal line is the maximum Ω Ratio [75]. In Figure 6.4(d), the horizontal line is the SN Ratio for the raw signal. For parts (b)-(d), the methods that have adequate performance (in accordance with the limits from the references) are highlighted in white.

Figure 6.4 shows that Wiener (N and O with and without band pass respectively) has the most consistent improvement in all criteria compared with the other methods. However, Wiener filtering requires a clean reference, which is available for this simulated data set, but will be unavailable in a real EMG-based control system. The results obtained using IMCRA SE along with band passing restored the DP Ratio, Ω Ratio and SN Ratio to within the ranges recommended in [75]. Figure 6.4(d) shows that band passing the signal improves the Ω Ratio regardless of any additional processing.

6.5.2. Classification accuracy

The changes in classification accuracy for each of the processing types was investigated using the method listed in Table 6.2. The classification accuracy results are shown in Figure 6.5.

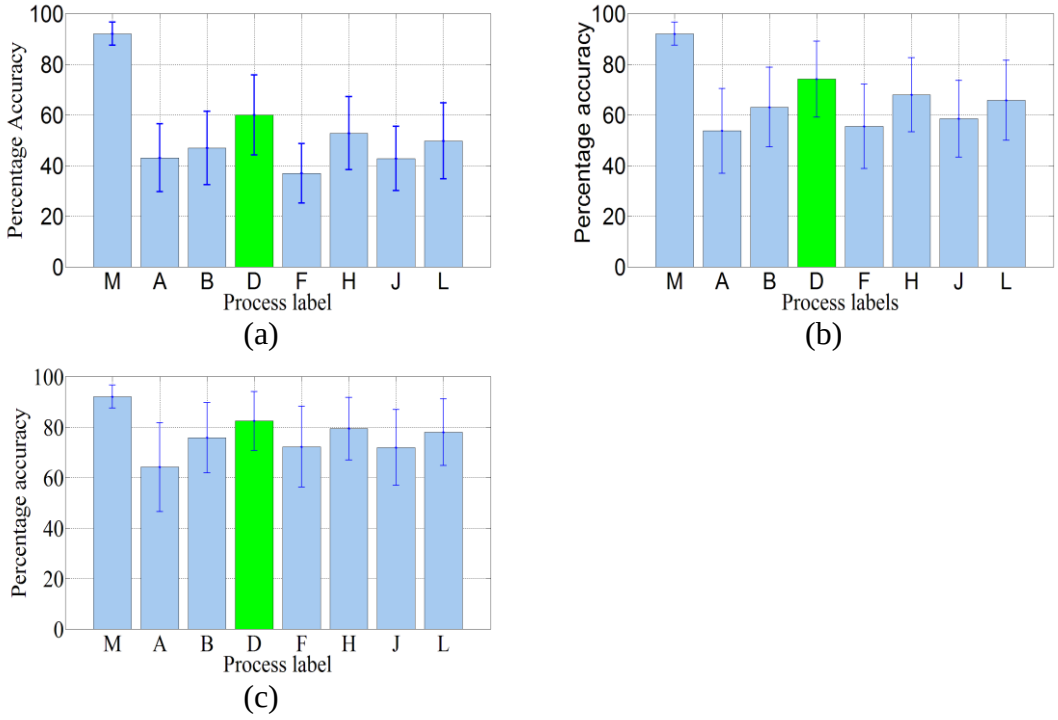

Figure 6.5 - Mean accuracies across all subjects of Data Set 2 for all processes with AWGN added (a) at -10dB, (b) at -5dB, (c) at 0dB

Figure 6.5 shows the improvement in classification accuracy when Data Set 2 has been contaminated with white noise at various levels relative to the mean power of the 'gesture' parts of each of the signals. The error bars are ±1 Standard Deviation (SD). Processes labels are defined in Table II. IMCRA with band pass is highlighted. In all parts of Figure 6.5, bar 'M' shows the accuracy for the unfiltered clean data, which is 92%. Figure 6.5 (a) show the results for noise added at -10dB relative to the mean gesture power, where the accuracy 'A' (signal with AWGN added) is 43%. IMCRA SE (labelled D in the graphs) is best at restoring the accuracy to 59.9%. There is a similar trend in improvement at -5dB in (b) and at 0dB in (c).

6.5.3. Classification accuracy using real noisy EMG

Data Set 4 has high levels of power line interference, so notch filtering is applied along with band pass filtering before IMCRA SE is applied. The classification

accuracy for all possible combinations of two channels was calculated (e.g. channels 1 and 2, then channels 1 and 3 up to channels 15 and 16), and then the mean across all these combinations was taken. The same process was repeated for all combinations of 4 channels, and then all combinations of 6, 8, 10, 12 and 14 channels. These results are shown in Figure 6.6.

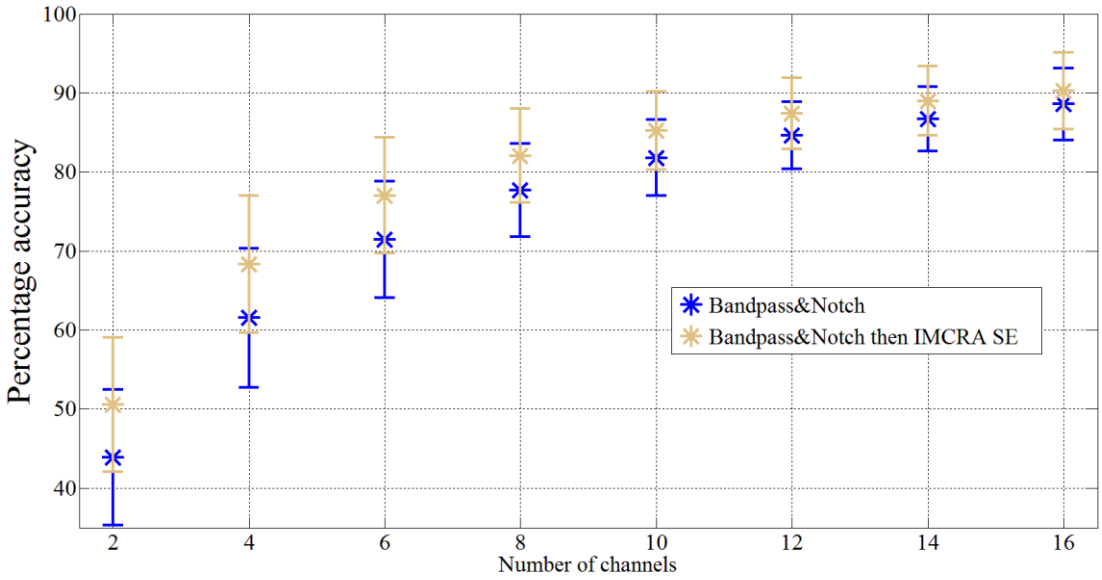

Figure 6.6 - Mean accuracies across all five subjects for Data Set 4

Figure 6.6 shows the classification accuracy for 2-16 channels with and without IMCRA SE. The error bars are ±1 standard deviation. Classification accuracy for Data Set 4 is high for all five subjects when all sixteen channels are used. As could be expected, the accuracy drops as fewer channels are used. The drop-off is lessened if IMCRA SE is applied, and the improvement is greater for fewer channels. For example, for two channels, the accuracy jumps from a mean of 43.9% to 50.6%. For four channels, the mean accuracy jumps from 61.5% to 68.3%. For sixteen channels, the mean accuracy across all subjects increases slightly from 88.58% to 90.2%.

The mean improvements range between 1.5× standard deviation for two channels to 1.3× standard deviation for 16 channels.

6.6. Discussion

Figure 6.4 shows that the measurements of signal quality found in [75] are affected in different ways by each of the methods, and that both MSNE and IMCRA SE restore the values of the measurements to within the acceptable ranges given in [75].

Confidence that noise is being removed is increased by the observation that the classification accuracy of the pattern recognition systems is improved when IMCRA SE is used on Data Sets 2 (with noise added) and 4 (with intrinsic noise). A possible mechanism by this is achieved might be that the 'overwhelming' measurement noise is reduced in the parts of the signals that have a low MVC [99].

IMCRA SE was shown to be superior to wavelet-based noise reduction and Empirical Mode Decomposition. This was tested using real myoelectric signals with artificially added white noise, as well as with intrinsically noisy signals. Figure 6.5 shows that, of all the methods tested, IMCRA SE is the most effective at recovering the classification accuracy in this situation.

IMCRA is sensitive to initial conditions: it is important that the first window consist only of noise. A test was performed in which the noise estimation started during a gesture. The IMCRA estimator assumed that this was the noise floor, so the rest of the signal was attenuated accordingly, which rendered the signals useless for pattern recognition.

The results from Data Set 2 changed mostly by a little either way if IMCRA SE was applied to the 'clean' signals. This indicated that the noise estimation was not overzealous.

The length of the window (L) is determined by the need for the classifier to respond within human reaction time: Changing L to 1024 for the real EMG increased the accuracy slightly for Data Set 4, but this is longer than the 300ms reaction time.

To determine the effects of varying parameters, the values of the smoothing factors are critical. The values of α and V determine the trade-off between signal attenuation and noise reduction. V must not be too high or too much of the weaker spectrogram components of the EMG will be excessively attenuated. The forgetting factor, α, a, must not be too low or the spectral peaks caused by gestures will be insufficiently strong. The values of α_d (recursive time-smoothing parameter for the noise) and α_s (smoothing parameter for second iteration of noise estimation) are also important. Most of the parameter values for IMCRA in [109, 133] were found to be lead to an improvement in signal quality and classification accuracy without any adjustment.

Figure 6.6 shows IMCRA SE can recover some classification accuracy for Data Set 4 (noisy real EMG) when fewer channels are used. There were diminishing returns on the use of IMCRA SE as more channels were used. It was discovered that increasing the number of EMG channels improves the classification accuracy for very noisy data even if noise reduction is not used. If there are fewer channels, then IMCRA SE provides its most significant improvement in accuracy.

IMCRA was found to give a greater improvement in the classification accuracy when alternative feature types were used. For example, the average percentage improvement in accuracy for autoregressive features was greater. However, the overall performance of autoregressive features was inferior.

The results have shown that band passing should always be performed regardless of the other noise reduction types employed.

There is a practical limit in terms of computational load. It may not be worth performing IMCRA SE on multi-channel EMG for the sake of a few percent improvement in classification accuracy. Instead, IMCRA SE is more suitable for data sets where there are only a few (2-4) noisy channels, which of course is a common number of channels in the current generation of forearm prostheses.

6.7. Empirical Mode Decomposition-based Filtering (EMDF) as an Alternative to Low Pass Filtering

In order to assess the usefulness of the EMG below 20Hz, it was decided to test whether it was possible to classify gestures based only on features extracted from the signal below 20Hz. This would include EMG, but in Data Set 2, there are also high levels of motion artifact noise in the 0-20Hz band. The data was put through a third-order low-pass Butterworth filter with a cut-off frequency of 20Hz. The accuracy was better than chance but was disappointing. The results indicated that there is some useful discriminatory information below 20Hz, which could be either the EMG or some repeatable property of the motion artifact that correlates to specific gestures.

It was hoped that EMDF (described in section 3.5.1) would remove motion artifact while retaining these useful low-frequency components of the EMG. High passing is

done to remove the often-overwhelming motion artifact noise. This also removes any low frequency EMG that may be present. An example is shown in Figure 6.7.

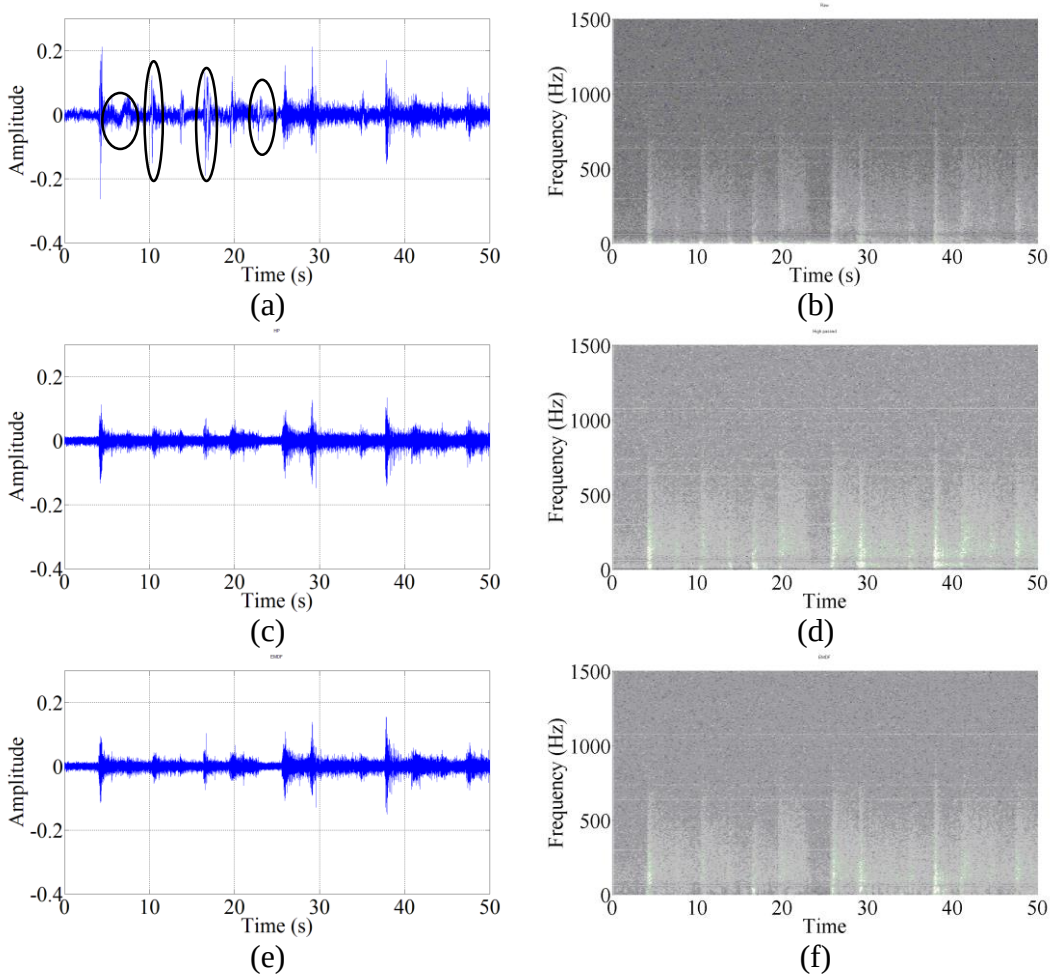

Figure 6.7 – (a) a time domain signal from Data Set 2. (b) The same signal in the time-frequency domain (c) signal after HPF, in Time Domain (d) signal after HPF, in time-frequency domain (e) EMDF applied in time domain (f) EMDF in time-frequency domain

Figure 6.7(a) shows an example of an EMG signal from Data Set 2 with some of the motion artifacts circled. The motion artifacts are also evident in the spectrogram of the signal Figure 6.7(b). The signal is high-pass filtered in Figure 6.7(c) and (d) and EMDF is applied using 100-sample windows in Figure 6.7(e) and (f). It appears that EMDF is better at preserving the lower-frequency structure. Despite this apparent retention of information, a commensurate improvement in classification accuracy was not observed.

6.8. Summary

This chapter has shown the potential of spectral noise estimation and noise reduction for improving the classification accuracy of a pattern recognition-based myoelectric control system. Firstly, the change in signal quality caused by IMCRA SE and MSNE for EMG signals with added AWGN was measured and found to be satisfactory. Spectral Enhancement techniques, compared against several other techniques, performed best at improving the classification accuracy in the presence of added and intrinsic noise, which implies that Spectral Enhancement was effective at preserving spectral information from the EMG while reducing the noise. The resulting improvement if the data is already clean is marginal, so the additional processing required for the spectral noise reduction is not advantageous.

The parameters of IMCRA SE were configured to respond appropriately to EMG. In this way, stronger EMG components were removed from noise estimations. Signal quality was restored and classification accuracy was improved for both AWGN and 'naturally' noisy data. The improvement in accuracy gained for the noisy data would make the operation of prosthetic hands easier.

7 Conclusion

In this thesis, novel methods of EMG activity detection and noise identification have been introduced. An algorithm designed for speech noise reduction has been shown to be effective for EMG signals for both white and intrinsic noise. These developments will ultimately lead to improvement in the performance of myoelectric control and automated clinical EMG analysis.

7.1.1. LBP Activity Detection

LBPAD takes advantage of the behaviour of 1-D LBP histogram bins in order to identify the presence of EMG in offline recordings. It allows accurate multi-channel activity detection with a lower FPR than the methods against which it was tested in Chapter 4. This was achieved without the need to tailor thresholds for each individual EMG recording in the data sets, which was necessary for energy and Bonato methods.

LBPAD must be tested in real-time in future work and implemented in a prosthetic under changing SNR conditions. The fitting of currently available commercial myoelectric prosthetic hands to patients requires manual calibration of threshold settings by clinicians according to each patient's ability. It is common for patients to return to the clinic for threshold values readjustment because conditions change such as muscle tone and sensor slippage. An investigation of the benefits of LBPAD to reduce the need for recalibration could be carried out by testing LBPAD in the presence of the common types of noise found in EMG, added artificially to clean real EMG at multiple SNRs. An understanding of the relationship between the LBP parameter values and the noise levels present in the EMG needs to be established, and the mathematical rigour behind 1-D LBPs must be developed further.

LBPAD has not been tested on recordings of slow, intentional movements. The possibility of modifying LBPAD to detect changes between gestures without going through 'rest' first should be investigated.

LBPAD should be adapted for and tested on other types of signal such as speech.

7.1.2. Contaminant identification

It is necessary to be able to identify the contaminant types present in EMG signals in order to be able to decide whether to discard or filter the signals, or to adjust the recording apparatus or telehealth setup to reduce the noise. Manual identification methods have existed for a while, but the method presented in Chapter 5 combines some of them to perform automated identification of five contaminants.

The contaminant identification system discussed in Chapter 5 is capable of producing a class label identifier for a single contaminant. Future work should focus on the identification of multiple contaminants that may be simultaneously present. Such a system may identify the dominant contaminant, as discerning the number and type of each contaminant may not be feasible. In this work, analysis was limited to isometric, isotonic contractions, which could be applied to calibration or verification contractions performed at the beginning and end of data acquisition. Additional work should investigate the effect of short analysis windows and the applicability of similar analysis in dynamic contractions for real-time assessment.

As discussed in section 3.5, the previous One-class SVM system [44] detected noise regardless of its type. The system presented here will misclassify previously unseen data types. To address this, future work should investigate the possibility of developing a confidence measure that uses the one-class SVM.

Another possible approach to the contaminant issue would be ‘brute force’, where the EMG is subjected to every type and combination of noise reduction methods until the best classification accuracy is achieved. Though this would be time-consuming, the results could form a basis against which to compare the classification from the SVMs. If the SVM classification was accurate, then the most appropriate filter for the identified contaminant(s) should be the ones that produced the highest classification accuracy.

Future work should identify the ranges of SNR within which the noise has non-negligible impact upon the signal quality. As well as the quality metrics discussed in Section 3.5, gesture classification accuracy could be used, which was done in this thesis as a signal quality metric in Chapter 6.

The ultimate aim of contaminant identification in the context of forearm prostheses is improvement in usability of the prosthetic. For telehealth, the ultimate aim is the transmission of clean biosignals that can be used for remote diagnosis. With this in mind, future work should focus on achieving real-time signal analysis and filtering.

7.1.3. Spectral Enhancement

In Chapter 6, Spectral Enhancement, which was developed for speech signals, was shown to have potential for use on EMG signals. An improvement in classification accuracy implied that the noise in the EMG signals had been reduced, particularly for instances where there was a low channel count, which is the case for the current generation of prosthetic control systems for hands.

More work is needed to tailor the spectral estimation mechanism in the spectral enhancement techniques based on the spectral properties of the EMG. For example, the best choice of statistical distributions for myoelectric signals need to be determined, though these problems have not yet been solved for speech [109]. Different distributions might be used depending on the MVC, as it has been shown that the distribution changes as MVC changes [134].

Because IMCRA SE reduces the measurement noise, it would be possible to compare it against the adaptive whitening filter in [99] for the purposes of improving amplitude estimation in EMG.

As there are usually multiple concurrent EMG channels, multi-channel versions of the spectral noise estimation techniques could be adapted to take advantage of the redundancy and crosstalk. IMCRA SE should be tested in a real time situation and the processing time then compared with other methods in real time such as wavelets and EMD.

The hope was that EMDF would preserve low-frequency information from the EMG better than a high-pass filter, and that this would lead to higher classification accuracy. The tests of EMDF performed as part of this work indicated that this was not the case. More work is needed to indicate conclusively whether EMDF has utility for EMG signals. For example, EMDF might be useful in the process of MUAP decomposition, which was not the focus of this work.

7.2. Combined system

The novel contributions could be integrated into a system as shown in Figure 7.1.

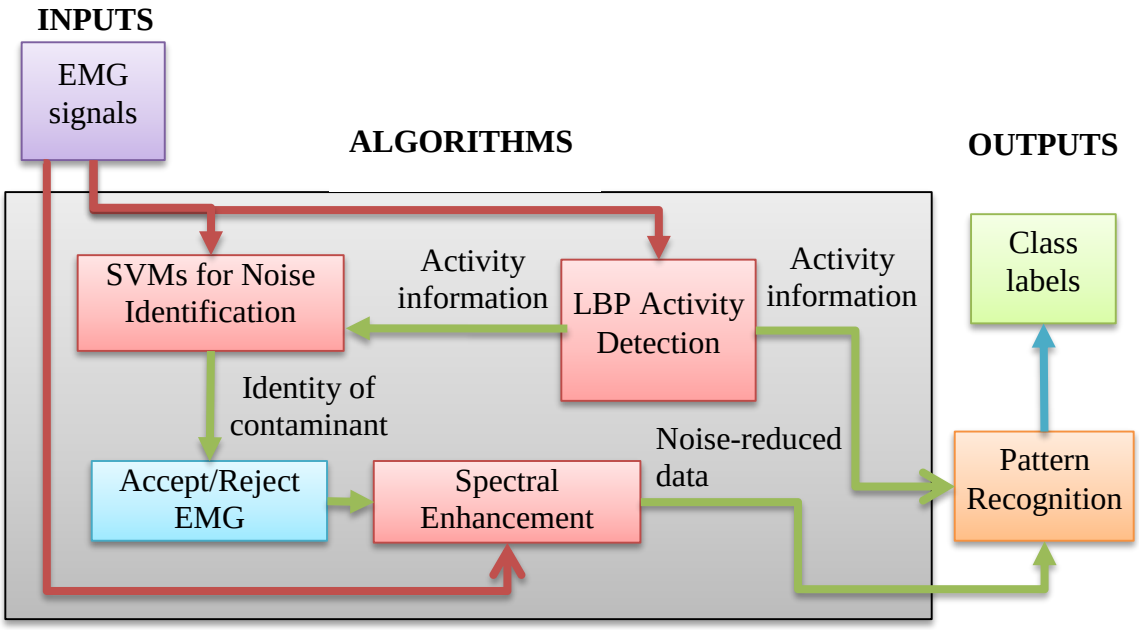

Figure 7.1 - Proposed structure of future system that incorporates LBPAD, SVM-based noise identification and Spectral Enhancement

Noise identification would be integrated into a pattern recognition system in a manner similar to that shown in Figure 7.2.

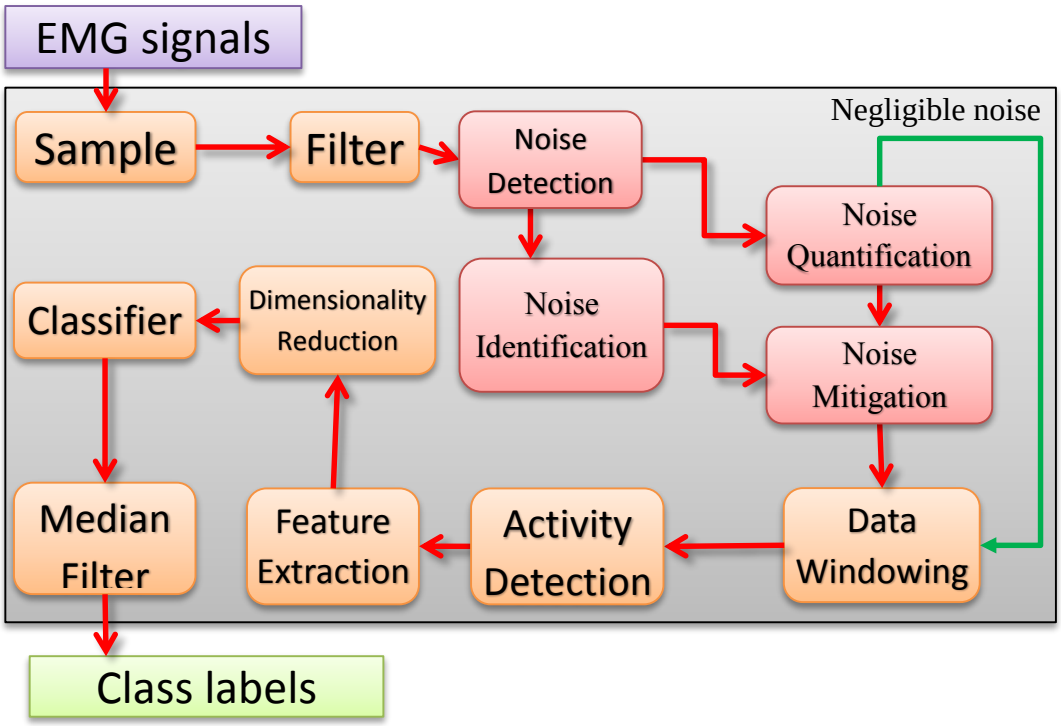

Figure 7.2 – Suggested pattern recognition system with additional stage for noise detection, identification, quantification and mitigation

Figure 7.2 shows a pattern recognition system with an additional stage for noise detection, identification, quantification and mitigation [5, 44, 73]. If the noise in the EMG has been deemed negligible, then the noise mitigation stage can be bypassed.

In this work, the classification accuracy is measured purely as the number of times that the classifier produces a correct class label. A more sophisticated approach [136, 137] is to measure the completion of tasks classed under Activities of Daily Living (ADL). This would be a logical next stage for any system that was to be used in clinical trials.

The effects of fatigue upon the performance of each of the novel algorithms should be investigated [25].

The gap between academic and industrial research for myoelectric prosthetic limb control is discussed in [138]. High classification accuracy in lab-based myoelectric controllers, but this is not reflected in the relatively small percentage of amputees who use myoelectric forearm prostheses. Future research should bear this in mind.

The algorithms presented here could contribute towards myoelectric toolboxes such as BioPatRec [139].

Blind Source Separation was discussed in 2.5.4. Degenerate Unmixing Estimation Technique (DUET) [140] is a BSS technique that is capable of separating an arbitrary number of sources from a few mixtures. DUET was tested during this PhD research on multi-channel EMG, and the physical meaning of the sources extracted from the EMG could not be identified. This is perhaps because DUET in its unmodified form does not account for either the 'tissue filter effect' or any reverberation. There is scope to develop an algorithm based on DUET for use with EMG signals.

7.3. The future of forearm myoelectric control

The main development in the near future of forearm myoelectric control will be the release of a commercialised pattern recognition control system in a lower-arm prosthetic. Longer term, the lessons learned from ambitious programmes such as

Revolutionizing Prosthetics will lead to prosthetics that are more functional and intuitive.

Several technologies could improve prostheses. Injectable wireless sensor implants have the advantages of invasive sensors without the problems associated with percutaneous sensing [36]. Osseointegration [141] is the permanent addition of a connector on the bone on the residual limb, to which a prosthetic can be attached. This would likely reduce sensor slippage for surface sensors.

Muscle Synergies are instances of multiple concurrent muscle movements, presumed to be initiated by a single neural command signal [142]. Unlike features that have been dimensionally reduced, synergies have a time dimension [65]. The feasibility of muscle synergies to refine EMG control is an area ripe for future research.

In the longer term, prosthetic hands will be made that perform better than natural hands in certain situations. Prosthetic hands will then be developed that are as good as or even superior to those with which we are born. Until then, incremental improvements, such as the tools presented in this thesis, will lead to a gradual improvement in the quality of life of prosthetic users.

Appendix A

Overview of IMCRA

In this appendix, IMCRA will be explained based on [109, 133]. The aim of IMCRA is to continuously estimate the noise in a speech signal without access to a noise reference, and to exclude stronger speech components from this noise estimate. A smoothed power spectrum is generated for each DFT bin across windows of the signal. The location of stronger speech components are estimated and excluded from a second smoothed spectrum. This STFT of the noisy signal is smoothed and Minimum Statistics is used to track the minimum. The second smoothed spectrum is used to generate a gain, which can be applied to the noisy signal to reduce noise. Once the noise estimate is made, its STFT can be subtracted from the STFT of the noisy speech (this step has been called Spectral Enhancement using IMCRA, or IMCRA SE, in this thesis, but was called IMCRA/OMLSA in [105]).

The noisy speech can be thought of as the clean speech plus additive noise:

$$y(n) = x(n) + d(n)$$

Where $y(n)$ is the noisy speech, $x(n)$ is the clean speech and $d(n)$ is the additive noise. The STFT of the speech is to be estimated by minimising some distortion measure. The STFT is:

$$Y(k,l) = X(k,l) + D(k,l)$$

where l is the time frame index (l=0,1,…,N-1) and k is the frequency bin index (k=0,1,…N-1). Subscripts can be used:

$$Y_{kl} = \sum_{n=0}^{N-1} y(n + lM)h(n)\, e^{-i\frac{2\pi}{N}nk}$$

where $h(n)$ is an analysis window of size N and is usually a Hamming window. M is the framing step. If an estimate of STFT of the clean speech is available, the ISTFT can be used to obtain an estimate of the clean speech:

$$\hat{x}(n) = \sum_{l} \sum_{k=0}^{N-1} \hat{X}_{tk} \tilde{h}(n - lM) e^{l\frac{2\pi}{N}(n-lM)}$$

The aim of IMCRA SE is to obtain an estimate of the clean speech and use it as $\hat{X}_{tk}$

The vector $\tilde{h}(n)$ is a synthesis window that is biorthogonal to the analysis window

$h(n)$ and the ISTFT is implemented by using the weighted overlap-add method. The steps for IMCRA are as shown in Figure 0.1

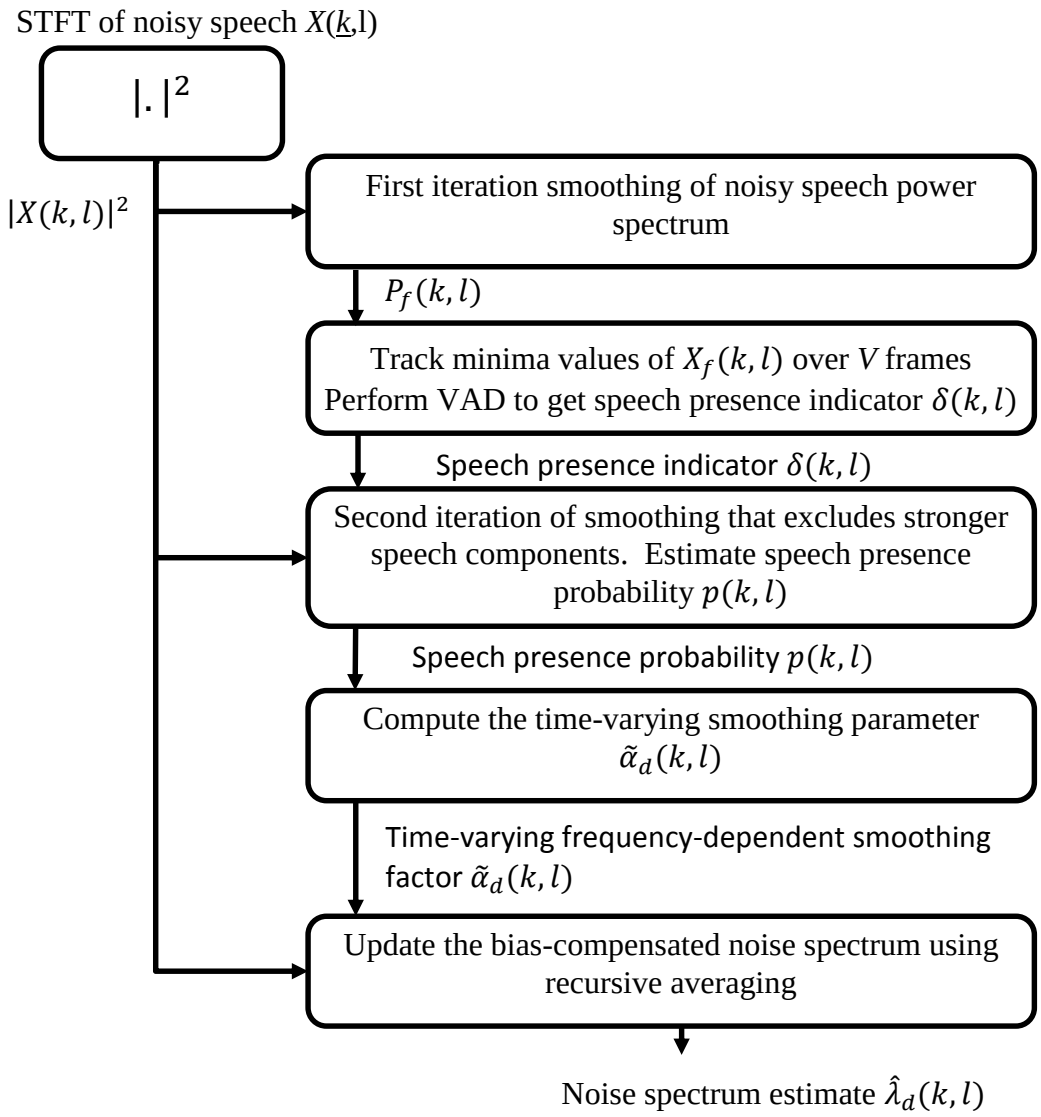

Figure 0.1 – IMCRA flow chart [109]

The noise spectrum estimate obtained from Figure 0.1 is used for IMCRA SE.

Choice of Probability Density Function

Distortion is defined as the difference between the STFT of the clean signal and the STFT of the estimated signal. $d(X_{kl}, \hat{X}_{kl})$ is a distortion measure between X_{kl} and the estimate of it $\hat{X}_{kl}$. The aim is to minimise the expected value of the distortion based on assumptions about the statistical distributions of the signal and noise [109]. Minimum Mean Square Error (MMSE) is used to estimate the speech content within

the STFT, and then calculate a gain function, which is used to attenuate the noise. Several distributions can be used in the MMSE spectral estimation:

- Gaussian, where the MMSE estimator uses a Wiener filter
- Gamma, where the MMSE estimator uses a scaled complementary error function $\mathrm{erfcx}(x)$
- Laplacian, where the MMSE estimator uses parabolic cylinder functions.

A choice is available because the best choice of estimator has not been solved for speech [109]. Neither has it been solved for EMG. Once a noise estimation has been performed using IMCRA, the spectrum of the noise estimation is subtracted from the noisy signal.

Appendix B

This appendix shows effect of IMCRA SE upon a trial from Data Set 2. Eight channels are shown in the time domain and time-frequency domain in Figure 0.1, Figure 0.2 and Figure 0.3. Throughout this appendix, the solid vertical lines indicate that the subject has been instructed to change gesture. Dashed vertical lines indicate that the subject has been instructed to rest.

The 23 gesture instructions are (starting from the first vertical solid bar):

Hand close, pronation, hand close, pronation, wrist extension,

rest,

Hand open, supination,

rest,

Wrist extension, pronation,

rest,

Supination, hand close, wrist extension, pronation, hand open, hand close, wrist flexion, supination, wrist flexion, wrist extension, hand open

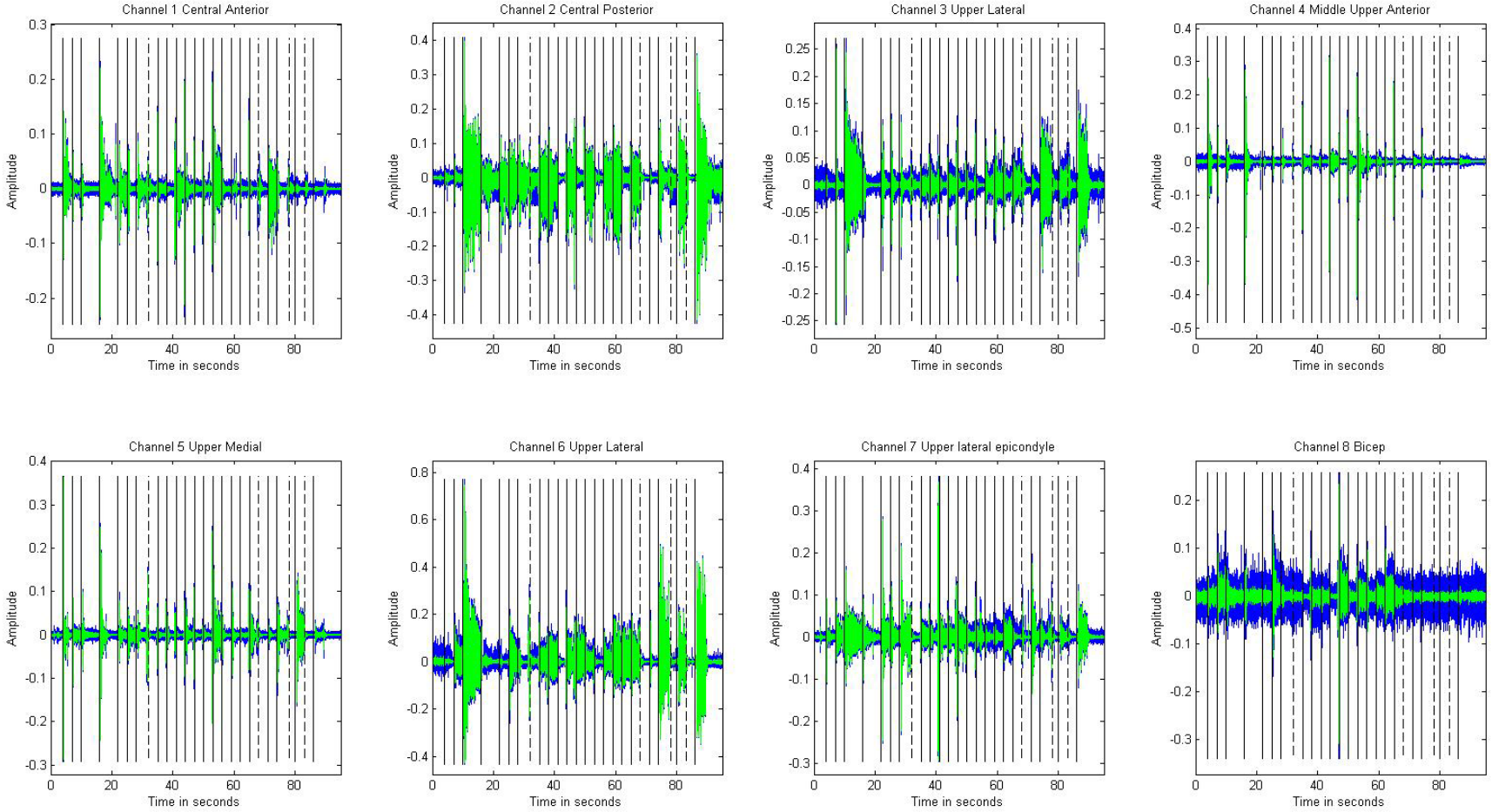

Figure 0.1 – The signals before and after IMCRA SE in the time domain, with the lighter colour representing the processed signal

APPENDIX B

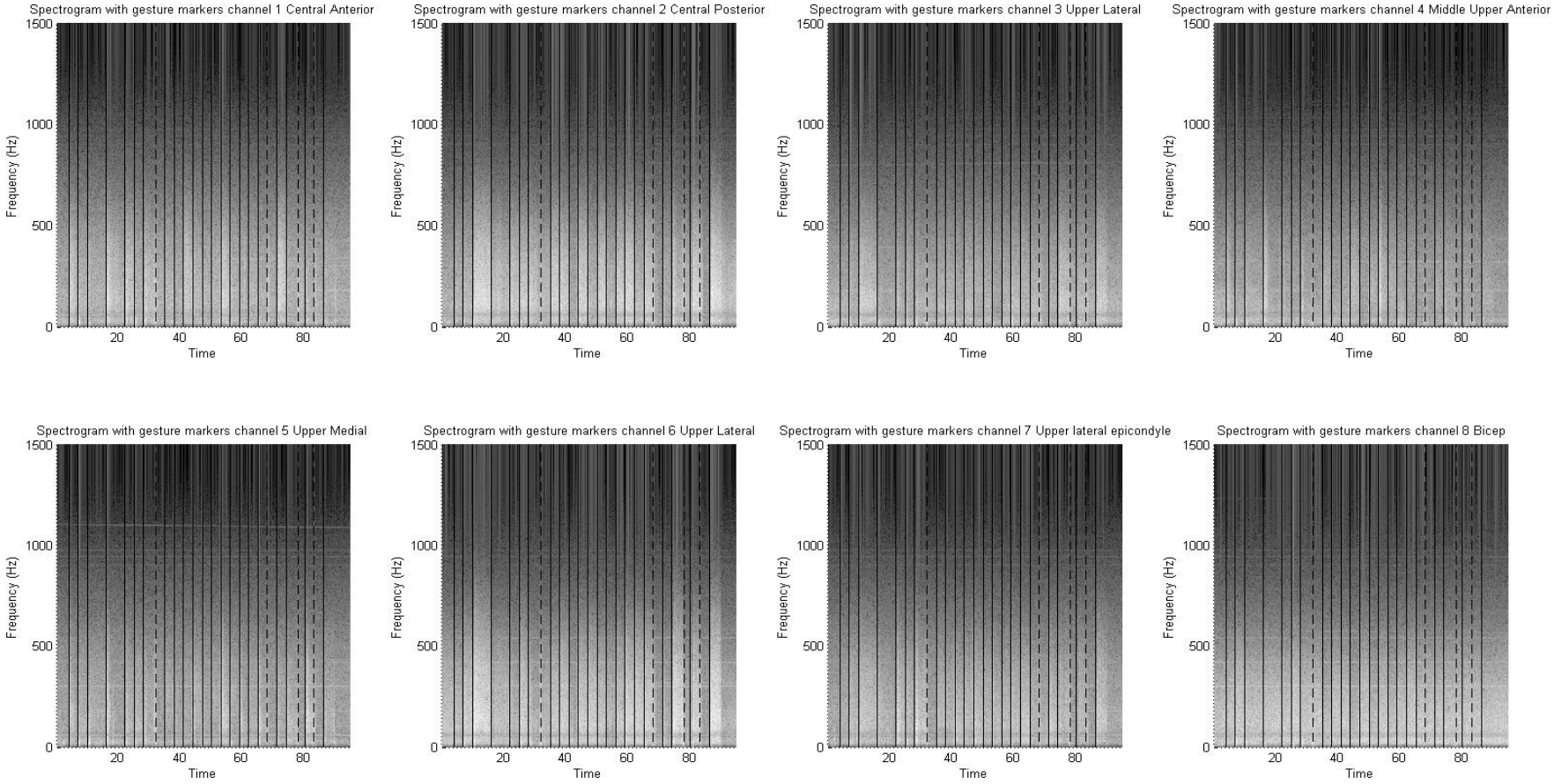

Figure 0.2 – STFT of the signals before IMCRA SE

APPENDIX B

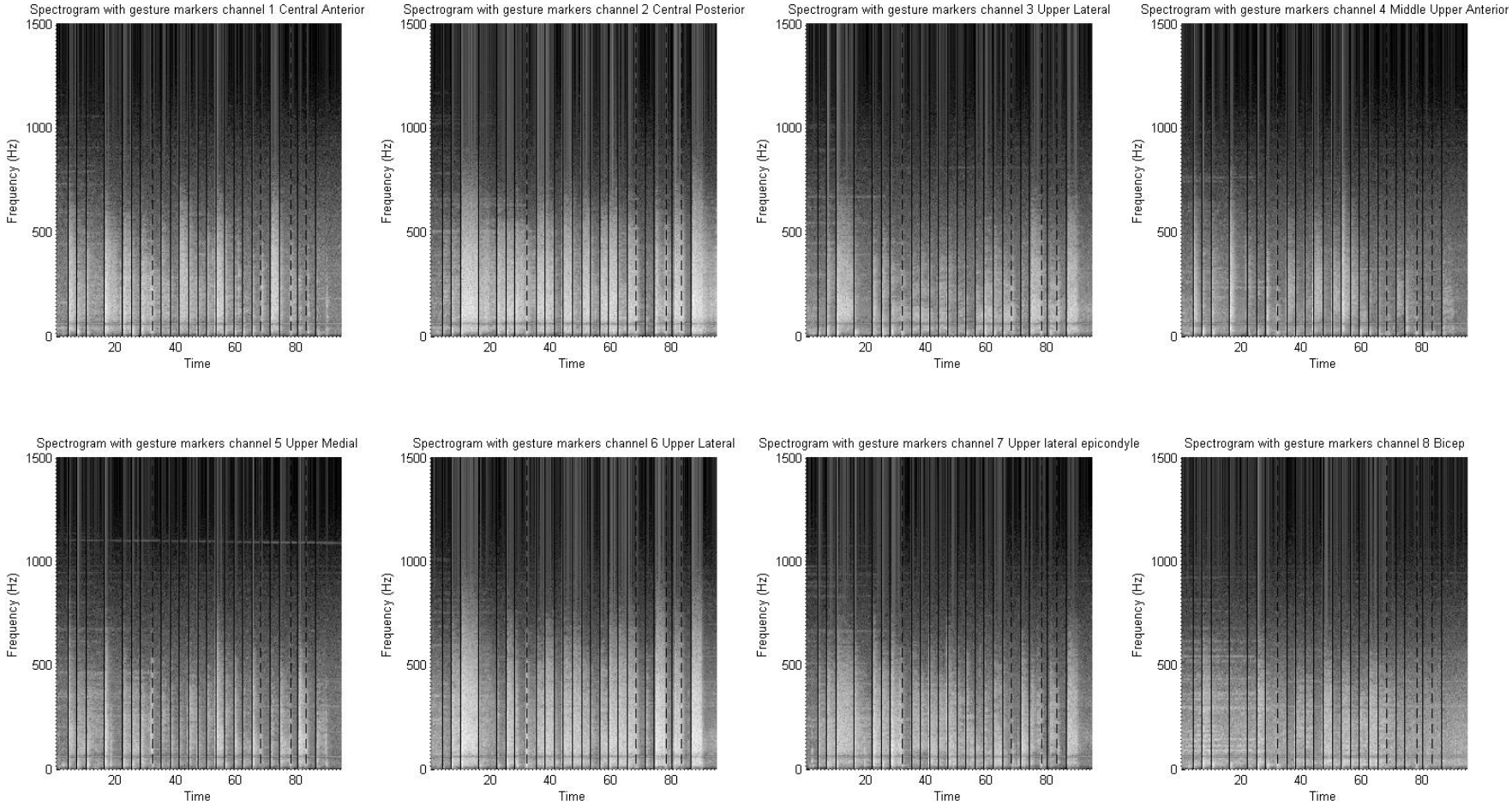

Figure 0.3 – STFT of the signals after IMCRA SE

References

[1] *Bionic Hand for 'Elective Amputation' Patient*. Available: http://www.bbc.co.uk/news/science-environment-13273348, (2011, Accessed 03/03/2014).

[2] E. D. Sherman, "A Russian bioelectric-controlled prosthesis," *Canad.Med.Ass.J.*, vol. 91, pp. 1268-1270, 12 Dec, 1964 1964.

[3] C. Castellini, E. Gruppioni, A. Davalli, and G. Sandini, "Fine detection of grasp force and posture by amputees via surface electromyography," *J Physiol Paris*, 10 April 2009.

[4] M. Asgharioskoei and H. Hu, "Myoelectric control systems—A survey," *Biomedical Signal Processing and Control*, vol. 2, pp. 275-294, 2007.

[5] P. McCool, G. D. Fraser, A. D. C. Chan, L. Petropoulakis, and J. J. Soraghan, "Identification of Contaminant Type in Surface Electromyogrpahy (EMG) Signals," *IEEE Transactions on Neural Systems and Rehabilitation Engineering*, in press.

[6] P. McCool, N. Chatlani, L. Petropoulakis, J. J. Soraghan, R. Menon, and H. Lakany, "1-D Local Binary Patterns for onset detection of myoelectric signals," in *Signal Processing Conference (EUSIPCO), 2012 Proceedings of the 20th European*, 2012, pp. 499-503.

[7] P. McCool, N. Chatlani, L. Petropoulakis, J. J. Soraghan, R. Menon, and H. Lakany, "Lower Arm Electromyography (EMG) Activity Detection using Local Binary Patterns," *IEEE Transactions on Neural Systems and Rehabilitation Engineering*, in press.

[8] P. McCool, L. Petropoulakis, J. J. Soraghan, and N. Chatlani, "Improved Pattern Recognition Classification Accuracy for Surface Myoelectric Signals using Spectral Enhancement," *Elsevier Biomedical Signal Processing and Control*, submitted.

[9] B. Hudgins, P. Parker, and R. N. Scott, "A new strategy for multifunction myoelectric control," *IEEE Transactions on Biomedical Engineering*, vol. 40, pp. 82-94, 1993.

[10] K. Englehart, B. Hudgins, P. A. Parker, and M. Stevenson, "Classification of the myoelectric signal using time-frequency based representations," *Medical engineering & physics*, vol. 21, pp. 431-8, Jul-Sep 1999.

[11] H. Daley, K. Englehart, L. Hargrove, and U. Kuruganti, "High density electromyography data of normally limbed and transradial amputee subjects for multifunction prosthetic control," *Journal of electromyography and kinesiology : official journal of the International Society of Electrophysiological Kinesiology*, vol. 22, pp. 478-84, Jun 2012.

[12] J. Earl E. Vanderwerker. *A Brief Review of the History of Amputations and Prostheses*. Available: http://www.acpoc.org/library/1976_05_015.asp, (1976, Accessed 10/3/2014).

[13] J. L. Collinger, B. Wodlinger, J. E. Downey, W. Wang, E. C. Tyler-Kabara, D. J. Weber, *et al.*, "High-performance neuroprosthetic control by an individual with tetraplegia," vol. 381, pp. 557-564, 2013/2/22/.

[14] J. d. R. Millán, F. Renkens, J. Mouriño, and W. Gerstner, "Noninvasive brain-actuated control of a mobile robot by human EEG," *IEEE Transactions on Biomedical Engineering*, vol. 51, pp. 1026-1033, June 2004 2004.

[15] O. Bai, P. Lin, S. Vorbach, J. Li, S. Furlani, and M. Hallett, "Exploration of computational methods for classification of movement intention during human voluntary movement from single trial EEG," *Clinical neurophysiology : official journal of the International Federation of Clinical Neurophysiology,* vol. 118, pp. 2637-55, Dec 2007.

[16] R. Reiter, "Eine neue Electrokunsthand," *Grenzgebiete der Medizin,* vol. 4, 1948.

[17] P. Zhou, M. M. Lowery, K. B. Englehart, H. Huang, G. Li, L. Hargrove, *et al.*, "Decoding a New Neural Machine Interface for Control of Artificial Limbs," *Journal of Neurophysiology,* vol. 98, pp. 2974-82, Nov 2007.

[18] *Revolutionizing Prosthetics*. Available: http://www.jhuapl.edu/prosthetics/program/details.asp, (2013, Accessed 04/03/2014).

[19] R. Garst, "The Krukenberg hand," *Journal of Bone & Joint Surgery, British Volume,* vol. 73-B, pp. 385-388, May 1, 1991 1991.

[20] S. Raspopovic, M. Capogrosso, F. M. Petrini, M. Bonizzato, J. Rigosa, G. Di Pino, *et al.*, "Restoring Natural Sensory Feedback in Real-Time Bidirectional Hand Prostheses," *Science Translational Medicine,* vol. 6, p. 222ra19, February 5, 2014 2014.

[21] *The Nobel Prize in Physiology or Medicine 1963*. Available: http://www.nobelprize.org/nobel_prizes/medicine/laureates/1963/, (2013, Accessed 16/10/2013).

[22] F. Martini, *Fundamentals of anatomy & physiology*: San Francisco : Benjamin Cummings, 2011.

[23] J. V. Basmajian, *Muscles alive : their functions revealed by electromyography*: Baltimore : Williams & Wilkins, 1985.

[24] A. Merlo, D. Farina, and R. Merletti, "A fast and reliable technique for muscle activity detection from surface emg signals," *IEEE Transactions on Biomedical Engineering,* vol. 50, pp. 316-323, March 2003 2003.

[25] *Electromyography: Physiology, Engineering, and Noninvasive Applications*, 2004.

[26] P. Konrad. (2001). *The ABC of EMG*.

[27] L. J. Hargrove, K. Englehart, and B. Hudgins, "A comparison of surface and intramuscular myoelectric signal classification," *IEEE Transactions on Biomedical Engineering,* vol. 54, pp. 847-853, 2007.

[28] H. J. Hermens, B. Freriks, R. Merletti, G. Hägg, D. F. Stegeman, J. Blok, *et al.* (1999). *SENIAM 8: European Recommendations for Surface ElectroMyoGraphy*.

[29] B. Freriks and H. J. Hermens. (1999). *SENIAM 9: European Recommendations for Surface ElectroMyoGraphy, results of the SENIAM Project*.

[30] D. F. Stegeman and H. J. Hermens. *Standards for surface electromyography: the European project "Surface EMG for non-invasive assessment of muscles (SENIAM)"*. (Accessed 24/4/2014).

[31] T. R. Farrell and R. F. f. Weir, "A comparison of the effects of electrode implantation and Targeting on Pattern Classification Accuracy for Prosthesis Control," *IEEE Transactions on Biomedical Engineering,* vol. 55, September 2008 2008.

[32] J. J. Baker, E. Scheme, K. Englehart, D. T. Hutchinson, and B. Greger, "Continuous Detection and Decoding of Dexterous Finger Flexions With Implantable MyoElectric Sensors," *IEEE Transactions on Neural Systems and Rehabilitation Engineering,* vol. 18, pp. 424-432, 2010.

[33] L. J. Hargrove, L. Guanglin, K. B. Englehart, and B. S. Hudgins, "Principal Components Analysis Preprocessing for Improved Classification Accuracies in Pattern-Recognition-Based Myoelectric Control," *IEEE Transactions on Biomedical Engineering,* vol. 56, pp. 1407-1414, 2009.

[34] H. Yonghong, K. B. Englehart, B. Hudgins, and A. D. C. Chan, "A Gaussian mixture model based classification scheme for myoelectric control of powered upper limb prostheses," *IEEE Transactions on Biomedical Engineering,* vol. 52, pp. 1801-1811, 2005.

[35] M. M. Lowery, R. F. f. Weir, and T. A. Kuiken, "Simulation of intramuscular EMG signals detected using implantable myoelectric sensors," *IEEE Transactions on Biomedical Engineering,* vol. 53, pp. 1926-1933, October 2006 2006.

[36] R. F. Weir, P. R. Troyk, G. A. DeMichele, D. A. Kerns, J. F. Schorsch, and H. Maas, "Implantable Myoelectric Sensors (IMESs) for Intramuscular Electromyogram Recording," *IEEE Transactions on Biomedical Engineering,* vol. 56, pp. 159-171, 2009.

[37] N. M. L. Celani, C. M. Soria, E. C. Orosco, F. A. d. Sciascio, and M. E. Valentinuzzi, "Two-dimensional myoelectric control of a robotic arm for upper limb amputees," *Journal of Physics: Conference Series,* vol. 90, p. 012086, 2007.

[38] S. D. Taffler and P. J. Kyberd, "Differences in the Activity of the Muscles in the Forearm of Individuals with a Congenital Absence of the Hand," *IEEE Transactions on Biomedical Engineering,* vol. 54, pp. 1514-1519, August 2007 2007.

[39] P. Bonato, T. D'Alessio, and M. Knaflitz, "A Statistical Method for the Measurement of Muscle Activation Intervals from Surface Myoelectric Signal During Gait," *IEEE Transactions on Biomedical Engineering,* vol. 45, pp. 287-299, 1998.

[40] G. Staude, C. Flachenecker, M. Daumer, and W. Wolf, "Onset Detection in Surface Electromyographic Signals: A Systematic Comparison of Methods," *EURASIP Journal on Advances in Signal Processing,* vol. 2001, p. 867853, 2001.

[41] W. S. Pease, H. L. Lew, and E. W. Johnson, *Johnson's Practical Electromyography*, 4 ed.: Lippincott Williams & Wilkins, 2006.

[42] J. Chu-Andrews and R. J. Johnson, *Electrodiagnosis: An Anatomical and Clinical Approach*, 1986.

[43] A. D. C. Chan and G. C. Green, "Myoelectric Control Development Toolbox."

[44] G. Fraser, A. D. C. Chan, J. R. Green, and D. MacIsaac, "Automated biosignal quality analysis for electromyography using a one-class support vector machine," *IEEE Transactions on Instrumentation and Measurement,* in press.

[45] K. Englehart and B. Hudgins, "A robust, real-time control scheme for multifunction myoelectric control," *IEEE Transactions on Biomedical Engineering*, vol. 50, pp. 848-854, 2003.

[46] R. Kato, T. Fujita, H. Yokoi, and T. Arai, "Adaptable EMG Prosthetic Hand using On-line Learning Method-Investigation of Mutual Adaptation between Human and Adaptable Machine," presented at the The 15th IEEE International Symposiumon Robot and Human Interactive Communication (RO-MAN06), Hatfield, UK, 2006.

[47] L. H. Smith, L. J. Hargrove, B. A. Lock, and T. A. Kuiken, "Determining the Optimal Window Length for Pattern Recognition-Based Myoelectric Control: Balancing the Competing Effects of Classification Error and Controller Delay," *IEEE Transactions on Neural Systems and Rehabilitation Engineering*, vol. 19, pp. 186-192, April 2011 2011.

[48] P. Parker, K. Englehart, and B. Hudgins, "Myoelectric signal processing for control of powered limb prostheses," *Journal of electromyography and kinesiology : official journal of the International Society of Electrophysiological Kinesiology*, vol. 16, pp. 541-8, Dec 2006.

[49] A. H. Al-Timemy, G. Bugmann, N. Outram, and J. Escudero, "Single Channel-Based Myoelectric Control of Hand Movements with Empirical Mode Decomposition," in *33rd Annual International Conference of the IEEE EMBS*, Boston, Massachusetts USA, 2011, pp. 6059-6062.

[50] X. Chen, X. Zhang, Z.-Y. Zhao, J.-H. Yang, V. Lantz, and K.-Q. Wang, "Multiple Hand Gesture Recognition based on Surface EMG Signal," pp. 506-509, 2007.

[51] K. Ito, M. Tsukamoto, and T. Kondo, "Discrimination of Intended Movements based on Nonstationary EMG for A Prosthetic Hand Control," in *ISCCSP 2008*, Malta, 2008.

[52] S. Micera, G. Vannozzi, A. M. Sabatini, and P. Dario, "Improving detection of muscle activation intervals," *IEEE Engineering in Medicine and Biology Magazine*, vol. 20, pp. 38-46, 2001.

[53] S. S. Haykin, *Neural networks and learning machines*: Harlow : Pearson Education, 2008.

[54] G. C. Matrone, C. Cipriani, E. L. Secco, G. Magenes, and M. C. Carrozza, "Principal components analysis based control of a multi-DoF underactuated prosthetic hand," *J Neuroeng Rehabil*, vol. 7, p. 16, 2010.

[55] J. M. Kilner, S. N. Baker, and R. N. Lemon, "A novel algorithm to remove electrical cross-talk between surface EMG recordings and its application to the measurement of short-term synchronisation in humans," *J Physiol*, vol. 538, pp. 919-30, Feb 1 2002.

[56] Q. Li, J.-h. Yang, X. Chen, Z. Liang, and Y.-x. Ren, "The decomposition of Surface EMG Signals Based on Blind Source Separation of Convolved Mixtures," in *2005 IEEE Engineering in Medicine and Biology 27th Annual Conference*, Shanghai, China, 2005.

[57] R. O. Duda, *Pattern classification*: New York : Wiley, 2001.

[58] A. B. Ajiboye and R. F. f. Weir, "A Heuristic Fuzzy Logic Approach to EMG Pattern Recognition for Multifunctional Prosthesis Control," *IEEE Transactions on Neural Systems and Rehabilitation Engineering*, vol. 13, pp. 280-291, September 2005 2005.

[59] S. Maier and P. v. d. Smagt, "surface emg suffices to classify the motion of each finger independently," in *9th International Conference on Motion and Vibration Control (MOVIC)*, 2008.

[60] F. V. G. Tenore, A. Ramos, A. Fahmy, S. Acharya, R. Etienne-Cummings, and N. V. Thakor, "Decoding of Individuated Finger Movements Using Surface Electromyography," *IEEE Transactions on Biomedical Engineering*, vol. 56, pp. 1427-1434, 2009.

[61] G. Kondo, R. Kato, H. Yokoi, and T. Arai, "Classification of Individual Finger Motions Hybridizing Electromyogram in Transient and Converged States," presented at the 2010 IEEE International Conference on Robotics and Automation, Anchorage Convention District, Anchorage, Alaska, USA, 2010.

[62] M. A. Oskoei and H. Huosheng, "Support Vector Machine-Based Classification Scheme for Myoelectric Control Applied to Upper Limb," *IEEE Transactions on Biomedical Engineering*, vol. 55, pp. 1956-1965, 2008.

[63] C.-C. Chang and C.-J. Lin, "LIBSVM: A library for support vector machines," *ACM Transactions on Intelligent Systems and Technology*, vol. 2, pp. 27:1--27:27, 2011.

[64] A. D. C. Chan and K. B. Englehart, "Continuous myoelectric control for powered prostheses using hidden Markov models," *IEEE Transactions on Biomedical Engineering*, vol. 52, pp. 121-124, 2005.

[65] J. Chiang, Z. J. Wang, and M. J. McKeown, "A Hidden Markov, Multivariate Autoregressive (HMM-mAR) Network Framework for Analysis of Surface EMG (sEMG) Data," *IEEE Transactions on Signal Processing*, vol. 56, pp. 4069-4081, August 2008 2008.

[66] A. M. Simon, L. J. Hargrove, B. A. Lock, and T. A. Kuiken, "A Decision-Based Velocity Ramp for Minimizing the Effect of Misclassifications During Real-Time Pattern Recognition Control," *IEEE Transactions on Biomedical Engineering*, vol. 58, pp. 2360-2368, August 2011 2011.

[67] S. Amsuss, P. Gobel, N. Jiang, B. Graimann, L. Paredes, and D. Farina, "Self-Correcting Pattern Recognition System of Surface EMG Signals for Upper Limb Prosthesis Control," *IEEE Transactions on Biomedical Engineering*, vol. PP, pp. 1-1, 2014.

[68] G. P. John, *Digital signal processing : principles, algorithms, and applications*. London: London : Prentice-Hall International UK, 1996.

[69] N. E. Huang, Z. Shen, S. R. Long, M. C. Wu, H. H. Shih, Q. Zheng, *et al.*, "The empirical mode decomposition and the Hilbert spectrum for nonlinear and non-stationary time series analysis," pp. 903-995, 1996.

[70] P. Flandrin, G. Rilling, and P. Goncalves, "Empirical mode decomposition as a filter bank," *Signal Processing Letters, IEEE*, vol. 11, pp. 112-114, 2004.

[71] P. Flandrin, P. Gonçalvès, and G. Rilling, "Detrending and Denoising with Empirical Mode Decomposition," presented at the EUSIPCO 2004, Vienna, Austria, 2004.

[72] C. Sapsanis, G. Georgoulas, A. Tzes, and D. Lymberopoulos, "Improving EMG based classification of basic hand movements using EMD," in *Engineering in Medicine and Biology Society (EMBC), 2013 35th Annual International Conference of the IEEE*, 2013, pp. 5754-5757.

[73] G. D. Fraser, A. D. C. Chan, J. R. Green, and D. T. MacIsaac, "Biosignal quality analysis of surface EMG using a correlation coefficient test for

normality," in *Medical Measurements and Applications Proceedings (MeMeA), 2013 IEEE International Symposium on*, 2013, pp. 196-200.

[74] J. G. Webster, "Reducing Motion Artifacts and Interference in Biopotential Recording," *IEEE Transactions on Biomedical Engineering,* vol. BME-31, pp. 823-826, 1984.

[75] C. Sinderby, L. Lindstrom, and A. E. Grassino, "Automatic assessment of electromyogram quality," *Journal of applied physiology,* vol. 79, pp. 1803-1815, November 1, 1995 1995.

[76] G. B. Moody, W. E. Muldrow, and R. G. Mark, "A noise stress test for arrhythmia detectors," *Computers in Cardiology,* vol. 11, pp. 381-384, 1984.

[77] G. D. Fraser, A. D. C. Chan, J. R. Green, and D. MacIsaac, "Removal of electrocardiogram artifacts in surface electromyography using a moving average method," in *2012 IEEE International Symposium on Medical Measurements and Applications Proceedings (MeMeA)*, 2012, pp. 1-4.

[78] Z. Ping, M. M. Lowery, R. F. Weir, and T. A. Kuiken, "Elimination of ECG Artifacts from Myoelectric Prosthesis Control Signals Developed by Targeted Muscle Reinnervation," in *27th Annual International Conference of the Engineering in Medicine and Biology Society, 2005. IEEE-EMBS 2005*, 2005, pp. 5276-5279.

[79] A. Phinyomark, C. Limsakul, and P. Phukpattaranont, "EMG denoising estimation based on adaptive wavelet thresholding for multifunction myoelectric control," in *Innovative Technologies in Intelligent Systems and Industrial Applications, 2009*, 2009, pp. 171-176.

[80] X. Ren, Z. Yan, Z. Wang, and X. Hu, "Noise reduction based on ICA decomposition and wavelet transform for the extraction of motor unit action potentials," *Journal of neuroscience methods,* vol. 158, pp. 313-322, 2006.

[81] D. K. Kumar, S. Poosapadi Arjunan, and V. P. Singh, "Towards identification of finger flexions using single channel surface electromyography--able bodied and amputee subjects," *Journal of neuroengineering and rehabilitation,* vol. 10, p. 50, 2013.

[82] J. P. Bello, L. Daudet, S. Abdallah, C. Duxbury, M. Davies, and M. B. Sandler, "A tutorial on onset detection in music signals," *IEEE Transactions on Speech and Audio Processing*, pp. 1-13, 2005.

[83] A. Benyassine, E. Shlomot, S. Huan-yu, D. Massaloux, C. Lamblin, and J. P. Petit, "ITU-T Recommendation G.729 Annex B: a silence compression scheme for use with G.729 optimized for V.70 digital simultaneous voice and data applications," *IEEE Communications Magazine,* vol. 35, pp. 64-73, 1997.

[84] S. J. Rastin, C. P. Unsworth, K. R. Gledhill, G. G. Coghill, M. Chadwick, and R. Robinson, "Iterative coupling of standardised earthquake detection and wavelet thresholding to determine simplified earthquake event waveforms (SEEW)," in *10th International Conference on Information Sciences Signal Processing and their Applications (ISSPA)*, 2010, pp. 173-176.

[85] S. Qizhu, S. Yining, D. Xiangfeng, and M. Zuchang, "Onset Determination of Muscle Contraction in Surface Electromyography Signals Analysis," in *2005 IEEE International Conference on Information Acquisition*, Hong Kong and Macau, China, 2005, pp. 384-387.

[86] D. E. Marple-Horvat and S. L. Gilbey, "A method for automatic identification of periods of muscular activity from EMG recordings," *Journal of neuroscience methods,* vol. 42, pp. 163-7, May 1992.

[87] J.-J. Ding, C.-J. Tseng, C.-M. Hu, and T. Hsien, "Improved onset detection algorithm based on fractional power envelope matched filter," presented at the 19th European Signal Processing Conference (EUSIPCO 2011), Barcelona, Spain, 2011.

[88] P. Masri and A. Bateman, "Improved modelling of attack transients in music analysis-resynthesis," in *Proceedings of the International Computer Music Conference*, 1996, pp. 100-103.

[89] E. J. Scheme, K. B. Englehart, and B. S. Hudgins, "Selective Classification for Improved Robustness of Myoelectric Control Under Nonideal Conditions," *IEEE Transactions on Biomedical Engineering,* vol. 58, pp. 1698-1705, 2011.

[90] A. Fougner, E. Scheme, A. D. C. Chan, K. Englehart, and O. Stavdahl, "Resolving the Limb Position Effect in Myoelectric Pattern Recognition," *IEEE Transactions on Neural Systems and Rehabilitation Engineering,* vol. 19, pp. 644-651, 2011.

[91] M. Zardoshti-Kermani, B. C. Wheeler, K. Badie, and R. M. Hashemi, "EMG Feature Evaluation for Movement Control of Upper Extremity Prostheses," *IEEE Transactions on Rehabilitation Engineering,* vol. 3, pp. 324-333, December 1995 1995.

[92] E. N. Kamavuako, K. B. Englehart, W. Jensen, and D. Farina, "Simultaneous and Proportional Force Estimation in Multiple Degrees of Freedom From Intramuscular EMG," *IEEE Transactions on Biomedical Engineering,* vol. 59, pp. 1804-1807, 2012.

[93] J. Zhao, Z. Xie, L. Jiang, H. Cai, H. Liu, and G. Hirzinger, "EMG Control for a Five-fingered Underactuated Prosthetic Hand Based on Wavelet Transform and Sample Entropy," in *2006 IEEE/RSJ International Conference on Intelligent Robots and Systems,* Beijing, China, 2006, pp. 3215-3220.

[94] K. Englehart, B. Hudgins, and P. A. Parker, "A wavelet-based continuous classification scheme for multifunction myoelectric control," *IEEE Transactions on Biomedical Engineering,* vol. 48, pp. 302-311, March 2001 2001.

[95] R. G. Willison, "Analysis of Electrical Activity in Healthy and Dystrophic Muscle in Man," *J. Neurol. Neurosurg.Psychiat.,* vol. 27, pp. 386-394.

[96] D. Graupe and W. K. Cline, "Functional Separation of EMG Signals via ARMA Identification Methods for Prosthesis Control Purposes," pp. 252-259, 1975.

[97] D. Peleg, E. Braiman, E. Yom-Tov, and G. F. Inbar, "classification of finger activation for use in a robotic prosthesis arm," *IEEE Transactions on Neural Systems and Rehabilitation Engineering,* vol. 10, pp. 290-293, December 2002 2002.

[98] D. Farina and R. Merletti, "Comparison of algorithms for estimation of EMG variables during voluntary isometric contractions," *Journal of Electromyography and Kinesiology,* vol. 10, pp. 337-349, 2000.

[99] E. A. Clancy and K. A. Farry, "Adaptive Whitening of the Electromyogram to Improve Amplitude Estimation," *IEEE Transactions on Biomedical Engineering*, vol. 47, p. 11, June 2000 2000.

[100] G. D. Fraser, A. D. C. Chan, J. R. Green, N. Abser, and D. MacIsaac, "CleanEMG; Power line interference estimation in sEMG using an adaptive least squares algorithm," in *Engineering in Medicine and Biology Society,EMBC, 2011 Annual International Conference of the IEEE*, 2011, pp. 7941-7944.

[101] G. D. Fraser, A. D. C. Chan, J. R. Green, and D. MacIsaac, "Detection of ADC clipping, quantization noise, and amplifier saturation in surface electromyography," in *Medical Measurements and Applications Proceedings (MeMeA), 2012 IEEE International Symposium on*, 2012, pp. 1-5.

[102] S. Taffler, "The use of the Hilbert Transform in EMG Analysis," presented at the MEC, University of New Brunswick, 1999.

[103] A. O. Andrade, S. Nasuto, P. Kyberd, C. M. Sweeney-Reed, and F. R. Van Kanijn, "EMG signal filtering based on Empirical Mode Decomposition," *Biomedical Signal Processing and Control*, vol. 1, pp. 44-55, 2006.

[104] A. O. Boudraa and J. C. Cexus, "EMD-Based Signal Filtering," *IEEE Transactions on Instrumentation and Measurement*, vol. 56, pp. 2196-2202, 2007.

[105] N. Chatlani and J. J. Soraghan, "EMD-Based Filtering (EMDF) of Low-Frequency Noise for Speech Enhancement," *Audio, Speech, and Language Processing, IEEE Transactions on*, vol. 20, pp. 1158-1166, 2012.

[106] S. Karlsson, J. Yu, and M. Akay, "Enhancement of Spectral Analysis of Myoelectric Signals During Static Contractions Using Wavelet Methods," *IEEE Transactions on Biomedical Engineering*, vol. 46, pp. 670-684, June 1999 1999.

[107] "A Method of Recognizing Finger Motion Using Wavelet Transform of Surface EMG Signal."

[108] A. Phinyomark, C. Limsakul, and P. Phukpattaranont, "A Comparative Study of Wavelet Denoising for Multifunction Myoelectric Control," in *International Conference on Computer and Automation Engineering 2009*, 2009, pp. 21-25.

[109] *Springer handbook of speech processing [internet resource]*: Berlin ; London : Springer, 2008.

[110] Y. Ephraim and D. Malah, "Speech enhancement using a minimum-mean square error short-time spectral amplitude estimator," *IEEE Transactions on Acoustics, Speech and Signal Processing*, vol. 32, pp. 1109-1121, 1984.

[111] R. Martin, "Spectral Subtraction Based on Minimum Statistics," presented at the EUSIPCO 1994, 1994.

[112] I. Cohen and B. Berdugo, "Speech enhancement for non-stationary noise environments," *Signal Processing*, vol. 81, pp. 2403-2418, 2001.

[113] T. Ojala, M. Pietikainen, and T. Maenpaa, "Multiresolution gray-scale and rotation invariant texture classification with local binary patterns," *IEEE Transactions on Pattern Analysis and Machine Intelligence*, vol. 24, pp. 971-987, 2002.

[114] S. He, J. J. Soraghan, B. F. O'Reilly, and D. Xing, "Quantitative Analysis of Facial Paralysis Using Local Binary Patterns in Biomedical Videos," *IEEE*

Transactions on Biomedical Engineering, vol. 56, pp. 1864-1870, July 2009 2009.

[115] N. Chatlani and J. J. Soraghan, "Local binary patterns for 1-D signal processing," 2010, pp. 95-99.

[116] Z. Qiming, N. Chatlani, and J. J. Soraghan, "1-D Local binary patterns based VAD used INHMM-based improved speech recognition," in *Signal Processing Conference (EUSIPCO), 2012 Proceedings of the 20th European*, 2012, pp. 1633-1637.

[117] L. Houam, A. Hafiane, A. Boukrouche, E. Lespessailles, and R. Jennane, "One dimensional local binary pattern for bone texture characterization," *Pattern Analysis and Applications*, pp. 1-15, 2012/09/01 2012.

[118] A. Benzaoui and A. Boukrouche, "1DLBP and PCA for face recognition," in *Programming and Systems (ISPS), 2013 11th International Symposium on*, 2013, pp. 7-11.

[119] M. H. Zweig and G. Campbell, "Receiver-operating characteristic (ROC) plots: a fundamental evaluation tool in clinical medicine," *Clin Chem*, vol. 39, pp. 561-77, Apr 1993.

[120] A. D. C. Chan and D. MacIsaac, "CleanEMG: Assessing the quality of EMG signals," presented at the 34th Conf. Med. Biol. Eng. Soc. and FICCDAT, Toronto, Canada 69826, 2011.

[121] E. A. Clancy, E. L. Morin, and R. Merletti, "Sampling, noise-reduction and amplitude estimation issues in surface electromyography," *Journal of Electromyography and Kinesiology*, vol. 12, pp. 1-16, 2002.

[122] A. Phinyomark, C. Limsakul, and P. Phukpattaranont, "A novel feature extraction for robust EMG pattern recognition," *arXiv preprint arXiv:0912.3973*, 2009.

[123] N. H. Lovell, S. J. Redmond, J. Basilakis, and B. G. Celler, "Biosignal quality detection: An essential feature for unsupervised telehealth applications," in *e-Health Networking Applications and Services (Healthcom), 2010 12th IEEE International Conference on*, 2010, pp. 81-85.

[124] A. Arvidsson, A. Grassino, and L. Lindstrom, "Automatic selection of uncontaminated electromyogram as applied to respiratory muscle fatigue," *Journal of applied physiology*, vol. 56, pp. 568-75, Mar 1984.

[125] E. Shwedyk, R. Balasubramanian, and R. N. Scott, "A Nonstationary Model for the Electromyogram," *IEEE Transactions on Biomedical Engineering*, vol. BME-24, September 1977 1977.

[126] C. Grönlund, K. Roeleveld, A. Holtermann, and J. S. Karlsson, "On-line signal quality estimation of multichannel surface electromyograms," *Medical and Biological Engineering and Computing*, vol. 43, pp. 357-364, 2005/06/01 2005.

[127] H. R. Marateb, M. Rojas-Martinez, M. Mansourian, R. Merletti, and M. A. Villanueva, "Outlier detection in high-density surface electromyographic signals," *Medical & biological engineering & computing*, vol. 50, pp. 79-89, Jan 2012.

[128] V. Agostini and M. Knaflitz, "An Algorithm for the Estimation of the Signal-To-Noise Ratio in Surface Myoelectric Signals Generated During Cyclic Movements," *IEEE Transactions on Biomedical Engineering*, vol. 59, pp. 219-225, 2012.

[129] N. Abser, D. MacIsaac, A. D. C. Chan, G. D. Fraser, and J. R. Green, "CleanEMG: Comparing interpolation strategies for power line interference quantification in surface EMG signals," presented at the 35th Conference of the Canadian Medical & Biological Engineering Society, Halifax, Canada, 2012.

[130] N. V. Thakor and Z. Yi-Sheng, "Applications of adaptive filtering to ECG analysis: noise cancellation and arrhythmia detection," *Biomedical Engineering, IEEE Transactions on,* vol. 38, pp. 785-794, 1991.

[131] P. S. Hamilton, M. G. Curley, R. M. Aimi, and C. Sae-Hau, "Comparison of methods for adaptive removal of motion artifact," in *Computers in Cardiology 2000*, 2000, pp. 383-386.

[132] N. Wiener, "The extrapolation Interpolation and Smoothing of Stationary Time Series with Engineering Applications," *J. American Statistical Association,* vol. 47, pp. 319-321, 1952.

[133] I. Cohen, "Noise spectrum estimation in adverse environments: improved minima controlled recursive averaging," *Speech and Audio Processing, IEEE Transactions on,* vol. 11, pp. 466-475, 2003.

[134] K. Nazarpour, A. H. Al-Timemy, G. Bugmann, and A. Jackson, "A note on the probability distribution function of the surface electromyogram signal," *Brain Research Bulletin,* vol. 90, pp. 88-91, 2013.

[135] E. A. Clancy and N. Hogan, "Probability density of the surface electromyogram and its relation to amplitude detectors," *Biomedical Engineering, IEEE Transactions on,* vol. 46, pp. 730-739, 1999.

[136] C. Cipriani, C. Antfolk, M. Controzzi, G. Lundborg, B. Rosén, M. C. Carrozza, *et al.*, "Online Myoelectric Control of a Dexterous Hand Prosthesis by Transradial Amputees," *IEEE Transactions on Neural Systems and Rehabilitation Engineering,* vol. 19, pp. 260-270, June 2011 2011.

[137] S. S. Roley, J. V. DeLany, C. J. Barrows, S. Brownrigg, D. Honaker, D. I. Sava, *et al.*, "Occupational therapy practice framework: domain & practice, 2nd edition," *Am J Occup Ther,* vol. 62, pp. 625-83, Nov-Dec 2008.

[138] N. Jiang, S. Dosen, K. Muller, and D. Farina. (2012) Myoelectric Control of Artificial Limbs - Is there a Need to Change Focus? *IEEE Signal Processing Magazine*. 150-152.

[139] M. Ortiz-Catalan, R. Branemark, and B. Hakansson, "BioPatRec: A modular research platform for the control of artificial limbs based on pattern recognition algorithms," *Source Code Biol Med,* vol. 8, p. 11, 2013.

[140] A. Jourjine, S. Rickard, and Ö. Yilmaz, "Blind Separation of Disjoint Orthogonal Signals - Demixing N Sources From 2 Mixtures," pp. 2985-2988, 2000.

[141] E. J. Rouse, D. C. Nahlik, M. A. Peshkin, and T. A. Kuiken, "Development of a model Osseo-Magnetic Link for intuitive rotational control of upper-limb prostheses," *IEEE Transactions on Neural Systems and Rehabilitation Engineering,* vol. 19, pp. 213-220, April 2011 2010.

[142] L. H. Ting and J. L. McKay, "Neuromechanics of Muscle Synergies for Posture and Movement," *Current Opinion in Neurobiology,* vol. 17, pp. 622-628, 2008.